1-1-2017

Axonal Transport, Parkin, And A-Synuclein; Novel Therapeutic Targets To Treat Methamphetamine Neurotoxicity

Bryan Andrew Killinger
Wayne State University,

AXONAL TRANSPORT, PARKIN, AND α-SYNUCLEIN; NOVEL THERAPEUTIC TARGETS TO TREAT METHAMPHETAMINE NEUROTOXICITY

by

BRYAN ANDREW KILLINGER

DISSERTATION

Submitted to the Graduate School

of Wayne State University,

Detroit, Michigan

in partial fulfillment of the requirements

for the degree of

DOCTOR OF PHILOSOPHY

2017

MAJOR: PHARMACEUTICAL SCIENCES

Approved By:

_____

Advisor: Date:

_____

_____

_____

ACKNOWLEDGEMENTS

I would like to express my appreciation for my family and friends who provided support and encouragement throughout my studies. Without their support my education, and the work completed at Wayne State, would have not been possible.

I would also like to thank my advisor Dr. Anna Moszczynska for providing me with the freedom to expolore new and exciting scientific endevours. With the guidance from Dr. Moszcynska and my other committee members, I was able to combine disperate scientific observations into a unified coherent dissertation. I would like to specifically thank all of my committee members including Dr. Aloke Dutta, Dr. Matthew Galloway, Dr. Bryan Yamamoto (Stark Neurosciences Institute, Indiana University), and Dr. Timothy Stemmler. The time and effort provided over the last several years and during the final review of the disseartation is very much appreciated.

I would also like to thank the many other faculty at Wayne State that provided me with support and guidance over the years. Specifically, Dr. George Corcoran was extremely supportive of my development in the department and in my future endevours. Dr. Steven Firestine provided invaluable consultation and guidance during the difficult process of forming a defending this dissertation. I would like to thank Dr. David Pitts for access to his workshop which was invaluable in the construction of custom equiptment. I would like to thank Dr. Randall Commissaris for providing the opportunity to give lectures for his courses.

I would like to thank the many lab memebers over the years that provided me with training and guidance in the lab. Specifically, Dr. Bin Liu who helped me learn many

techniques early on in the lab. Dr. Ping Qui for providing me a breadth of knowledge about laboratory techniques used to address key scientific questions. I would also like to thank Dr. Yuran Xie for constant support and scientific input on the direction of my project. The scientific input from Dr. Xie was often invaluable for finding the most important questions that needed to be addressed in my research. I would also like to thank Dr. Wu Kai for his consulation and support, as he was always willing to chat about “big picture” concepts.

There are too many individauls to thanks specifically. Everyone in the Pharmaceutical Sciences department was in some way part of my success. I would like to thank all these individuals whom I didn’t have time to metion specifically.

TABLE OF CONTENTS

LIST OF TABLES

LIST OF FIGURES

CHAPTER 1: INTRODUCTION

1.1 Methamphetamine abuse

1.1.1 Prevalence of methamphetamine abuse

Methamphetamine (METH) is a commonly abused illicit psychostimulant. Originally synthesized from ephedrine in 1893 by chemist Nagai Nagayoshi [1], METH gained widespread popularity as an illicit recreational drug in the 1960's [2]. Interestingly, METH was famously used by Adolph Hitler during World War II possibly to alleviate symptoms of idiopathic Parkinson's disease [3]. Today METH remains a drug of widespread abuse in the United States and around the world [4-9]. METH use, particularly in the USA, is fueled by the ease of its manufacture, widespread availability [10], and addictive properties [11]. Approximately 1-2% of Americans have used METH in their lifetime [12], which pales in comparison to more popular illicit drugs (e.g. cocaine, heroin, marijuana), but still remains worrisome because of the health risks associated with METH use. The majority of METH in the United States is imported by criminal organizations based in Mexico [13, 14]. METH is also produced by clandestine synthesis which often results in severe injury to the person performing the synthesis [13]. The illicit manufacture, continued use, and abuse of METH remains a public health problem in the USA.

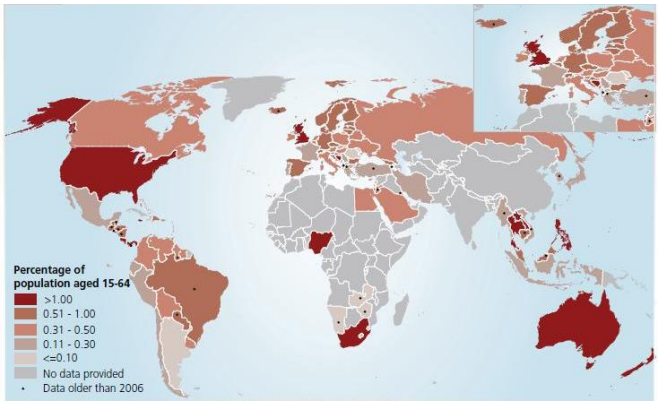

Figure 1: Prevalence of methamphetamine use. The map depicts the percentage of the population of individual countries that use amphetamine type stimulants. (Source = United Nations Office on Drugs and Crime, World Drug Report, 2016)

1.2 Methamphetamine toxicity

METH abuse predominantly produces two main toxic effects: cardiovascular toxicity and neurotoxicity. Cardiovascular toxicity, which accounts for most METH related deaths and emergency room visits, manifests as cardiac dysrhythmias, myocardial infarction, and aortic dissection [15-19]. Approximately 1.5% of METH users eventually perish as a result of their drug use [20]. However, many, but not all, METH users recover from their addiction and these users may face cognitive impairments, impaired motor function, increased risk of stroke, risk of developing parkinson's disease, and possibly lasting psychosis due to METH-induced neurotoxicity [21-24].

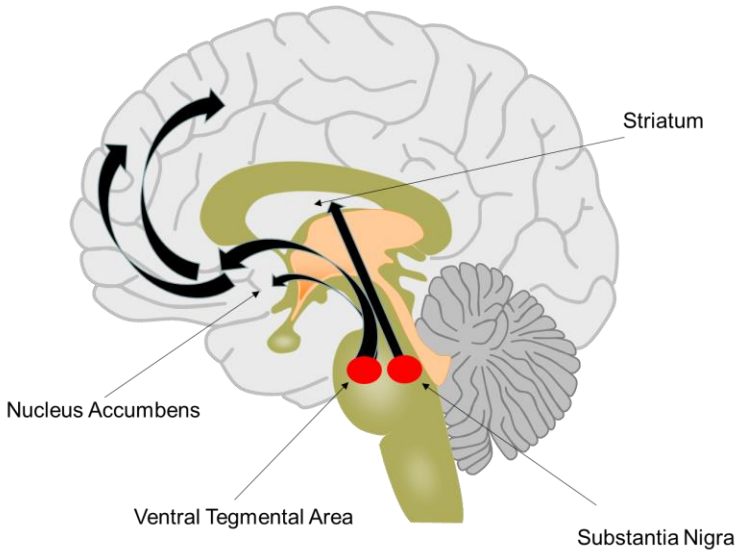

Figure 2. Dopamine pathways of the central nervous system. Mesolimbic DA projections originate in the ventral tegmental area and project to the nucleus accumbens. The nigrostriatal pathway includes DA neurons that project from the substantia nigra to the dorsal striatum. Meso cortical dopamine projections originate in the midbrain and project throughout the neocortex.

1.2.1 Methamphetamine Neurotoxicity

METH neurotoxicity is primarily characterized by damage to the neurons of the nigrostriatal dopamine (DA) pathway [25]. DA neurons in the nigrostriatal pathway originate in the substantia nigra pars compacta (SNpc) and project to the dorsal striatum [26]. Heavy METH users have reduced dopamine transporter (DAT), a transporter protein specific for DA neurons, binding in the striatum following abstinence [27]. METH abusers also have reduced DA levels in the striatum [28]. Because both DA and DAT are specific to dopaminergic (DAergic) neurons it is assumed that DAergic nerve terminals of the striatum are destroyed following heavy METH use [29]. Despite massive damage to

DAegic nerve terminals of the striatum in rodent models of METH neurotoxicity, the DAergic neuron cell bodies in the SNpc remain relatively intact [30]. METH users also show significant activation of microglia in the striatum [31]. Microglia are activated in response to CNS injury [32, 33], and therefore the activation of microglial in the striatum of METH users suggest damage to striatal DAergic axons. However, microglia activation is not restricted to the striatum and was also observed in the midbrain, thalamus, and throughout the cortex [31].

Several studies suggest that DAergic nerve terminals recover following abstinence from METH [34, 35] (Figure 3). Because large scale synaptogenesis is not thought to occur in the adult brain, the apparent recovery of DAergic nerve terminals in the striatum may be due to neuroadaptations in response to METH, as opposed to the gross axotomy of DAergic axons. METH neurotoxicty likely involves a combination of both damage to striatal DAergic axons and neuroadaptation of nigral striatal DAergic neurons.

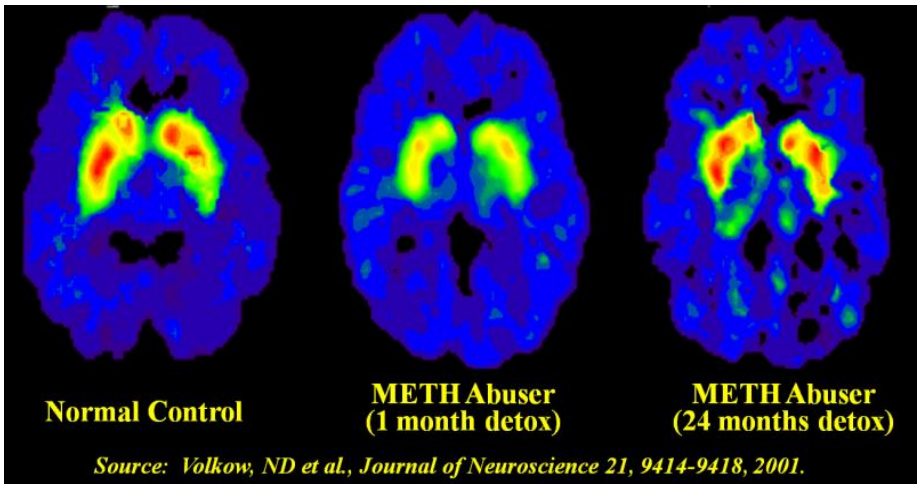

Figure 3. Recovery of striatal dopamine in human methamphetamine abusers following prolonged abstinence from methamphetamine (Volkow, 2001, Neuroscience). Depicted are positron emission topography images of the human METH users that were administered radiolabled, methylphenidate, a dopamine transporter (DAT) ligand. Red, yellow, and blue depicts decreasing DAT density, respectively. Shown here are the PET images from a drug naïve control, METH abuser following detox, and METH user following 24 months of abstinence. (Figure used with written permission from publisher)

1.2.2 The role of hyperthermia

METH can induce life threatening hyperthermia in both humans and animal models of METH neurotoxicity [36-38]. In animal models of METH neurotoxicity METH-induced hyperthermia is directly proportional to the neurotoxic outcomes of METH [39]. Prevention of hyperthermia by lowering environmental temperature inhibits METH-induced neurotoxicity [40, 41] while enhancing hyperthermia increases METH-induced neurotoxicity [42]. It remains unclear why hyperthermia plays such an important role in METH neurotoxicity. Likely explanations for the hyperthermia effect include the increased production of reactive oxidative species generation (ROS), toxic effects outside the CNS (e.g. liver toxicity), impaired the blood brain barrier (BBB), and enhance misfolding of cellular proteins [43].

1.2.3 Behavioral consequences of methamphetamine exposure

The primary behavioral effect of METH is the potent activation of motor behaviors. Motor behaviors includes the activation of locomotor activity (e.g. walking or running) and stereotypy (e.g. repetitive movements). Amphetamines activate nigral striatal DAergic pathway by increasing extracellular dopamine in the striatum [44]. Amphetamines increase extracellular DA in the striatum primarily through the interactions with DAT (Salahpour et al., 2008). METH, like all amphetamines, produces differential effects on locomotor

activity with low doses increasing locomotor activity and high doses decreasing locomotor activity [45-47]. Although high-dose METH decreases locomotor activity, it subsequently increases stereotypy [47]. The motor effects of METH are primarily due to DA activation in the nigrostriatal DAergic pathway [48, 49]. Locomotor effects of amphetamines can be blocked or increased by the knockout [50] or overexpression of DAT [51], respectively. Exposure to neurotoxic doses of METH can result in long-term motor abnormalities and insensitivity to METH-induced locomotor activation [45].

1.2.4 Rodent models of methamphetamine neurotoxicity

The rodent METH binge model is a convenient method to study the neurotoxic effects of METH. The METH binge model involves 4 administrations of relatively high doses of METH (10 mg METH / kg body weight) administered every 2 h. This binge model has several key advantages. The first advantage of binge model is robust depletion of monoamines in the striatum [52], that to some extent, recapitulates monoamine depletions seen in human users [28]. The second advantage is the severe hyperthermia produced during binge METH [53]. The third advantage of the binge METH model is the high level of experimental control afforded by an acute exposure to METH. Other paradigms, such as drug self-administration, produce heterogenous exposure to METH, which ultimately results in a high level of variability in the data obtained that can obscure the accurate analysis of METH's action [54].

Binge METH results in the permanent, at least in part, loss of striatal DA axons and terminals [55, 56] which requires METH-induced hyperthermia [40]. Externally cooling animals during binge METH can attenuate many of the neurotoxic effects [53]. When

rodents are treated with high doses of METH in a cold room (i.e. 4°C) METH neurotoxicity is essentially prevented (Ali et al., 1994, Bowyer et al., 1994). Binge METH models require that animals achieve body temperatures of 41-42°C to observe robust neurotoxicity in the striatum (Bowyer et al., 1994, Yuan et al., 2006). Because 41-42°C body temperature can be fatal, the animals can be cooled during binge METH by placing them on ice (Halpin et al., 2013). Despite external cooling of rats during binge METH the mortality rate in high-dose METH experiments can still be 40-50% [57]. This mortality rate is not reflected in human users [20] (~1.5% mortality after 30 years of METH abuse), bringing into question the utility of a binge METH treatment regime. Furthermore, METH induced hyperthermia of 42°C is sufficient to denature many proteins [58] and multiple organ failure. These consequences of hyperthermia make the specificity of the drug effect in METH binge models difficult to discern from the more global/gross toxicity due to a cellular heat shock response or organ failure.

Binge METH may not completely approximate human METH use. In humans the METH-induced reductions of striatal DAergic neuron markers recover given sufficient abstinence from METH [35]. The transient nature of METH-induced loss of striatal DAergic markers suggests neuroadaptations of DA neurons, and not gross axotomy of DA neurons, is a key components of METH neurotoxic effect in humans. Several alternative METH neurotoxicity animal models have been developed to better approximate human METH use. Chronic METH model, which is similar to METH binge model, involves exposure to high doses of METH over long periods of time (often several weeks). The chronic METH model has the advantage of lower mortality rates and less hyperthermia

when compared to binge METH models. However, this model suffers from a key drawback, in that METH is still administered by the experimenter, termed non-contingent administration, and not actively administered by the animal, termed contingent administration. Humans actively administer METH (i.e. contingent administration) and therefore non-contingent administration does not mimic human METH use. Drug self-administration models have been used since 1962 to study drug addiction [59, 60] but used only recently to study METH neurotoxicity. METH self-administration does not produce neurotoxicity seen in binge METH models [61-63]. Only when animals are allowed to self-administer METH for ~18 hours a day for weeks at a time meaningful reductions (~40-50%) in striatal DAergic markers are observed [64, 65]. Interestingly, the reduction in striatal DAergic markers appears transient similar to what is seen in human METH users. Therefore, METH self-administration may be a more accurate model of human METH neurotoxicity than classical non-contingent models.

1.2.5 Molecular mechanisms of methamphetamine neurotoxicity

1.2.5.1 Dopamine

METH-induced DAergic neurotoxicity is due to several drug effects at the DAergic nerve terminal. The primary effect of METH is releasing of DA from pre-synaptic vesicles and pre-synaptic nerve terminals via interaction with vesicular monoamine transporter 2 (VMAT2) [66-70] and DAT [71, 72], respectively. Free DA in the presynaptic terminal readily auto-oxidizes into a reactive dopamine quinone, which subsequently forms adducts with and damages cellular components [73-75]. DA released into the cytosol following METH produces excess oxidative stress damaging the nerve terminal [14, 74, 76]. METH

also binds to and reverses the function of DAT. Because DAT is the primary clearance mechanism of DA in the synapse, METH ultimately increases an efflux of DA out of the nerve terminal. Treatments that increase or decrease the available DA (i.e. vesicular, cytosolic, and extracellular DA stores) prior to METH treatment, appear to increase or decrease the neurotoxicity observed, respectively [68, 77].

1.2.5.2 Neuroinflammation

Neuroinflammation plays an important role in several neurodegenerative diseases [78]. Neuroinflammation occurs with infection or toxic insult in the CNS. The neurotoxic insult of METH activates several neuroinflamatory responses that can activate microglia in the striatum [31, 79]. Microglia release proinflammatory cytokines which can induce cell death [80]. METH also increases the immunoreactivity of the reactive gliosis protein, glial fibrillary acidic protein (GFAP), in the striatum [81]. Induction of GFAP, termed reactive gliosis, in the CNS is a general response to injury or toxic insult [82]. Astrocytes, unlike microglia, can play a neuroprotective role [83].

1.2.5.2 Oxidative Stress

Oxidative stress is an important mechanism of METH neurotoxicity. METH can induce toxic hydroxyl radicals and superoxide [74, 84]. METH increases cytosolic DA concentrations through interactions with VMAT2 increasing auto-oxidation of DA [85]. In humans, the increase in cytosolic DA can be metabolized by MAO-B, producing hydrogen peroxide and the metabolite DOPAC [86, 87]. Hydrogen peroxide can then produce hydroxyl radicals via the Fenton reaction [88]. Hydroxyl radicals are highly reactive and can damage a wide variety of cellular components [89].

1.2.6 Role of parkin in methamphetamine neurotoxicity

1.2.6.1 Cellular functions of parkin

Parkin is an E3 ubiquitin ligase [90] expressed in neural bodies and neurites, but not glia, throughout the brain [91]. Parkin ubiquitinates damaged/dysfunctional proteins so they can be degraded by the proteasome. The ubiquitination of proteins and subsequent degradation of ubiquitinated proteins via the proteasome is referred to, collectively, as the ubiquitin proteasome system (UPS). Parkin has numerous proposed substrates including DAT [92, 93].

1.2.6.2 Methamphetamine impairs parkin function

METH impairs parkin function [94, 95]. Binge METH results in the transient reduction in parkin levels of striatal synaptosomes. The loss of parkin occurs within the first 24 h and returns to basal levels at 48 h following binge METH [94]. The METH-induced loss parkin coincides with increased 4-hydroxynonanal modified proteins and decreased proteasomal activity in the striatum [94]. Treatment with the antioxidant compound, vitamin E, prevented these effects, and prevented the loss of striatal DA [94].

1.2.6.3 Neuroprotective effects of parkin

The overexpression of parkin protects against METH-induced neurotoxicity [96]. However, parkin knockout mice are not hypersensitive to the neurotoxic effects of METH [97]. The lack of hypersensitivity could be due to phenotype adaptations to compensate for the loss of parkin. Mutations in PARK2, the gene encoding parkin, have been found in patients with the neurodegenerative disease Parkinson's disease (PD). The overexpression of parkin in the SNpc has shown some neuroprotective efficacy in PD models [98-102].

PD and METH neurotoxicity are similar in that both involve damage to the nigrostriatal DAergic pathway. METH neurotoxicity models have been used to mimic the neurodegeneration of PD [103].

1.2.6.4 Parkin modulates dopamine release in the nigrostriatal DA pathway

As an E3 ubiquitin ligase, parkin is thought to exert neuroprotective effects by enhancing the removal of damaged/misfolded proteins. However, numerous studies now demonstrate that parkin plays a "non-classical" role in DA neurons of the nigrostriatal pathway [98, 104-106]. Studies manipulating parkin expression in nigrostriatal DA neurons suggest parkin modulates DA activity of these neurons, independently of parkin mediated neuroprotection via enhanced degradation of damaged substrates [97, 98, 104]. In general, loss of parkin appears to impair DA utilization while overexpression of parkin enhances DA utilization. DA utilization is a general term that refers to the normative the process of DA synthesis, packaging, release, and reuptake [105].Therefore, parkin's effects on DA utilization may be through enhanced DA synthesis [98], packaging into vesicles [105], or release [106-108].

1.2.7 Role of α-synuclein in methamphetamine neurotoxicity

α-Synuclein is a small intrinsically disordered protein of unknown function. Several proposed functions of α-synuclein include SNARE mediated vesicle exocytosis, lysosomal function, and possibly intracellular vesicle transport [109]. α-Synuclein is expressed ubiquitously throughout the body and is abundantly expressed in the brain [110]. α-Synuclein aggregation is important for the progression of PD, and correspondingly, has been the subject of intense study. Large cytoplasmic inclusions rich in α-synuclein are a

hallmark of PD. Similar aggregates have been observed in METH neurotoxicity models [111]. α-Synuclein is a possible substrate for parkin [112], however, parkin mediated ubiquitination does not appear to directly control α-synuclein turnover [113]. Furthermore, any direct interactions between α-synuclein and parkin are likely transient and weak [113].

Increasing the expression of α-synuclein is toxic to dopamine neurons [114-117]. Preliminary studies have suggested the METH can increase expression of α-synuclein in the striatum [118, 119]. The METH-induced increase in striatal α-synuclein and oxidative stress may lead to toxic aggregation and neurotoxicity [120]. Knockdown of α-synuclein in rats can protect against METH induced loss of TH and DA [121, 122]. α-Synuclein modulates DA release via interactions with calcium channels [123] which could result in increased METH-induced DA release in the striatum.

DA, which is structurally similar to METH, is known to bind to α-synuclein [124] and subsequently promote its aggregation [124, 125]. Therefore, METH may also bind to α-synuclein, inducing a conformation change similar to that seen with DA, and increasing α-synuclein aggregation [126]. However, METH binding to α-synuclein was determined using a nanopore assay and another technique is needed to confirm the interaction between METH and α-synuclein.

α-Synuclein forms a stable tetramer in vivo [127]. Destabilization of this tetramer is a hypothesized initiating mechanism for the aberrant aggregation and neurodegeneration in PD [128]. It is unknown if METH can affect α-synuclein tetramer stability. Interactions between α-synuclein and cellular lipids stabilizes the n-terminus α-helix conformation of α-synuclein and drive the formation of higher-order α-synuclein oligomers. Disruption of

interactions between α-synuclein and cellular lipids can impair tetramer/oligomer formation. DA forms adducts with α-synuclein stabilizing the aggregation prone protofibril α-synuclein species [129], and impairing α-synuclein lipid binding [130]. Presumably, METH-induced increase in free cytoplasmic DA would promote α-synuclein adduct formation, and subsequently impair tetramer formation, possibly resulting in the toxic aggregation of α-synuclein. The aggregation of α-synuclein may be directly involved in METH-induced neurotoxicity and may help explain the apparent increased incidence of PD in METH users [24]. However, any direct relationship between METH neurotoxicity and α-synuclein remains untested and unclear.

1.2.8 Role of axonal transport in methamphetamine neurotoxicity

1.2.8.1 Axonal transport defined

Neurons are highly polarized cells that transmit and receive electrical/neurochemical signals. Neurons consist of three distinct parts including the cell body, the axon, and the axon terminal. Axons are appendages that project from the cell body to a distal location. The point at which the axon ends is termed the nerve terminal or button. Nerve terminals are the "business end" of the neuron in that they are heavily enriched in cellular machinery involved in neurotransmission (e.g. receptors, neurotransmitter filled vesicles, membrane transport proteins etc.). Neurotransmitters can have rapid turnover at the nerve terminal, and therefore, synthesis of neurotransmitters occurs locally at the nerve terminal to ensure constant availability of these important signaling molecules. However, other important nerve terminal components such as proteins and organelles are not normally generated at the nerve terminal because nerve terminals

lack the genetic information and protein synthesizing machinery. Axonal transport is the process by which neurons supply nerve terminals with proteins and organelles to meet the requirements of the nerve terminal. Axonal transport is also important in the trafficking of cellular components back to the cell body. Axonal transport becomes especially crucial for the healthy function of neurons, whose subcellular compartments, are vastly separated from each other by space and time. For example, human peripheral neurons can have axons that project a distance 10^6 greater than the radius of the cell body.

Axonal transport is responsible for the trafficking of cellular cargo to the distal nerve terminal. Known cargos that are actively transported via axonal transport include mitochondria [131], lipid vesicles [132, 133], soluble proteins [134], and membrane proteins (embedded in lipid vesicles)[135].

1.2.8.2 The machinery of axonal transport

Axonal transport of cargo can either be toward the nerve terminal (i.e. anterograde) or towards the cell body (retrograde). Motor proteins, such as kinesin and dyenin, are a main driving force of axonal transport. Motor proteins utilize ATP to generate motive force carry their cargo along the axon. Cargo can move in the axon by either slow or fast axonal transport [136] and the directionality of transport switches rapidly, often with long pauses between periods of rapid movement. Numerous adapter proteins and motor proteins are thought to regulate the axonal transport of specific cargo in a complex signaling network. (See figure 4 for summary)

Microtubules (MT) are required for axonal transport. MT are long polymers consisting of α- and β-tubulin heterodimers. MT are highly dynamic structures that cycle

between elongation (rescue) and rapid depolymerization (sometimes referred to as catastrophe) [137]. Axonal transport requires stable and long-lived MT. Compounds that depolymerize MT inhibit axonal transport and compounds that stabilize MT enhance axonal transport [138, 139].

1.2.8.3 The role of tubulin post-translational modifications in axonal transport

There are several known post translational modifications (PTM) of α-tubulin including detyrosination (DetyTUB) and acetylation (AcetTUB). Following α-tubulin synthesis the c-terminal tyrosine residue is proteolytically removed by an unidentified carboxypeptidase, generating DetyTUB. DetyTUB can be re-tyrosinated by tubulin tyrosine ligase [140, 141]; however, the removal of the remaining glutamate residue makes the detyrosination irreversible. DetyTUB is associated with long lived stable MT [142] required for axonal transport, although the PTM does not itself confer stability. AcetTUB is generated by two acetyltransferases, MEC-17 (also known at αTAT1 or α-tubulin N-acetyltransferase 1) and ARD1-NAT1, that acetylate lysine 40 of α-tubulin [143]. α-Tubulin can only be acetylated when following its incorporation into a MT polymer. AcetTUB can be deacetylated by histone deacetylase 6 (HDAC6) and sirtuin-2 [144, 145]. Although AcetTUB is not thought to directly impart stability to MT per se, AcetTUB is highly enriched on stable long-lived MT polymers.

1.2.8.4 Role of axonal transport in neurodegeneration

Axonal transport dysfunction has been implicated in several neurodegenerative diseases including Parkinson's disease and Alzheimer's disease [146-148]. Many studies suggest that deficits in axonal transport impair the removal of damaged/dysfunctional

cellular components (e.g. proteins) and organelles (e.g. mitochondria), ultimately resulting in neurodegeneration [149]. It remains unclear whether axonal transport deficits are a cause of neurodegeneration or a symptom of neurodegenerative processes.

1.2.8.5 Possible role of axonal transport in METH neurotoxicity

It is unknown whether METH can impair axonal transport. There are several preliminary studies that suggest METH can impair MT stability. Endothelial cells treated with METH show reduced levels of AcetTUB, suggesting a loss of MT stability [150]. As previously mentioned, the reduction in striatal DAergic nerve terminal markers following METH are partially reversible given sufficient abstinence from METH. Therefore, it is possible that axonal transport is impaired/downregulated following METH exposure and subsequently recovers following abstinence from METH.

1.2.8.6 The use of MT stabilizing compounds as axonal transport enhancing drugs

Several recent investigations have found that new class of MT stabilizing drugs, called epothilones, can be used to enhance axonal transport in neurons of the CNS [139, 151, 152]. Epothilone D is a particularly promising compound for the enhancement of axonal transport. Systemic treatment with Epothilone D results in increased the number of stable MT in CNS neurons [152]. Several treatments with Epothilone D can delay neurodegeneration in several animal models of PD and AD [152, 153]. Epothilone D potently stabilizes MT polymers [154], and readily accumulates in the brain [155], making it a good candidate for treatment of axonal transport deficits in the CNS. Epothilone D was in clinical trial for Alzeihmers disease but these trials have since been discontinued, possibly due to issues with efficacy and safety.

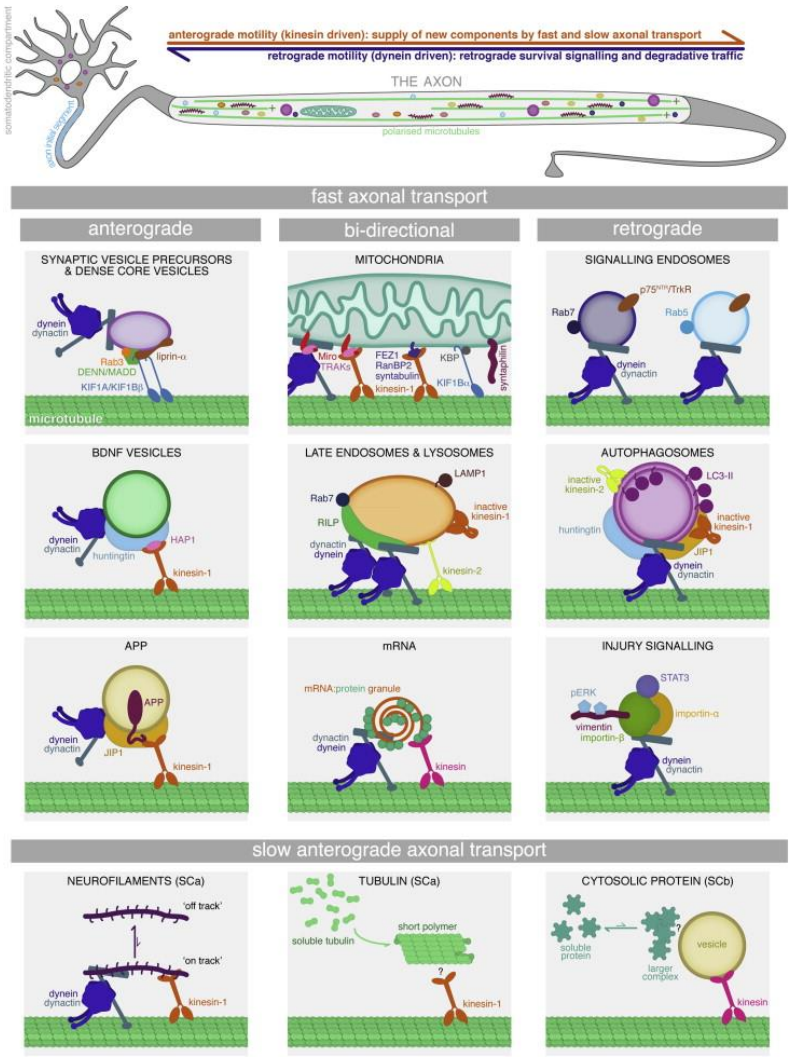

Figure 4. Axonal transport. (Maday S, Twelvetrees AE, Moughamian AJ, Holzbaur EL (2014) Axonal transport: cargo-specific mechanisms of motility and regulation. Neuron 84:292-309.) Axonal transport occurs over the entire length of the axon. The processes can either transport cargo to or from the cell nerve terminal (anterograde and retrograde transport, respectively). Axonal transport is involved with the trafficking of numerous cellular cargoes including vesicles, mitochondria, mRNA, neurofiliments, tubulin, and cytosolic proteins. Motor proteins kinesin and dynein are the main driving force for anterograde and retrograde transport, respectively. Both motor proteins require intact microtubule polymers. (Figure used with written permission from publisher).

1.3 Project Overview

1.3.1 Project Rationale

There are currently no therapeutic interventions to inhibit or reverse the neurotoxic effects of METH on the central nervous system (CNS). The process of axonal transport as well as the proteins parkin and α-synculein have proposed roles in METH neurotoxicity. Investigation into these factors, and how they relate to METH neurotoxicity, could provide insight into possible therapeutic targets to treat METH neurotoxicity.

1.4 Specific Aims and Hypothesis

1.4.1 Aim 1

Establish the presence of axonal transport deficit in the nigrostriatal DA pathway following neurotoxic administration of METH. Hypothesis: Neurotoxic regimen of METH will result in axonal transport impairment.

1.4.2 Aim 2

Restore DAergic terminal function via enhancing axonal transport in the nigrostriatal DA pathway. Hypothesis: Stabilization of microtubules will restore METH-induced decreases in striatal DAergic markers.

1.4.3 Aim 3

Determine whether deficit in E3 ligase parkin mediates the METH-induced impairment in axonal transport. Hypothesis: Loss of parkin will potentiate METH-induced impairment of axonal transport.

1.4.4 Aim 4

Investigate whether altered assembly of α-synuclein species mediates the METH-induced impairment in axonal transport. Hypothesis: METH will alter α-synuclein multimerization leading to impaired axonal transport.

CHAPTER 2: VALIDATION OF DRUG SELF-ADMINISTRATION AS A METH TOXICITY MODEL

2 Background

Methamphetamine (METH) abuse results in long-term depletion of striatal DAergic nerve terminal components [35]. This depletion may be partially due to damage to striatal DAergic axons [31, 55]. Therefore, a good model to study METH abuse should produce long-lived DA depletion in the striatum similar to what is observed in human METH users [27, 35, 156-158].

Rodent drug self-administration is an old technique commonly used to study the addictive properties of drugs [159]. Only recently, drug self-administration procedures have been employed to specifically study the neurotoxic properties of METH [62, 63, 160]. The use of self-administration for the study of METH neurotoxicity remains speculative because rodent METH self-administration models fail to produce robust neurotoxicity in the striatum, unless the self-administration sessions are significantly prolonged [160]. Furthermore, rodent drug self-administration does not engender the same pattern of drug taking in humans. Rodents will self-administer METH at regular intervals [161] while human users generally administer several large doses over the period of several days. This can be explained because the half-life of METH is significantly shorter in rats, making frequent administration necessary to maintain a steady blood levels [162].

METH self-administration models have some advantages over models that use non-contingent administration. First, METH self-administration may better approximate human abuse. Human abusers are not passively administered METH, but instead, undergo many

complex behaviors to seek out and take METH. These complex behaviors and the environmental stimuli associated with them, make the administration of METH "contingent." Contingent administration requires that operant conditioning is controlling the drug taking/seeking behavior. Like with all operant behaviors, a discrimitive stimulus signals the availability of reinforcing stimulus. The reinforcing stimulus "drives" behavior by increasing its probability in the future. METH is a potent reinforcer that can easily shape the operant behavior of lever pressing in rodents. Numerous studies have demonstrated that self-administered (i.e. contingent) drugs produce distinct neurochemical responses in the brain [65, 163], which are likely to influence the development of neurotoxicity. As eluded to, this phenomenon is likely a result of the complicated learning and drug seeking behaviors during self-administration. As most profoundly demonstrated by hollerman, J.R. and Schultz, W. (1998), where the simple light stimulus signaling drug administration drastically altered the subsequent activity of DA neurons [164].

Here we explored the use of a short-access self-administration protocol to study METH neurotoxicity in the striatum.

2.1 Materials and methods

2.1.1 Chemicals and materials

D-methamphetamine HCl (METH) (Sigma-Aldrich, St. Louis, MO) was dissolved in sterile saline to a concentration of 0.5 mg METH / mL saline. METH solutions were sterile filtered through a 0.22 μm membrane. Ketamine (100 mg / mL), xylazine (20 mg / mL), surgical drapes, wound clips, silk sutures, and surgical gauze was purchased from Henry Shein Animal Health (Dublin, OH). Precision grain based food pellets were

purchased from Bioserve (Flemington, NJ). Catheter plugs, catheter extenders, and 22 ga Renathane catheter tubing was purchased from Braintree Scientific (Braintree, MA). Heparin/dextrose catheter lock solution and 22 ga blunt needles were purchased from SAI infusion. Infusion harnesses and tethers were purchased from Instech Laboratories (Plymouth Meeting, PA). Operant chambers and MED-PC software were purchased from Med Associates (Fairfield, VT).

2.1.2 Subjects

Adult male Long-Evans rats (Envigo, Indianapolis, IN) between the weights of 200-250g were used. All animals were fasted overnight before lever training. For the remainder of the study animals were allowed ad libitum access to food and water. For the duration of the study all animals were singly housed in clear bottom polycarbonate cages with Sani-Chip bedding. Animals were inspected upon arrival for signs of abnormalities such as disease and/or distress. Following an acclimation period of 7 days each animal was weighed and assigned a study number. For the duration of the study animals were be weighed on a weekly basis and on days of drug self-administration.

All animals were implanted with a chronic indwelling jugular catheter. The catheter was flushed daily with 1 mL sterile saline and filled with 0.5 mL heparine/dextrose catheter lock solution. Between flushing the catheter was plugged using a 22 ga stainless steel catheter plug. Animals whose catheter lost patency prior to the end of study was removed from the study. All catheter solutions were sterile filter through a 0.22 μm filter and drawn up in the biohood.

2.1.3 Jugular Catheter Surgery

Animals were anesthetized with a mixture of ketamine (100 mg ketamine / kg body weight) xylazine (6 mg xylazine / kg body weight). To maintain surgical plane anesthesia booster shots of ketamine (20 mg ketamine /kg body weight) were administered. All anesthetic agents were administered via intraperitonal (i.p.) injection.

Once the animal has reached a deep state of anesthesia (does not respond to tail pinch) the animal's hair was removed from both incision sites. (See Figure 5)

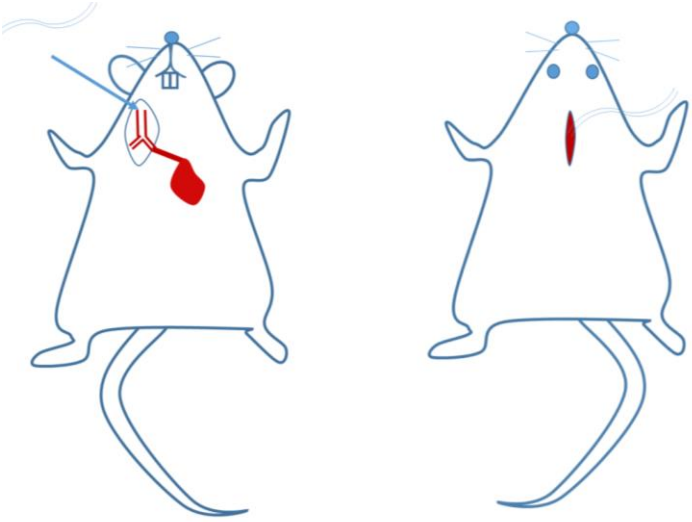

Figure 5. Jugular catheter surgery incision sites. The drawing depicts the site of surgical incisions for the implantation of the chronic intradwelling catheter in rats. The jugular catheter is implanted into the jugular vein (arrow) and inserted just proximal to the right atrium.

Petroleum based ointment was placed in each of the animal's eyes prior to surgery. Both incision sites were then cleaned thoroughly with both betadine and isopropyl alcohol (scrubbing the site 3 times with each solution; in an outward circular motion). The animal was then placed in dorsal recumbancy and small 0.25'' incision was made on the right side of the animal's neck. Using blunt dissection methods, the animal's jugular vein was

exposed just anterior to the pectoral muscle. The jugular vein was isolated from surrounding tissue and tied with a sterile silk suture to stop blood flow to the heart. A small incision was made in the jugular vein, the catheter inserted, and then was tied into place using another sterile silk suture just posterior to the catheter insertion site. The catheter was flushed with sterile saline and blood was briefly drawn into the catheter line to ensure correct placement. The catheter was then cleared with sterile solution. The animal was then flipped over and an incision made between in the scapular region. Forceps were used to separate the skin from the underlying tissue and muscle. Once an area was cleared under the skin, connecting both incisions, the catheter line was then closed using a 22-gauge steel plug and pulled through the dorsal incision site. At this time the catheter line was secured to muscle in the neck and back using silk sutures. Once secure the catheter was flushed with locking solution consisting of 0.5 mL heparin/dextrose. The incision sites are closed using sutures or wound clips. Animal was then placed on warming pad to recover. During recovery, the catheter line could be cut to the desired length (approximately 1 inch from incision site).

2.1.4 Methamphetamine self-administration behavioral procedures

Initial lever training was conducted prior to the catheter surgery. During the training phase animals are placed on limited food access (food removed approximately 5pm night prior to training and returned following training the next day). Animals then are allowed to respond for three 30 min sessions of fixed ratio (FR) 1. Animals are limited to 30 rewards per session. Once animal has reached the maximum session rewards at FR1 schedule of reinforcement they can then undergo catheter surgery. Following recovery from catheter

surgery (7-10 days) the wound clips and/or sutures are removed from incision sites. The animal was then allowed to administer METH (0.1 mg METH / kg bodyweight / per infusion) on an FR1 schedule for 7 consecutive days. Each drug infusion results in a 20s timeout to prevent accidental overdose. Following 7 consecutive days of responding on FR1 schedule, animals were placed on FR5 schedule on day 8. Animals were then allowed to respond for 7 days on FR5 schedule. Behavioral output was continuously recorded with MEDPC software. (See table 1)

2.1.5 High-Performance Liquid Chromatography

Procedures were conducted as previously described [165]. All procedures were conducted on ice or under refrigeration. Briefly, tissues were sonicated in 0.5 mL of 0.3 N perchloric acid for 30 s, and the resulting homogenate was centrifuged for 30 min at 12,000 x g. The pellet was dissolved in 1M NaOH overnight at 4°C, and protein concentration was determined using the bicinchoninic acid (BCA) protein assay (ThermoScientific). To measure DA content, 20 µl of the supernatant was injected into mobile phase containing 90 mM sodium dihydrogen phosphate monohydrate, 50 mM citric acid, 1.7 mM 1-octane sulfonic acid, 50 µM EDTA, and 10% acetonitrile (ThermoScientific), at a flow rate of 0.5 mL/min. Samples were separated using a C-18 reverse-phase column (150 X 3.2, 3 µM particle size; ThermoScientific). DA and its metabolites were then detected electrochemically (electrode 1: -150 V, electrode 2: +220 V). Final values are reported as picograms of analyte per microgram of protein.

2.1.6 Immunohistochemistry

Rats were euthanized via live decapitation, the brain removed, and cut to separate the right and left hemispheres. The left hemisphere was placed into 50 mL of 4% paraformaldehyde in PBS. The brain was kept in the paraformaldehyde solution for 3 days at 4°C, and then transferred to 10% glycerol (1 day) and 20% glycerol (1 day). Fixed brains were then flash frozen in isopentane cooled with slurry of ethanol and dry ice. 30 µM sagittal sections were then cut using cryostat (Thermoscientific) and the sections rehydrated in PBS for 1 h. Sections were then incubated in blocking buffer (PBS, 0.1% Triton X-100, 1% m/v bovine serum albumin) for 1 h at room temperature. Sections were incubated overnight at 4°C with anti-TH antibody (EMDMillipore) in blocking buffer. Sections were then incubated with blocking buffer containing Alexa Fluor® 488 goat anti-mouse (Invitrogen, Carlsbad, CA) diluted 1:400 for 2.5 h at room temperature. DRAQ5 (Invitrogen) was used according to the vendor protocol to stain nuclei. Sections were then mounted using Fluoromount (SouthernBiotech, Birmingham, AL). Slides were imaged using a Leica SP3 laser scanning confocal microscope (Leica, Wetzlar, Germany). The non-compressed raw single z-plane images were exported from the Leica Image Analysis Suite (Leica). These images were then analyzed using Imaris co-localization analysis software (Bitplane South Windsor, CT). For each image automatic thresholding and masking functions were used to prevent interference from signal noise and variations in signal intensity. The resulting percent co-occurrence in the TH channel was normalized to non-treated control for ease of graphical comparison. The final value represents the percentage of signal overlap within the TH signal.

Table 1. Self-Administration parameters.

	Lever Training	Acquisition Day 1-7	Maintenance Day 8-21
Schedule	**1**	**1**	**5**
Session length (min)	**30**	**180**	**180**
Max Rewards	**30**	**999**	**999**
Timeout (s)	**0**	**20**	**20**
Reward	**Food Pellet**	**0.1mg/kg METH**	**0.1mg/kg METH**

2.2 Results

2.2.1 Lever Training

Food deprived rats quickly acquired the lever press behavior on a FR1 schedule of reinforcement. All animals met the criteria of 30 rewards (food pellets) by the third day of lever training. The lever press behavior for several animals was "hand shaped" by manually delivering the pellet as the rat's behavior more closely approximated a lever press.

2.2.2 Methamphetamine intake during self-administration

Following the implantation of jugular catheters animals were allowed to respond for METH. Responding on day 1 was relatively robust with animals administering approximately 1.5 mg METH / kg bodyweight (Figure 6). The robust responding on day 1 was likely due to prior lever training. Animal responding slightly decreased within the first few days to 1 mg METH / kg bodyweight. By day 7 responding had stabilized to about 1.75 mg METH / kg BW.

On day 8 the FR1 was increased to an FR5. Correspondingly, responding increased 5-fold of that seen using the FR1 schedule. For the remainder of the study animals self-administered approximately 1.75 mg METH / kg bodyweight.

Animals that were allowed to respond for infusions of saline showed extinction of lever press behavior within the first three days. Responding remained very low for the remainder of the study.

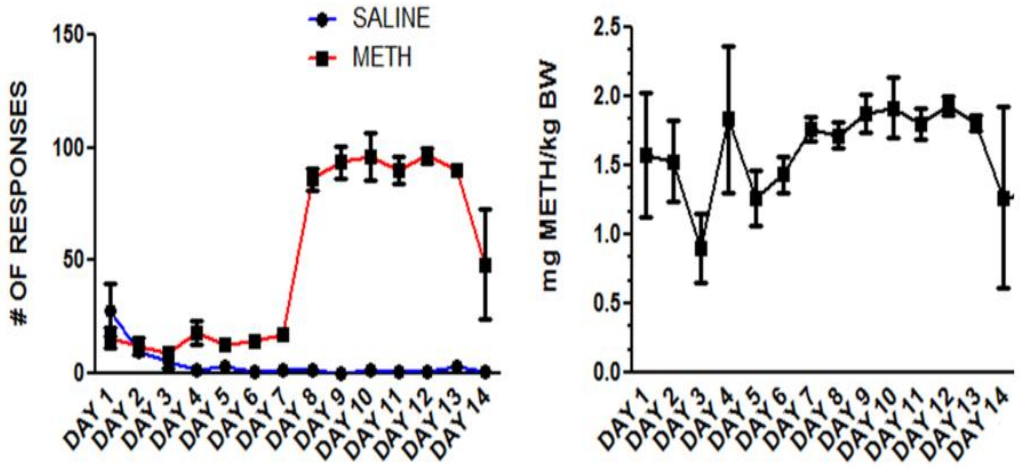

Figure 6. Responding during self-administrations session. The mean number of responses (left) and drug intake (right) during 14 days of self-administration. Each daily session was 4 h in length. Animals trained under an FR1 for first seven days and a FR5 for the remaining 7 seven days. Each response consists of a single lever press. Each injection consisted of 0.1 mg METH / kg bodyweight or saline. n =4.

2.2.3 Gross dopamine axon pathology of the striatum following methamphetamine self-administration

Binge METH results in large scale axotomy of the striatal dopaminergic axons in rats [55]. TH staining of the striatum shows dense DAergic axon enervation in animals that self-administered both saline and METH (Figure 7). The overall intensity of TH staining and the morphology of TH axons were indistinguishable from saline and METH exposed animals. (Figure 7)

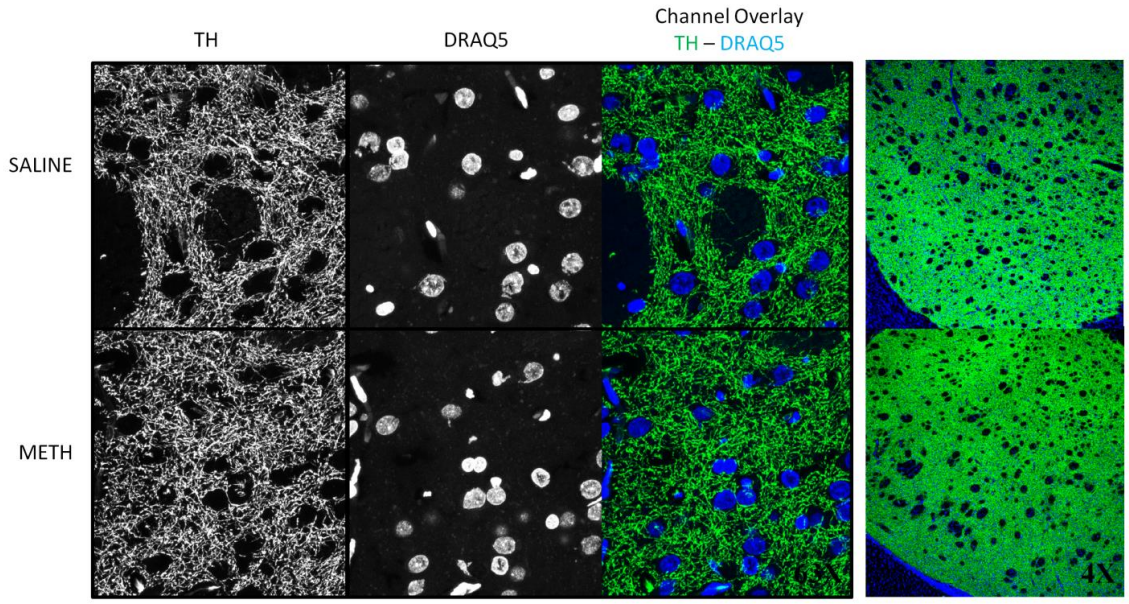

Figure 7. Striatal DAergic axons 21 days following methamphetamine self-administration. Fixed brain slices were stained with an antibody specific for tyrosine hydroxylase (TH) and a dye specific for nuclei (DRAQ5). Tissue was then imaged using confocal microscopy. High contrast images of both channels are displayed in the first two columns. Pseudo colored images of overlaid channels are shown in the last two columns. Low magnification images of the entire striatum depicted on the right. The top panel include images from a rat that was only exposed to saline during selfadministration session and the bottom panels depict a rat that self-administered methamphetamine for 14 consecutive days. Images depict a lack of damage/destruction to striatal dopaminergic axons following methamphetamine self-administration.

2.2.4 Striatal dopamine content following methamphetamine self-administration

Binge METH results in large dopamine loss in the rat striatum [166]. Following METH self-administration, we measured dopamine and dopamine metabolite content in the striatum. We observed little difference in the striatal dopamine content of rats exposed to saline or METH (Figure 8). Dopamine metabolites were also similar between saline and METH treated animals (Data not shown).

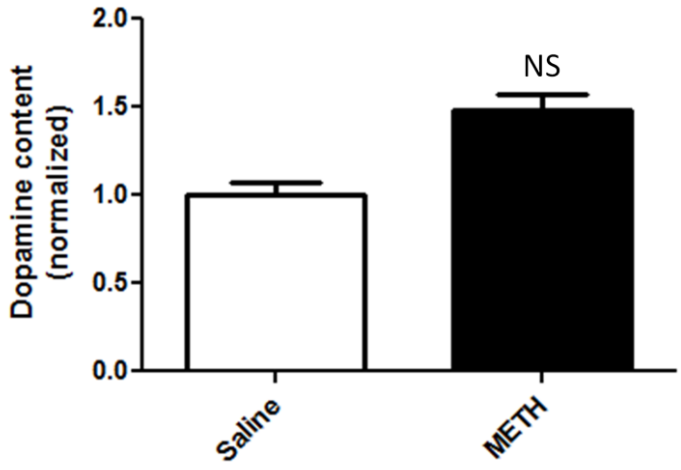

Figure 8. Striatal dopamine content 21 days following methamphetamine self-administration. Dopamine was separated by HPLC and measured by electrochemical detection. Striatal dopamine content was normalized to saline treated animals. Student t-test was conducted to compare treatment groups (NS). n = 3-4.

2.3 Discussion

Here we determined that rats would readily respond for an intravenous injection of 0.1 mg METH / kg bodyweight. The level of responding observed here is slightly less than other METH self-administration studies [65, 160]. However, those studies use Sprague Dawley rats and here we used Long-evans rats. Genetic differences between rat strains can affect the robustness of drug self-administration acquisition and maintenance [167, 168].

Our findings suggest that Long-Evans rats are less robust responders for METH than Sprague Dawley rats.

The main objective here was to determine if METH self-administration would result in detectable DAergic neurotoxicity in the striatum. We did not observe signs of neurotoxicity following 14-day exposure to METH self-administration. Striatal dopamine levels and TH axon abundance/morphology were similar between saline and METH exposed animals. This finding is in agreement with numerous studies that show only extended access can produce symptoms of neurotoxicity [160, 169]. The lack of toxicity is likely due to the short access to METH. Longer exposures (>12 h) seem to be required for detectable neurotoxicity in the striatum. The lack of toxicity may also be due to the relatively modest METH intake observed here with Long Evans rats. During the 4 h session most animals self-administered approximately 1.5-2.0 mg METH / kg bodyweight. This level of exposure may be sufficient to engender robust addictive behaviors (e.g. cue induced reinstatement) but likely insufficient for neurotoxicity.

2.4 Conclusions

Daily short access METH self-administration does not produce neurotoxicity in the striatum. The short access daily exposure, commonly used for addiction studies, is likely not a good model to study the neurotoxic effects of METH. Future studies utilizing self-administration to model METH neurotoxicity should focus on extended access paradigms, as described elsewhere [65]. Otherwise, METH neurotoxicity studies in rodents should focus on non-contingent administration.

CHAPTER 3 -- THE ROLE OF AXONAL TRANSPORT IN METHAMPHETAMINE NEUROTOXICITY

Results in chapeter three are transcribed from the peer-reviewed manuscript: "Killinger BA, Moszczynska A (2016) Epothilone D prevents binge methamphetamine-mediated loss of striatal dopaminergic markers. Journal of Neurochemistry 136:510-525". Killinger B. was responsible for designing, conducting, writing, and reporting results transcribed in chapter 3. Moszczynska A. was responsible for writing, editing, and reviewing the manuscript prior to acceptance by the Journal of Neurochemistry. The following work was conducted to begin to address the possibility that axonal transport may play in role in METH neurotoxicity. Furthemore, it was conducted to determine if the neuroprotective compound, epothilone d, could prevent/reverse the neurotoxic effects of METH.

3 Background

Methamphetamine (METH) is a widely abused neurotoxic psychostimulant. When administered in high doses, METH induces long-term deficits in striatal dopaminergic (DAergic) markers, including the dopamine transporter (DAT), tyrosine hydroxylase (TH), dopamine (DA), and DA metabolites [170-173]. To some extent, the loss of DAT, TH, DA, and its metabolites is due to physical loss of axonal terminals [55]. Extended abstinence from METH results in partial recovery of these DAergic markers in experimental animals and humans [35, 52, 55, 173-175], suggesting compensatory changes within the nigrostriatal DA pathway. There is little evidence that DAT and TH are locally synthesized in the axons in the adult brain; therefore, axonal transport might be required to restore DAT

and TH to DAergic terminals. Axonal transport impairment is an early marker of several neurodegenerative diseases [146] and may also precede development of METH neurotoxicity or play a role in predisposing METH users to development of Parkinson's disease [176]. It is not known whether METH alters axonal transport in the nigrostriatal DA pathway.

Axonal transport requires cytosolic polymers called microtubules (MTs) that consist of heterodimers of the cytoskeletal proteins α-tubulin and β-tubulin. Several post-translational modifications (PTMs) of α-tubulin, including detyrosination, tyrosination, and acetylation, are thought to play a role in regulating MT structure and function [177]. Specifically, acetylated (AcetTUB) and detyrosinated (DetyTUB) α-tubulin are highly enriched in stable long-lived MTs [178], are present in axons [179], and preferentially recruit the anterograde motor protein kinesin [180, 181]. Conversely, β-III-tubulin (βIIITUB) imparts dynamicity to MTs [182], is highly expressed in somatic neurons [183], and confers resistance to taxane-mediated MT stabilization [184, 185]. In axons, tyrosinated α-tubulin (TyrTUB) is enriched in newly formed MTs and in a highly dynamic MT population that is sensitive to nocodazole-mediated depolymerization [186]. Overall, MTs enriched with DetyTUB and/or AcetTUB are more rigid and support axonal transport, whereas MTs enriched with TyrTUB and/or βIIITUB are more dynamic and impede axonal transport. Although early alterations in MT structure and function have been reported in several models of DA neuron neurodegeneration [153], it is not known whether neurotoxic METH treatment alters MTs in the nigrostriatal DA pathway.

Epothilone D (EpoD) is a neuroprotective taxane-like compound that stabilizes MTs, promotes MT assembly, and ultimately enhances axonal transport in neurons [151]. Treatment with EpoD increases the number of stable MTs that are highly enriched with AcetTUB [187, 188]. Recently, it was shown that systemic injection of EpoD could attenuate 1-methyl-4-phenyl-1,2,3,6-tetrahydropyridine (MPTP)-induced loss of DAergic neurons in the nigrostriatal DA pathway of mice through stabilization of MTs and subsequent promotion of axonal transport [153]. It is currently unknown whether EpoD treatment can prevent METH-induced deficits in striatal DAergic markers.

The primary objective of this study was to investigate whether axonal transport plays a role in the development of deficits in DAergic markers in nigrostriatal axons in response to binge METH. We hypothesized that METH treatment would destabilize MTs in striatal DAergic axons, which would subsequently impair axonal transport from the substantia nigra pars compacta (SNpc) to the dorsal striatum. To investigate this hypothesis, we employed a moderately toxic METH regimen to avoid extensive damage to DAergic axons and examined striatal MTs at a time point when they are expected to be maximally destabilized [153]. To assess MT stability, we utilized antibodies against specific PTMs of α-tubulin and antibody against βIIITUB. Using immunofluorescent staining we identified a significant decrease in AcetTUB, a marker of stable MTs, in TH-positive striatal axons in rats treated with binge METH. Our second objective was to investigate the effects of the MT-stabilizing compound EpoD on the development of METH-induced DAergic deficits and MT dynamics within the striatum. We hypothesized that EpoD treatment would prevent the METH-induced loss of striatal DAergic markers.

To test this hypothesis, we administered two treatment regimens of EpoD alone or in combination with binge METH to adult Sprague-Dawley rats. Low doses of EpoD prevented decreases in the levels of DA, TH, and DAT and in the levels of AcetTUB in the striatum. High doses of EpoD potentiated METH-induced deficits in DA, DA metabolites and DAT and METH-induced acetylation of striatal MTs. In conclusion, our data suggest that binge METH has destabilizing effect on axonal transport in the nigrostriatal DA axons, which can be prevented by low doses of MT-stabilizing drug EpoD.

3.1.1 Materials and Methods

3.1.2 Subjects

A total of 71 adult male Sprague-Dawley rats (Harlan, Indianapolis, IN) weighing 350-400 g (on postnatal day 80) were used for experiments. All animal procedures were conducted in strict adherence to the Wayne State University Institutional Animal Care and Use Committee approved protocol # A-05-07-13.

3.1.3 Drug Treatments

D-Methamphetamine HCl (Sigma-Aldrich, St. Louis, MO, USA) was dissolved in sterile saline (0.9% NaCl) to a final concentration of 10 mg/mL. Binge METH treatment consisted of four successive intraperitoneal (i.p.) injections of METH (10 mg/kg METH-HCl, 8 mg/kg freebase METH) administered at 2-h intervals at ambient temperature of 21–22°C. In our hands, this METH regimen leads to moderate deficits in DA (20–25%) when measured at 7 days after the administration of the drug.

EpoD (Abcam, Cambridge, UK) was dissolved in dimethylsulfoxide (DMSO) to a final concentration of 0.5 mg/mL (working solution for low doses) and 5 mg/mL (working

solution for high doses). Rats in the EpoD groups were treated with either low doses of EpoD (EpoDL) or high doses of EpoD (EpoDH). Specifically, the EpoDL group received a single injection of 0.3 mg/kg EpoD 30 min prior to METH or saline, 0.1 mg/kg during METH or saline binge (1 h after the 3rd injection), and 0.1 mg/kg 24 h after the last injection of METH or saline. The EpoDH group received a single injection of 3 mg/kg EpoD prior to METH or saline, 1 mg/kg during METH or saline treatment, and 1 mg/kg after the last injection of METH or saline. All the rats received < 0.4 mL/kg DMSO. Exposure to DMSO was minimized to avoid the potentially confounding side effects of DMSO [171, 189-192]. Rectal temperatures were measured using a Thermotemp rectal probe (Physitemp, Clifton, NJ, USA). All the rats were killed via live decapitation 3 days after the last METH or saline injection. The details of the overall study design are summarized in Fig. 9. The 3rd-day time point was chosen for brain analysis because a previous study on axonal transport impairment showed that MPTP-induced changes to MTs occurred early (i.e., within 3 days) after the neurotoxic insult and prior to DAergic axon loss [153]. In rats, binge METH toxicity, manifested by deficits in DAergic markers, develops over approximately 3 days [40, 174, 193].

3.1.4 Tissue collection

All tissues were collected on ice, and the brains were rinsed with ice-cold phosphate-buffered saline. To measure total protein and neurotransmitter levels, both the striatum and SNpc were dissected from the right hemisphere using blunt dissection methods. The resulting tissue pieces were then immediately placed on dry ice and stored at −80°C until assayed. The left hemisphere was post-fixed in paraformaldehyde for 72 h at 4°C. The post-fixed brains were processed as previously described [96].

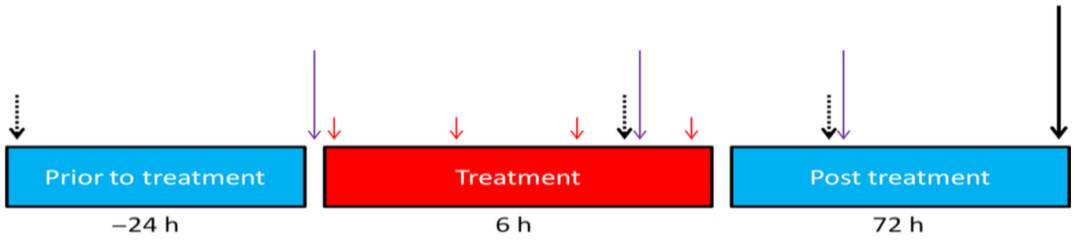

Figure 9. Study design to investigate methamphetamines effects on axonal transport. Study Design. Adult male Sprague–Dawley rats weighing 350–400 g were used for all experiments. Methamphetamine chloride (METH HCl) (4 × 10 mg/kg, i.p.) or saline (1 mL/kg) was administered to rats at 2-h intervals (solid red arrows). The animals were killed 3 days after the last METH or saline injection (solid black arrow) and assessed for the levels of tubulins and dopaminergic (DAergic) markers in the striatum and substantia nigra pars compacta (SNpc). A separate group of rats was treated with a microtubule-stabilizing drug epothilone D (EpoD) or vehicle 24 h before, during (after the 3rd injection) and 24 h after binge METH or saline treatment (purple arrows). Three 30-min open-field motor activity measurements were performed for both groups at times indicated by dotted black arrows. The second group of animals was also killed at 3 days after the last METH or saline injection and assessed for striatal tubulins and DAergic markers.

3.1.5 Western blot

Western blot analysis was conducted as previously described [96]. Polyvinylidene difluoride membranes were probed with one of the following primary antibodies: anti-DAT (1 : 500; Santa Cruz Biotechnology, Santa Cruz, CA, USA), anti-β-actin (1 : 5000; Cell

Signaling Technology, Danvers, MA, USA), anti-DetyTUB (1 : 1000; Millipore Corporation, Billerica, MA, USA), anti-TyrTUB (1 : 1000; Millipore), anti-AcetTUB (1 : 1000; Cell Signaling), anti-βIIITUB (1 : 1000; Abcam), anti-α-tubulin (1 : 1000; Santa Cruz Biotechnology), anti-dynein (1 : 1000; Santa Cruz Biotechnology), anti-kinesin heavy chain (1 : 1000; Santa Cruz, Biotechnology), anti-GFAP (1 : 1000; abcam), anti-caspase-3 (1 : 1000; Cell Signaling), or anti-4-hydroxynonenal (4-HNE (1 : 500, R&D Systems, Minneapolis, MN, USA) and appropriate secondary antibodies. The blots were developed using a LAS4000 Bioimager (GE Healthcare, Piscataway, NJ, USA). All the blots contained at least two samples representative of each experimental condition. Immunoreactivity was quantified using ImageJ software (National Institutes of Health, Bethesda, MD, USA).

3.1.6 Immunohistochemistry

Fixed brain tissues were processed as previously described [96]. Citrate buffer antigen retrieval (ThermoFisher, Waltham, MA, USA) was applied to all tissue sections. The sections were incubated overnight at 4°C with an anti-TH antibody and antibodies specific for one of the following: AcetTUB, TyrTUB, DetyTUB, βIIITUB, or α-tubulin – all of which were diluted 1 : 500 in the blocking buffer. The sections were then incubated for 2.5 h at 21°C with the blocking buffer containing diluted (1 : 400) Alexa Fluor® 488 goat anti-mouse (Invitrogen, Carlsbad, CA, USA) and Alexa Fluor 598 goat anti-rabbit (Invitrogen) antibody. DRAQ5 (Invitrogen) was used to stain nuclei. The sections were then mounted using Fluoromount mounting medium (Southern Biotech, Birmingham, AL, USA). The immunostaining was imaged using the Leica TCS SPE-II laser scanning

confocal microscope (Leica, Wetzlar, Germany). Non-compressed raw single z-plane images were exported from the Leica Image Analysis Suite (Leica). These images were then analyzed using Imaris co-localization analysis software (Bitplane South Windsor, CT, USA). For each, image automatic thresholding and masking functions were used to prevent interference from signal noise and variations in signal intensity. The resulting percent co-occurrence in the TH channel was normalized to that in the non-treated control for ease of graphical comparison. The final value represents the percentage of signal overlap within the TH signal.

3.1.7 High-performance liquid chromatography

The procedures were conducted as previously described [165]. All the procedures were conducted on ice or under refrigeration. Briefly, the tissues were sonicated in 0.5 mL of 0.3 N perchloric acid for 30 s, and the resulting homogenate was centrifuged for 30 min at 12 000 × g. The pellet was dissolved in 1 M NaOH overnight at 4°C, and protein concentrations were determined using the bicinchoninic acid protein assay (ThermoScientific). To measure DA content, 20 μL of the supernatant was injected into the mobile phase containing 90 mM sodium dihydrogen phosphate monohydrate, 50 mM citric acid, 1.7 mM 1-octane sulfonic acid, 50 μM EDTA, and 10% acetonitrile (ThermoScientific), at a flow rate of 0.5 mL/min. The samples were separated using a C-18 reverse-phase column (150 × 3.2, 3 μM particle size; ThermoScientific). DA and its metabolites were then detected electrochemically (electrode 1: −150 V, electrode 2: +220 V). The final values are reported as nanograms of analyte per microgram of protein.

3.1.8 Open-field motor activity

The gross motor activity of all the animals was assessed using the Opto-Varimex 4 Auto Track open-field Plexiglass chamber (Columbus Instruments, Columbus, OH, USA). At the beginning of each session, the animals were placed in the middle of the Plexiglass chamber, and their subsequent movement and position were recorded continuously. For each animal, gross motor activity was assessed for three 30-min sessions. The sessions were conducted the day before METH treatment, immediately after the third METH injection (before the 2nd EpoD dose), and 24 h after the last METH injection (before the 3rd EpoD dose). Locomotor activity was calculated automatically from the raw beam-break data by the Opto-Varimex software.

3.1.9 Functional observational battery

FOB assessments are useful to catalog neurotoxic effects when little is known about the potential neurotoxicity of a drug. Therefore, we conducted a shortened FOB based on[194] 24 h after binge METH. Briefly, technicians were blinded to all treatment conditions and only provided with animal identification numbers. Prior to the FOB, each technician was given instructions on how to document each of the scaled (1=least response, 5=most response) and quantal (i.e., was the clinical sign present or absent?) scores. Each animal was assessed by three different technicians. A specific measure was reported only if there was >90% interobserver agreement.

3.1.10 Statistical analysis

Datasets containing two experimental groups were analyzed using unpaired two-tailed Student's t-test with and without Bonferroni correction for multiple comparisons. To analyze datasets with three or more groups, one-way analysis of variance (anova) followed

by Tukey's post hoc test was performed. Two-way anova was performed on selected datasets to determine whether there was an interaction between METH and EpoD effects. Two-way repeated measures anova with Student–Newman–Keuls post hoc test was used to analyze the core body temperature data. Acclimation behavior was analyzed using simple linear regression analysis. All graphs were generated using GraphPad Prism 5 (GraphPad Software Inc., La Jolla, CA, USA), and all statistical operations were performed using SPSS (IBM). Statistical significance was set at $p < 0.05$.

3.2 Results

3.2.1 The effects of binge METH on DAergic markers in the striatum

Prior to the treatments, an average core body temperature of the animals was 36.6°C, which is the normal temperature for adult rats (Fig. 10a). Saline treatment did not significantly affect core body temperature at any time point. One hour after the first injection of METH, the rats had an average temperature of 38.9°C. Core body temperatures of the METH-treated animals significantly increased at 1, 3, 5, and 7 h after the first METH injection compared to saline controls. Core body temperatures were the highest at 5 and 7 h after the first METH injection, with mean values of 39.8°C and 40.5°C, respectively.

Compared to striatal whole-tissue lysates from saline-treated rats, there was a significant reduction in both DAT (−68%) and TH (−33%) immunoreactivity in striatal whole-tissue lysates from METH-treated animals at 3 days after the last injection of the drug (Fig. 10b and d). There was no significant difference in DAT or TH immunoreactivity between saline and METH rats in the SNpc tissue lysates (Fig. 10c). The loss of striatal DAT and TH was verified in fluorescently labeled brain slices, which showed a visible and

proportional reduction in DAT and TH signal within the striatum of the METH-treated rats compared with the striatum of the saline controls (Fig. 10e). High-contrast single-plane images of TH-labeled striatal axons in the striatum showed swollen axons and fragmented TH immunoreactivity 3 days after METH (Fig. 10f).

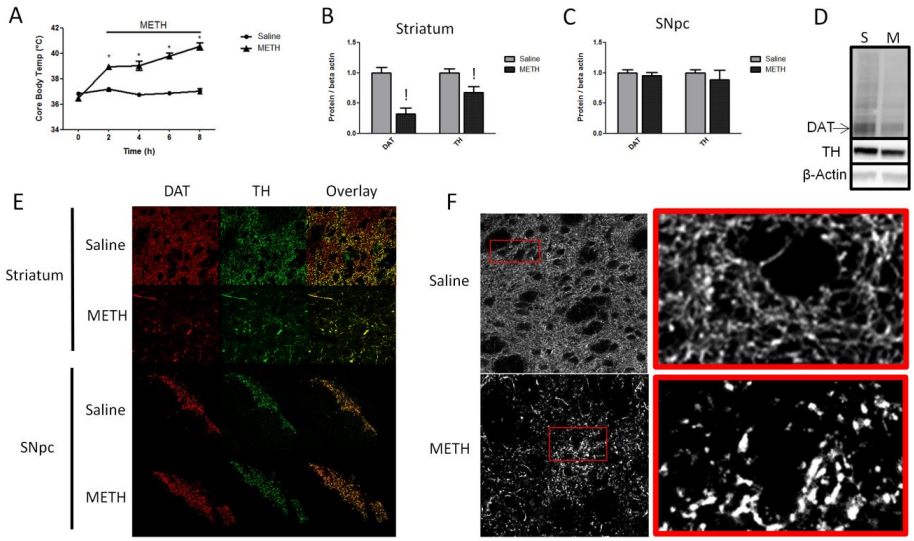

Figure 10. Levels of dopaminergic (DAergic) markers in the rat striatum and substantia nigra pars compacta (SNpc) 3 days after binge methamphetamine (METH). Rats were treated with four successive intraperitoneal (i.p.) injections of either saline (SAL) (1 mL/kg) or METH-HCl (10 mg/kg) at 2-h intervals. Three days later, the animals were killed and brain tissue was harvested. (A) Core body temperature of animals during binge METH or SAL treatment measured 1 h after each injection. METH induced significant hyperthermia over time ***$p < 0.001$ SAL vs. METH, two-way anova with repeated measures followed by Student–Newman–Keuls *post hoc* test, $n = 5$). (B and C) Quantified dopamine transporter (DAT) and tyrosine hydroxylase (TH) immunoreactivities in the striatum (B) and SNpc (C). METH significantly reduced DAT (−68%) and TH (−33%) immunoreactivity in the striatum (*$p < 0.025$, **$p < 0.01$, Student's two-tailed *t*-test with Bonferroni correction, $n = 5$) and not in the SNpc. (D) Representative western blot images of DAT (72 kDa), TH (64 kDa), and β-actin (45 kDa) from rats administered saline (S) or METH (M). β-Actin immunoreactivity was used as a loading control. All band density values were normalized to the saline controls. (E) Fluorescently labeled DAT (red) and TH (green) in brain tissue slices of the striatum and SNpc. The images depicting the striatum are magnified 40× to show individual axons; the SNpc images are magnified 4× to show

the total surface of this area. Channel overlay shows co-localization of green and red signal in yellow. (F) High-contrast images of TH immunoreactivity in striatal brain slices show the morphology of TH-labeled striatal axons. All data are expressed as mean ± SEM.

3.2.2 The effects of binge METH on microtubules in the nigrostriatal dopamine pathway

AcetTUB, DetyTUB, TyrTUB, and βIIITUB immunoreactivities were detectable in both the SNpc and the striatum (Fig. 11a). There were no detectable differences in the immunoreactivity of any of the tubulins in the SNpc tissue lysates between the saline- and METH-treated rats (Fig. 11b). The immunoreactivity of both βIIITUB and DetyTUB was significantly lower (−10% and −14%, respectively) in the striatal lysates of the METH-treated animals compared to the lysates of the saline-treated controls (Fig. 11c). AcetTUB and TyrTUB immunoreactivity in striatal lysates did not differ between saline- and METH-treated animals. The ratio of TyrTUB to DetyTUB was significantly higher (+26%) in striatal lysates of animals treated with METH than in saline controls (Fig. 11d).

Because MT PTMs that are assessed in total tissue lysates are not specific for DAergic axons, we probed striatal tissue sections with anti-TH antibody and antibodies against different tubulins to assess METH effect on MTs in DAergic axons. The results showed high basal levels of DetyTUB, AcetTUB, and βIIITUB in the striatum (Fig. 11f, g, and h). In agreement with previous reports, these MT populations were differentially expressed in axons and cell bodies; more specifically, DetyTUB and AcetTUB were more enriched in axons as opposed to the cell bodies. DetyTUB, AcetTUB, and βIIITUB were highly expressed in DAergic axons as well as in the surrounding TH-negative axons and cell bodies (Fig. 11f, g, and h). In the rats treated with METH, DAergic axons were

enriched with βIIITUB (Fig. 11h) and deficient in both AcetTUB (Fig. 11f) and DetyTUB (Fig. 11g). The immunofluorescence co-occurrence analysis revealed a significant loss of AcetTUB in the TH-positive axons (−52%) 3 days after binge METH as compared to saline controls (Fig. 11e). There was also a loss of DetyTUB (−33%) in these axons as well; however, it did not reach statistical significance. TyrTUB was not readily detectable in the TH-positive axons and, therefore, not quantified (data not shown).

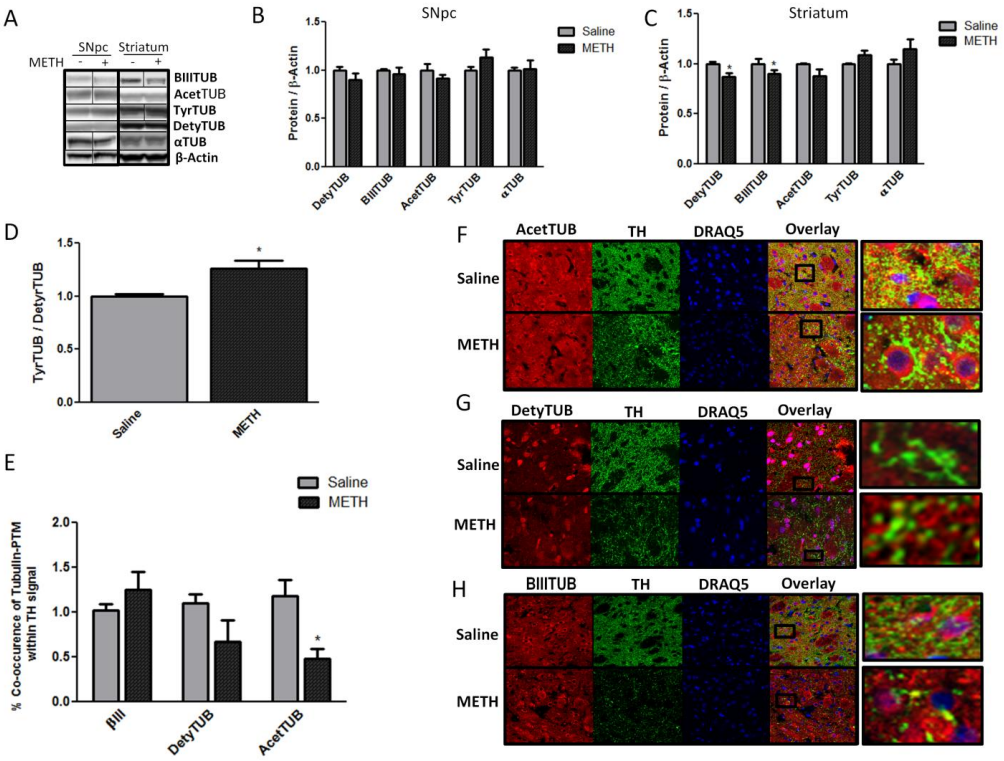

Figure 11. Tubulins in the striatum and substantia nigra pars compacta (SNpc) 3 days after methamphetamine (METH) treatment. Rats were treated with four successive intraperitoneal (i.p.) injections of either saline (SAL) (1 mL/kg) or METH-HCl (10 mg/kg) at 2-h intervals and killed 3 days later. (A–C) Western blot analysis of lysates from the striatum (B) and SNpc (C) labeled with antibodies specific for detyrosinated α-tubulin

(DetyTUB, 50 kDa), tyrosinated α-tubulin (TyrTUB, 50 kDa), βIII tubulin (βIIITUB, 52 kDa), acetylated α-tubulin (AcetTUB, 50 kDa), α-tubulin (αTUB, 50 kDa), and β-actin (45 kDa) (loading control). (A) Representative western blot images for (B) and (C). METH significantly decreased the immunoreactivity of DetyTUB (−14%) and βIIITUB (−10%) in striatal but not nigral tissue lysates (*$p < 0.05$ Student's two-tailed t-test without Bonferroni correction for multiple comparisons, $n = 5$). (D) Compared to saline, METH increased the ratio of TyrTUB to DetyTUB in striatal lysates (+26%, *$p < 0.05$ Student's two-tailed t-test, $n = 5$). (F–H) Images of fixed striatal brain slices fluorescently labeled for (F) AcetTUB, (G) DetyTUB, and (H) βIIITUB (all depicted in red) as well as for tyrosine hydroxylase (TH) (green) and nuclei (blue). (E) Quantification of co-occurrence of tubulins and TH in striatal tissue slices. Co-occurrence is defined as the percentage of TH signal that contains the tubulin signal above a threshold. METH significantly decreased the immunoreactivity of AcetTUB (−52%) and DetyTUB (−33%) in TH-positive striatal axons (*$p < 0.017$, Student's two-tailed t-test with Bonferroni correction $n = 5$). All band density values and co-occurrence values were normalized to the respective saline controls. The data are expressed as mean ± SEM.

3.2.3 The effects of EpoD on METH-induced alterations to microtubules in the striatum

Treatment with EpoDL slightly increased DetyTUB immunoreactivity in the striatum following saline (+36%) and markedly following METH (+78%) when compared with DMSO/saline treatment (Fig. 12a). When compared with EpoDL/saline treatment, DetyTUB increased in EpoDL/METH group by 31%. Treatment with EpoDH had little effect on the tubulins when administered alone, but when EpoDH was administered with METH, it resulted in a substantial loss of DetyTUB signal compared to DMSO/saline (−60%) and EpoDH/saline (−62%) group. All treatments minimally affected total striatal TyrTUB immunoreactivity. Compared to DMSO/saline controls, AcetTUB levels were reduced in the animals treated with both DMSO/METH and EpoDH/METH (−36% and −70%, respectively). Compared to EpoDH/saline, EpoDH/METH decreased AcetTUB levels by 67%. In contrast, the animals treated with EpoDL/METH had AcetTUB levels similar to those treated with DMSO/saline and those treated with EpoDL/saline. The

animals treated with DMSO/METH and EpoDH/METH had markedly lower levels of striatal βIIITUB compared with the DMSO/saline-treated animals (−46% and −55%, respectively) (Fig. 12b). α-Tubulin levels were similar across all the treatment groups. The animals treated with METH exhibited a small loss of the motor protein dynein (−28%) (Fig. 12c). In contrast, the animals treated with EpoDL and EpoDH together with METH did not show the loss of dynein in the striatum. Striatal kinesin signal was significantly greater in the striatal lysates of animals treated with EpoDH/METH (162%), but unchanged in all other treatment groups. EpoDL decreased the ratio of TyrTUB to DetyTUB in the striatum when administered with METH treatment (−70%) (Fig. 12d). The animals treated with EpoDH/METH showed a 2.8-fold increase in the ratio of TyTUB to DetyTUB compared to animals treated with DMSO/SAL.

The core body temperature profiles for the rats used in this experiment (Figs 12-14) are shown in Fig. 14a. The average core body temperature (36.8°C) remained unchanged at all time points after treatment with DMSO/saline, EpoDL/saline, or EpoDH/saline (Fig. 14a). The animals treated with METH displayed significant hyperthermia at 1, 3, 5, and 7 h after the first injection of METH as compared to saline controls. A maximum mean body temperature of 39.8°C was observed in the DMSO/METH and EpoDH/METH group at 3 h after the first METH injection. The EpoDL/METH group reached 40.0°C 7 h after METH. There were no significant differences in hyperthermia between DMSO/METH-, EpoDL/METH-, and EpoDH/METH-treated rats with the exception of EpoDL/METH versus EpoDH/METH group comparison at 7 h after the first METH injection. Even though the maximum core

body temperatures in DMSO/METH group were lower in the second than in the first experiment (39.8°C vs. 40.5° C), the deficits in DAT and TH between the experiments were not very different (−68% and −33% vs. −50% and −27%). The loss of AcetyTUB was higher, whereas the loss of DetyTUB was comparable in the second experiment (−36% vs. −12% and −16% vs. 14%, respectively), suggesting that the METH-induced changes in MT PMTs do not depend on temperature. In support, there was no correlation between AcetyTUB or DetyTUB immunoreactivity and METH-induced hyperthermia (not shown).

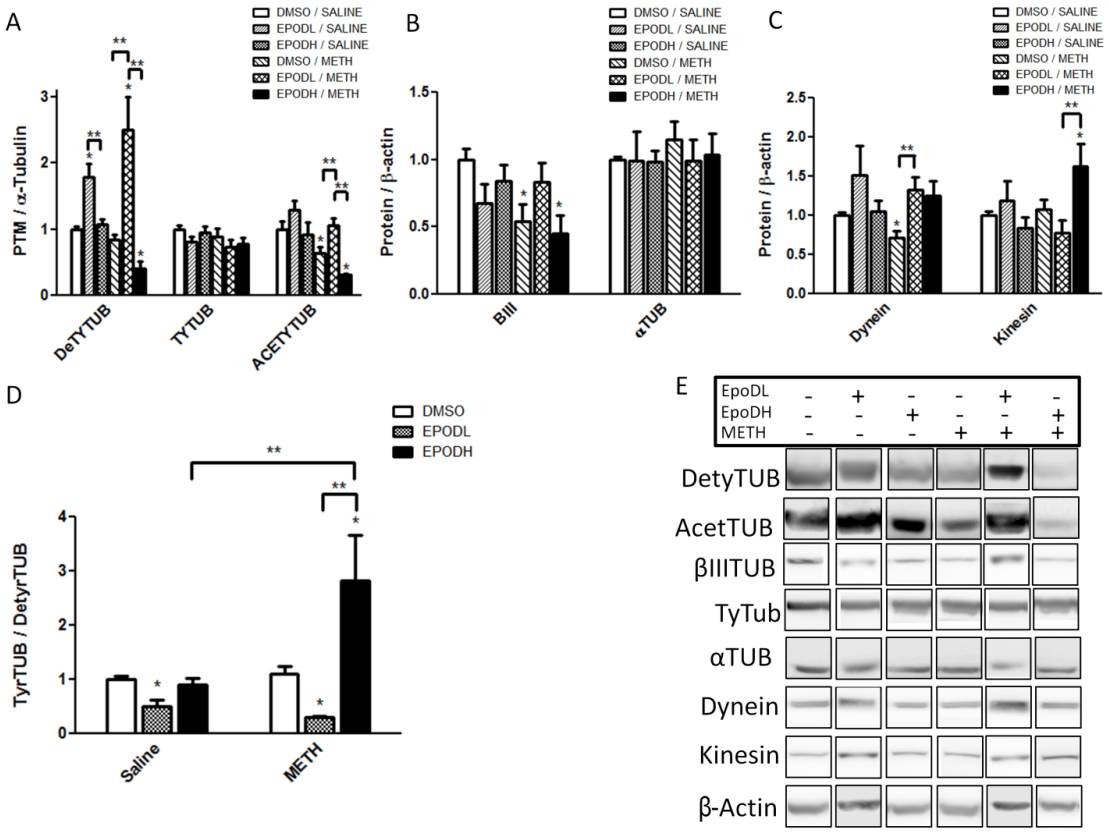

Figure 12. Striatal tubulins in rats treated with epothilone D (EpoD) and methamphetamine (METH). Rats was divided into six subgroups. Two subgroups were treated with four successive intraperitoneal (i.p.) injections of either saline (SAL) (1 mL/kg) or METH-HCl (10 mg/kg). The remaining subgroups were treated with SAL or METH and with a low dose of epothilone (EpoD) (EpoDL; 0.5 mg/kg), high dose of EpoD (EpoDH; 5 mg/kg) or dimethylsulfoxide (DMSO) administered in 3 i.p. injections before, during, and after binge METH or saline. All animals were killed 3 days later and the striatal lysates were analyzed for (A) post-translational modifications of α-tubulin (α-TUB): detyrosinated α-tubulin (DetyTUB, 50 kDa), tyrosinated α-tubulin (TyrTUB, 50 kDa), and acetylated α-tubulin (AcetTUB 50 kDa), (B) tubulin isoforms: α-TUB (50 kDa) and βIII tubulin (βIIITUB, 52 kDa), and (C) motor proteins: kinesin (heavy chain, 120 kDa) and dynein (95 kDa). α-TUB was used as a loading control for DetyTUB AcetTUB and TyrTUB while β-actin (45 kDa) was used as a loading control for other proteins. The immunoreactivities were normalized to saline/DMSO-treated controls. (A) Compared to METH alone, EpoDL/METH treatment increased, whereas EpoDH/METH treatment decreased the immunoreactivity of DetyTUB (+112% and −52%, respectively) and AcetyTUB (+66% and −52%, respectively). The DetyTUB and AcetyTUB in EpoDH/METH rats were also significantly decreased when compared with EpoDH/SAL controls (−62% and 67%, respectively). (B–D) In the EpoDH/METH-treated rats, βIIITUB immunoreactivity was decreased (−55% vs. DMSO/SAL) kinesin immunoreactivity was increased (+95% vs. EpoDH/SAL) and the ratio of TyrTUB to DetyTUB was increased (2.8-fold and 3.1-fold vs. DMSO/SAL and EpoDH/SAL, respectively). (E) Representative western blot images. All data are expressed as mean ± SEM. *$p < 0.05$, **$p < 0.01$ treatment vs. DMSO/SAL, #$p < 0.05$, ##$p < 0.01$, EpoD/SAL vs. EpoD/METH, ∏ (bracket) $p < 0.05$ differences within SAL and METH subgroups, one-way anova followed by Tukey's post hoc test, $n = 4–13$. Analysis of DetyTUB and AcetTUB data by two-way anova with Tukey post hoc test revealed co-treatment (DMSO, EpoD) x treatment (SAL, METH) interaction for DetyTUB and TyrTUB/DetyTUB ratio ($F(2.42) = 2.82$, $p < 0.05$ and $F(2,43) = 6.29$, $p < 0.01$, respectively).

3.2.4 The effects of EpoD on METH-induced decreases in the levels of DAergic markers in the striatum

Treatment with EpoDL alone increased striatal DA content by 40% without significantly affecting the levels of DA metabolites 3,4-dihydroxyphenylacetic acid (DOPAC) or homovanillic acid (HVA) (Fig. 13a–c). Conversely, the animals treated with EpoDH exhibited reduced striatal DA content (−50%) without significant reduction in striatal DOPAC or HVA content. The animals treated with METH alone had lower striatal

DA and DOPAC tissue concentrations (−63% and −48%, respectively) compared to the saline-treated animals. EpoDL reduced the METH-induced deficit in DA (to −43%) whereas EpoDH increased it (to −92%). Similar reductions in striatal DOPAC content were found in the EpoDL/METH-treated rats and in the rats treated with METH alone (−48%), while EpoDH/METH-treated rats showed 77% deficit in DOPAC. The ratio of the DOPAC to DA was similar in the animals treated with DMSO/saline, EpoDL/saline, and EpoDH/saline. Following METH, rats treated with DMSO or EpoDH showed a significant increase in the ratio of DOPAC to DA compared to the control rats (~ 2-fold and ~ 3.8-fold, respectively); EpoDL restored DOPAC/DA ratio to the control value, that is, the animals treated with EpoDL/METH had a similar ratio of DOPAC to DA as the DMSO/saline-treated controls (Fig. 13d).

Both EpoDL and EpoDH significantly increased DAT (2.3-fold and 1.6-fold, respectively) (Fig. 13e), but not TH (Fig. 13f), immunoreactivity in the striatal lysates. The animals treated with DMSO/METH had significant reductions in both DAT (−50%) and TH (−27%). Although there was a significant reduction in striatal DAT when comparing EpoDL/saline- to EpoDL/METH-treated rats (−57%), the EpoDL/METH-treated animals had DAT levels that were similar to those of the DMSO/saline-treated animals, indicating a ‘rescue’ of DAT levels by EpoDL. The animals treated with EpoDH/METH showed drastic reductions in striatal DAT immunoreactivity (> 80%). The loss of TH in the EpoDH/METH-treated animals was similar to that in the DMSO/METH-treated animals. Reductions in TH were not observed in the EpoDL/METH-treated animals compared to DMSO/saline controls. Compared to EpoDL/saline controls, EpoDL/METH treatment

decreased DA, DOPAC, DAT, and TH levels to similar extents as METH treatment compared to saline treatment (by 59%, 36%, 57%, and 18%, respectively). EpoDH/METH-induced decreases in relation to EpoDH/saline controls (−86%, −69%, −94%, −36%) where larger than those induced by DMSO/METH compared to DMSO/saline controls.

To assess inflammatory response in the experimental groups, GFAP immunoreactivity was measured in striatal lysates by western blotting analysis. Compared to DMSO/saline controls, GFAP immunoreactivity was significantly increased in the striatum 3 days after DMSO/METH (+57%) and EpoDH/METH (+69%) treatment (Fig. 13g). In contrast, GFAP expression was not significantly increased in the animals treated with EpoDL/METH. Although full-length pro-caspase-3 (~ 35 kDa) was detected in all the lysates, the activated cleaved caspase-3 (~ 15 kDa) was not detected in striatal lysates under any treatment condition. Striatal levels of 4-HNE were slightly increased (~ 10%) after binge METH alone (data not shown).

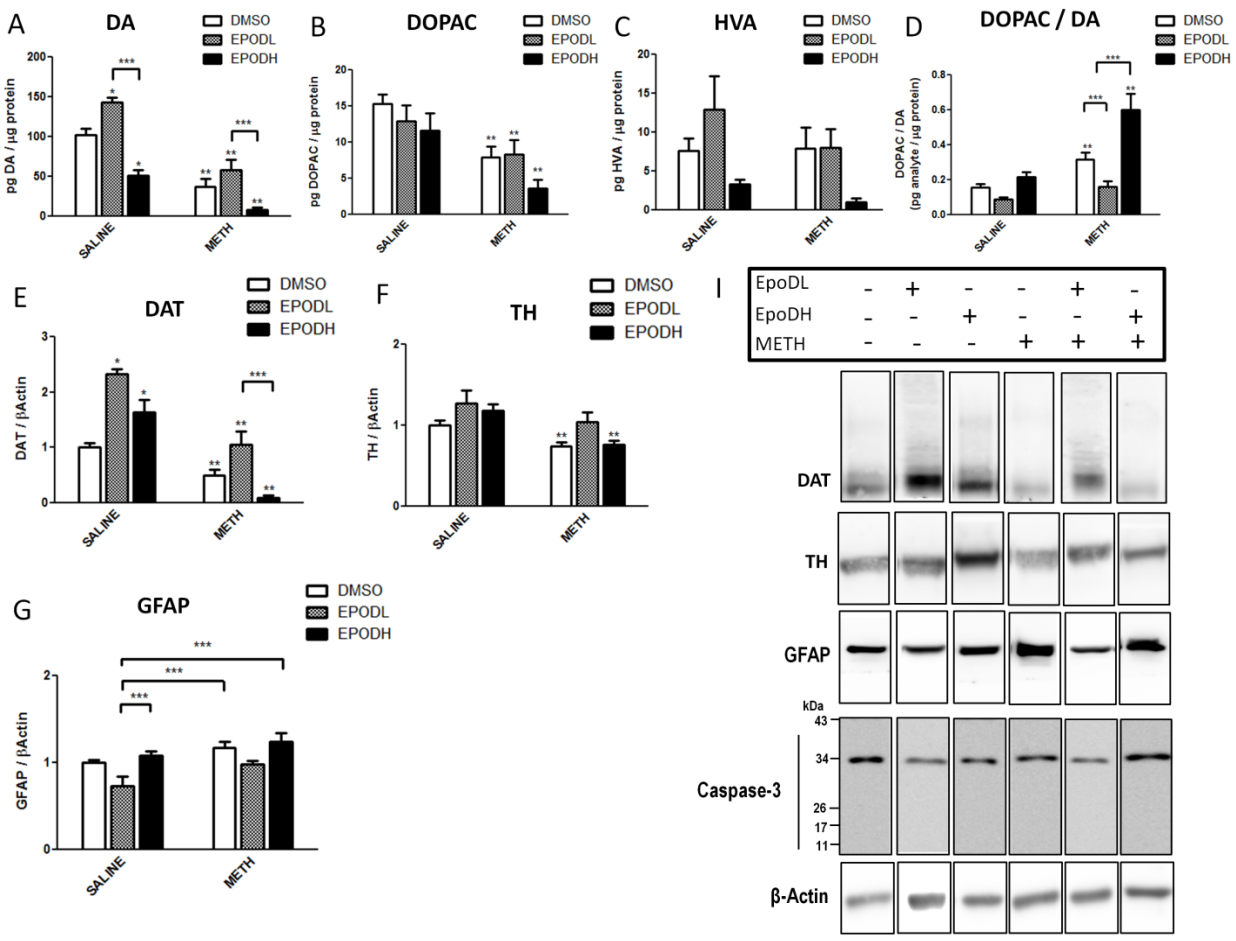

Figure 13. Striatal dopaminergic (DAergic) markers in rats treated with epothilone D (EpoD) and methamphetamine (METH). A group of rats was divided into six subgroups. Two subgroups were treated with four successive intraperitoneal (i.p.) injections of either saline (SAL) (1 mL/kg) or METH-HCl (10 mg/kg). The remaining subgroups were treated with SAL or METH and with a low dose of epothilone (EpoD) (EpoDL; 0.5 mg/kg), high dose of EpoD (EpoDH; 5 mg/kg) or dimethylsulfoxide (DMSO) administered in 3 i.p. injections before, during, and after binge METH or saline. All animals were killed 3 days later and the striatal lysates were analyzed for (A–F) DAergic markers, (G) glial fibrillary acidic protein (GFAP, 50 kDa), and (H) caspase-3 (35 and 17 kDa). β-Actin was used as a loading control. EpoDL and EpoDH alone both increased dopamine transporter (DAT) immunoreactivity (2.3-fold and 1.6-fold, respectively) while they have the opposite effects on DA (+40% and −50%, respectively). EpoD administration potentiated the METH-induced deficits in striatal (A) DA (−63% vs. 92%), (B) 3,4-dihydroxyphenylacetic acid (DOPAC) (−48% vs. −77%), and (F) dopamine transporter (DAT, 60–80 kDA) (−50% vs.

−90%) as well as in (D) the METH-induced increase in DOPAC/DA ratio (2-fold vs. 3.8-fold). Compared to DMSO/SAL group, DA and DAT content in EpoDL/METH group was decreased by 43% and 50%, respectively, while compared to EpoDL/SAL group these markers were decreased by 59% and 57%, respectively. (F) Tyrosine hydroxylase (TH, 60 kDa) content in EpoDH/METH group significantly decreased in relation to EpoDH/SAL group (−36%). (G) DMSO/METH and EpoDH/METH treatment increased GFAP immunoreactivity (+57% and +69%, respectively). (H) Neither treatment activated caspase-3. (H) Representative western blot images. Band density values were normalized to DMSO/SAL values. All data are expressed as mean ± SEM. *$p < 0.05$, **$p < 0.01$, ***$p < 0.001$, treatment vs. DMSO/SAL; #$p < 0.05$, ##$p < 0.01$, ###$p < 0.001$, EpoD/SAL vs. EpoD/METH; ∏ (bracket) $p < 0.05$ differences within SAL and METH subgroups; one-way anova followed by Tukey's post hoc test, n = 4–13. Analysis of DA, DAT, and DOPAC/DA data by two-way anova with Tukey post hoc test revealed co-treatment (DMSO, EpoD) × treatment (SAL, METH) interaction for DAT and DOPAC/DA ratio ($F(2.43) = 7.17$, $p < 0.01$ and $F(2,44) = 5.79$, $p < 0.01$, respectively).

3.2.5 Behavioral response of rats to EpoD and METH

Figure 14b–d depicts the analysis of motor activity counts 24 h before, during (after the 3rd METH injection), and 24 h after binge METH. Prior to METH administrations, the animals in all treatment groups displayed similar locomotor activity profiles (Fig. 14b). A similar pattern of locomotor activity was maintained across all the sessions by the animals treated with DMSO/saline and EpoDH/saline. The animals treated with EpoDL/saline or EpoDL/METH displayed increased stereotypy (seen as dense green nodules) during the treatment phase. The animals treated with DMSO/METH also displayed more stereotypy than DMSO/saline controls, but less than EpoDL/METH-treated rats (Fig. 14c). The animals treated with EpoDH/METH displayed less stereotypy than the other two METH groups; instead, they maintained hyperlocomotion during METH administration (Fig. 14b). The treatment with EpoDL/METH produced the highest levels of stereotypy and the greatest suppression of distance traveled. During the post-treatment phase (24 h post-

METH), the animals treated with METH showed significant reduction in the overall motor activity when compared with saline controls regardless of EpoD dose.

During the pre-treatment session, the animals from all groups displayed normal acclimation behavior that was characterized by a marked negative correlation between the distance travelled and the duration of the session (Fig. 14d). The animals treated with either DMSO/saline, EpoDL/saline, or EpoDH/saline exhibited similar acclimation behavior throughout all behavioral sessions. In the animals treated with DMSO/METH, EpoDL/METH, or EpoDH/METH, the slope between the distance traveled and time was lost during the treatment session because of emergence of stereotypy, with animals from the EpoDH group simultaneously maintained locomotor activity and stereotypy. During the post-treatment session, the slope for DMSO/METH and EpoDL/METH groups recovered slightly (to 23% and 10%, respectively, of their pre-treatment values) (Fig. 14d).

Table 2 shows the results of the FOB conducted 24 h after the final dose of METH. Animals treated with DMSO/saline and EpoD/saline had similar FOB scores and a 0% mortality rate. Although DMSO/METH-treated animals showed slightly less arousal than DMSO/saline-treated controls, and the mortality rate was much higher (42%). EpoD/METH was associated with an even higher mortality rate (50%). Nearly 70% of the animals in the EpoD/METH group displayed overt clinical abnormalities associated with

gross toxicity, whereas only 16% of the DMSO/METH group displayed overt clinical abnormalities.

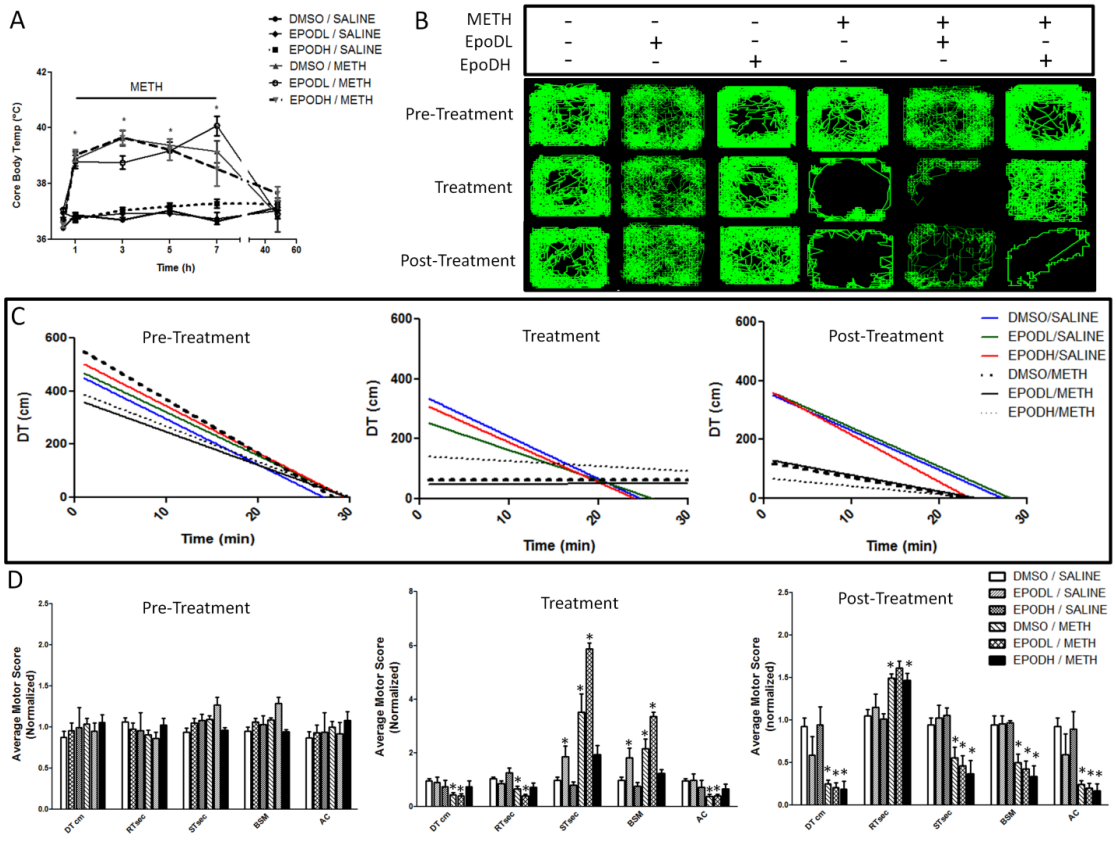

Figure 14. Locomotor activity of rats treated with epothilone D (EpoD) and methamphetamine (METH). Rats was divided into six subgroups. Two subgroups were treated with four successive intraperitoneal (i.p.) injections of either saline (SAL) (1 mL/kg) or METH-HCl (10 mg/kg). The remaining subgroups were treated with SAL or METH and with a low dose of epothilone (EpoD) (EpoDL; 0.5 mg/kg), high dose of EpoD (EpoDH; 5 mg/kg) or dimethylsulfoxide (DMSO) administered in 3 i.p. injections before, during, and after binge METH or saline. (A) Core body temperatures were recorded before METH (0.5 h) and 1 h after each METH or SAL injection. METH induced significant hyperthermia over time (***$p < 0.001$ SAL vs. METH, two-way anova with repeated measures followed by Student–Newman–Keuls post hoc test, n = 3–11). (B) Representative activity maps. Continuous green line traces animal's movement during each

30-min session. The animals treated with EpoDH/METH displayed less stereotypy (seen as dense green nodules) than other METH groups; instead, they maintained hyperlocomotion during METH administration. (C) Quantification of total motor activity counts during the 30-min open-field tests performed 24 h before METH (pre-treatment), after the third METH injection (treatment), and 24 h after the last METH injection (post-treatment). The rats treated with EpoDL/SAL or EpoDL/METH displayed increased stereotypy during the treatment phase. The animals treated with DMSO/METH also displayed more stereotypy than DMSO/saline controls but less than EpoDL/METH-treated rats. (D) Acclimation behavior during each of the 30-min locomotor activity sessions. Linear regression analysis was performed between the distance traveled and time. All data are expressed as mean ± SEM. *$p < 0.05$, treatment vs. DMSO/SAL; #$p < 0.05$, EpoD/SAL vs. EpoD/METH; ∏ (bracket) $p < 0.05$, differences within SAL and METH subgroups; one-way anova followed by Tukey's post hoc test, n = 4–13. Analysis of stereotypy data by two-way anova with Tukey post hoc test revealed a trend for co-treatment (DMSO, EpoD) × treatment (SAL, METH) interaction for total time spent in stereotypy (ST) ($F(2,36) = 7.17$, $p = 0.073$). Abbreviations: DT, total distance traveled; RT, total time at rest; ST, total time spent in stereotypy; AT, total ambulatory time; BSM, bursts of stereotypy; HC, horizontal counts; AC, ambulatory counts; EpoDL, low-dose EpoD; EpoDH, high-dose EpoD.

Table 2. Functional Observation Battery

Parameter	DMSO/Saline [C] (n=3)	EpoDH/Saline[C] (n=3)	DMSO/METH[C] (n=6)	EPODH/METH[C] (n=7)
Click Response[A]	5.4 ± 0.29	4.4 ± 0.96	3.2 ± 0.83	2.7 ± 0.92
Arousal[A]	6.4 ± 0.29	5.7 ± 1.06	4.3 ± 0.98	3.5 ± 0.65
Home Cage Posture[B]	0/3	1/3	1/6	5/7
Porforin[B]	0/3	0/3	1/6	5/7
Piloerection[B]	0/3	0/3	1/6	4/7
Mortality Rate	0/9 (0%)	0/9 (0%)	6/14 (42%)	7/14 (50%)

3.3 Discussion

Our first important finding was the loss of stable MTs in striatal DAerigic axons following binge METH. Although we report the loss of a few tubulins in the striatum, only the loss of AcetTUB appeared to be specific for striatal DAergic axons. Our second significant finding was that the treatment with the MT-stabilizing drug EpoD could prevent the METH-mediated loss of AcetTUB and the loss of striatal DAergic markers when administered at a low dose while potentiating METH-mediated losses of DAergic markers and markers of stable MTs when administered at a high dose. Finally, we demonstrated that EpoD treatment produced acute effects on METH-induced hyperlocomotion and stereotypy, raising the possibility that MT stabilization has an effect on DA signaling.

Binge METH administration results in both reversible and irreversible loss of striatal DAergic markers with the latter being considered a manifestation of 'classic' METH neurotoxicity. These 'classic' neurotoxic effects of METH are mediated, in part, by oxidative stress [195] and can induce reactive gliosis and pro-apoptotic caspase-3 cleavage throughout the striatum [40, 196, 197]. We observed only a mild increase in the immunoreactivity of the reactive gliosis marker GFAP and no signal for cleaved caspase-3 in the striatum of METH-treated animals (Fig. 13i). Striatal levels of 4-hydroxynonenal were also only slightly increased (~ 10%) after binge METH (data not shown). These results suggest that the METH-induced oxidative stress and loss of DAergic terminals was modest and that the marked deficits in DA, DAT and DOPAC were, in most part, reversible and caused by other than neurodegeneration mechanisms. Consequently, the MT alterations we are describing predominantly reflect combination of transient METH effects

on MTs and neuroadaptive responses in DAergic neurons, and not ‘classic’ neurotoxicity per se (i.e., a physical loss of DAergic axons). This interpretation is further supported by a relatively modest reduction in striatal DA content (~ 22%) observed 7 days following the same regimen of binge METH (data not shown). DA deficits are normally much greater (> 60%) in ‘classic’ METH neurotoxicity models at this time point [40, 198]. We did observe swollen axons with discontinuous TH signal in the striatum following METH; these axons were similar to the ‘empty’ axons lacking vesicles, mitochondria, and other components detected in the nigrostriatal DA pathway in 1-methyl-4-phenylpyridinium (MPTP)-treated mice [153]. Some of these TH-positive axons are likely irreversibly damaged [55], but the GFAP and TH data suggest that most axons are not. The lack of gross neurotoxicity is likely explained by the lack of severe hyperthermia (≥ 41°C), which is a crucial determinant of METH-induced neurotoxicity [40, 193]. In our hands, the METH-treated animals displayed acute hyperthermia; however, the effect was modest (average core body temperature of approximately 40°C). Some of the effects of METH on DAergic markers at regimens that do not increase core body temperatures above 40.5°C are short-lasting [52, 173, 174, 193], a finding that agrees with higher DA loss at 3 days than at 7 days after METH in our drug regimen. Although small, the increase in GFAP immunoreactivity was present in DMSO/METH and EpoDH/METH groups, but not in EpoDL/METH group, suggesting that administration of EpoDL with METH prevented METH-triggered reactive gliosis. Lack of caspase-3 activation in the striatum indicates that EpoDH did not augment METH-mediated toxic events such as mitochondrial dysfunction or oxidative stress in striatal neuronal cell bodies [199].

The heterogeneity of α-tubulin PTMs in polymerized MTs is thought to impart their different functions [200-202]. MTs that are enriched in AcetTUB and DetyTUB preferentially recruit the anterograde motor protein kinesin and promote axonal transport [180, 203], whereas TyrTUB is highly enriched in newly formed and dynamic MTs [186]. In agreement with recent findings in endothelial cells [150], we found that METH exposure led to the loss of AcetTUB, which is highly enriched in stable MTs. The loss of AcetTUB was more pronounced in TH-positive striatal axons than in striatal tissue lysates (Fig. 11), suggesting some level of specificity of this effect for striatal DAergic axons. METH also resulted in a significant increase in the ratio of TyrTUB to DetyTUB, further suggesting the loss of stable MTs within the striatum. The increased ratio of TyrTUB to DetyTUB may also be indicative of the increased recruitment of CAP-glycine proteins [204, 205], which are required for initiation of dynein-mediated retrograde axonal transport [206], possibly to remove cellular components oxidatively damaged by METH [207, 208].

The βIIITUB deficit observed in METH-treated rats could reflect decreased levels of MTs in DAergic axon [209]. This scenario is unlikely because the co-occurrence of βIIITUB with TH immunostaining was not decreased. Alternatively, given the known MT-destabilizing effects of βIIITUB over-expression [184], the loss of striatal βIIITUB might reflect increased MT stability in non-DAergic striatal components, such as neurons, in response to METH. βIIITUB has numerous functions, including a role in mitochondrial respiration, neurogenesis, axonal guidance and intracellular trafficking as well as axonal maintenance, including association of MTs with kinesin [182, 210-212]. METH-mediated alterations in any of these functions or adaptive responses to METH effects could be

reflected in the βIIITUB deficit [199, 213, 214]. In summary, our results suggest that METH exposure resulted in the loss of stable MTs in striatal DAergic axons, an effect that would impede axonal transport and could account for the transient (i.e., reversible) loss of striatal DA, DOPAC, DAT, and TH observed 3 days after METH.

The loss of AcetTUB can impair axonal transport [215]. Since EpoD increases AcetTUB levels [153, 188], we hypothesized that EpoD would attenuate the METH-induced deficits in AcetTUB and, ultimately, the loss of striatal DAergic markers. Only the low dose of EpoD (EpoDL) produced the desired effects. EpoDL prevented the METH-mediated loss of AcetTUB (Fig. 4), DA, DAT, and TH (Fig. 13). As the deficits in striatal DAergic markers were similar in DMSO/METH and EpoDL/METH rats when compared to their respective controls, the EpoDL protection likely involved keeping DAergic markers at the physiological levels via axonal transport and not via attenuation of neurodegeneration. In agreement, EpoDL increased striatal DetyTUB levels and, consequently, the ratio of DetyTUB to TyrTUB while administered alone and in combination with METH, supporting also the data on a robust effect of epothilones on MT stability [216-218]. In contrast, co-administration of EpoDH with METH resulted in a potentiation of the METH-induced loss of AcetyTUB and in a drastic loss of DetyTUB and DAergic markers. Lack of an effect of EpoD and METH, alone or in combination, on TyrTUB levels suggests the lack of their effect on the formation of new MTs [217]. Collectively, our data indicate that the low-dose EpoD stabilized MTs and restored the levels several striatal DAergic markers decreased by METH, whereas high-dose EpoD impaired MT function and potentiated the depletion of striatal DA and DAT induced by

METH. It was not surprising given the known neurotoxic potential of taxols [219]. Consequently, treatments with EpoD at doses outside the 'therapeutic window' may produce unintended neuropathy in humans, particularly those with already compromised CNS such as METH users. Neuroprotective EpoD doses are likely different for different species. The high dose of EpoD was chosen based on the results from a previous study in which this dose was found to be neuroprotective against MPTP in mice [153]. Mice differ from rats and humans in responses to DAergic toxins. In humans, recent phase 1 clinical trials testing EpoD effects against Alzheimer disease employed much smaller dose of EpoD than the dose in the investigation of Cartelli and colleagues.

The animals treated with EpoDH/METH exhibited a drastic increase in kinesin levels. Motor protein kinesin is guided from the cell body to the axon by tyrosination of α-tubulin [181]. Therefore, the METH-induced increases in kinesin might reflect an adaptational response in moderately destabilized striatal MTs in the axons or cell bodies surrounding the striatal DAergic axons. Previous findings have suggested a role of kinesin in the initial neural plasticity and development of drug addiction [220, 221]. METH exposure induces dendritic spines plasticity in the dorsal striatum [222]. Therefore, the increase in kinesin observed in the EpoDH/METH group could be explained by an increase in dendritic plasticity in this brain area. Future studies are needed to determine the specificity and function of METH-induced kinesin up-regulation.

In the striatum, DAergic innervation constitutes a few % of total pool of striatal components. EpoD- and METH-induced alterations in tubulin PTMs and in MT-associated proteins observed in the striatal whole-tissue lysates were 10% or greater; therefore, it is

likely that the METH-induced alterations of MTs are not exclusive to DAergic axons. Nevertheless, the METH-induced changes in particular MT PMTs within DAergic axons might be different from the changes induced by the drug within other striatal components.

EpoDL alone increased striatal DA, suggesting that EpoD increased the DA vesicle pool, possibly by promoting anterograde axonal transport of DA-containing vesicles [223, 224]. EpoDH had the opposite effect on the striatal DA content, causing a marked reduction in the neurotransmitter. It remains unclear why the two EpoD doses produced the opposite responses. Administration of high EpoD doses can result in overstabilization of MTs [225], with a consequent impairment of axonal transport [226]. We did not observe an increase in AcetyTUB after EpoDH alone in the striatal lysates; however, such increase might have occurred in DAergic axons. Alternatively, EpoD may have had an effect on DA synthesis and/or metabolism [227, 228]. As expected [229], METH treatment increased the ratio of DOPAC to DA. EpoDH treatment exacerbated the METH-induced increase in the ratio of DOPAC to DA, whereas EpoDL produced the opposite result than EpoDH, seemingly suppressing METH-induced increase in the DOPAC/DA ratio. EpoDL treatment alone had similar effect on the DAT as it had on DA levels, whereas striatal TH levels remained relatively unchanged (Fig. 13), suggesting that EpoDL treatment preferentially enhances anterograde transport of the DAT and DA storage vesicles in relation to TH. This differential effect may be explained by differences in cargo transport rates. In general, membrane proteins are transported by fast axonal transport, whereas cytosolic proteins primarily by slow axonal transport [230]. Consequently, the DAT could have been transported at a higher rate than TH, causing EpoD enhancement of axonal transport at the

3rd-day time point more obvious for the DAT than for TH. On the other hand, TH, DA, and DAT all can be transported by fast axonal transport [135, 231] and, therefore, the observed differences might not be simply because of different axonal transport velocities. EpoD may have differentially affected retrograde axonal transport or terminal turnover (degradation) of these DAergic markers (they are degraded by different cellular processes: the proteasome, enzymatic metabolism, and lysosome, respectively). In the absence of METH, EpoDL and EpoDH both increased the levels of striatal DAT but had different effects on MT stability. Literature data indicate that both stabilization and destabilization of MTs can induce increased trafficking of the DAT to the plasma membrane [232, 233], thus indicating the importance of proper balance in MT dynamics. In the presence of METH, EpoDH decreased the immunoreactivity of DAT. This could have resulted from METH-mediated inhibition of DAT axonal transport overcoming the effect of EpoDH.

It can be speculated that enhancing anterograde transport of DA storage vesicles and DAT would increase cytosolic DA levels within DA terminals and would exacerbate METH neurotoxicity [199]. In our study, EpoDL increased striatal DAT and DA levels and decreased the METH-induced loss of DAergic markers. The increase in DAT was higher than the increase in DA; this might have resulted in increased release of DA via the DAT and, consequently, prevented DA-mediated oxidative stress. Our behavioral data (Fig. 14) support this scenario. EpoDH alone also increased the striatal DAT levels, but resulted in drastic depletions of DAT and DA contents following METH. The additive DA and DAT depleting effects of EpoDH and METH was likely a consequence of destabilization of MTs by both drugs via their depolarization [218, 234] and/or changes to DAergic markers

metabolism or turnover. Finally, since binge METH impairs mitochondrial function and decreases ATP [199], a deficit in ATP may have contributed to decreased transport of DAergic markers, and mitochondria, to the terminals.

METH-induced DA release induces locomotor activation and binge METH can result in long-lasting alterations in locomotor behavior [45, 235]. As expected, METH alone increased stereotypy during its administration as well as disrupted normal acclimation behavior and suppressed locomotor activity 24 h after METH exposure (Fig. 6). EpoDL alone increased stereotypy during the treatment session, but had little effect on locomotor activity 24 h following treatments. This suggests there may be some acute effects of EpoD on signaling in the nigrostriatal DA pathway. The influence of MT stability on DA signaling and local DA synthesis may account for this effect [227, 228]. These studies showed decreased DAergic neurotransmission in mice with decreased MT stability, manifested by decreased levels of DA and its metabolites, decreased DA synthesis and release, decreased levels of DA D2 receptor, and decreased locomotor activity during the day. The EpoDL-induced increase in MT stabilization evoked opposite effects with up-regulation of DAT levels possibly reflecting an adaptive response to the increase in DA release. Administration of EpoDL with METH appeared to exacerbate the METH-induced effects on stereotypy, likely because of combined effect on DA release. Animals in the EpoDL/METH group displayed a nearly 2-fold increase in this measure compared to DMSO/METH-treated animals, whereas EpoDH suppressed METH-induced stereotypy. The dose-dependent biphasic effect of EpoD on METH-induced stereotypy during the treatment paralleled EpoDL effects on DAergic markers observed on the 3rd day. METH-

induced stereotypy is mediated mainly by post-synaptic D1 receptors in the striatum [236]. Hence, the data suggest that the EpoDL-mediated changes in MTs and DAergic markers occurred during METH administration and increased DA efflux. It is plausible that the 'protective' effect of EpoDL involved decreasing the levels of free intracellular DA and, consequently, preventing DA-mediated oxidative stress, a notion supported by lack of increased GFAP expression. The EpoDL protection could have also involved keeping up proper axonal transport not only of DAergic markers but also of mitochondria and removal of damaged components from DAergic terminals [237]. In contrast, the EpoDH-induced potentiation of METH-induced losses in DAergic markers could have been mediated by impaired anterograde transport of these markers and mitochondria, as well as by impaired removal of damaged neuronal components because of inhibition of their retrograde transport or autophagy [238-240]. The emergence of hyperlocomotion instead of stereotypy in EpoDH/METH rats suggests a decrease in DAergic neurotransmission and supports the notion of an impaired transport of DA-containing vesicles. An alternative explanation for the decreased DAergic neurotransmission in these rats is EpoDH-mediated suppression of DAT activity with a resultant decrease in the reverse transport of DA and an increase in free cytosolic DA and its metabolism. This is supported by the increased DOPAC/DA ratio in EpoDH/METH rats. An increase in free DA accompanied by a deficit in ATP (because of an impaired transport of mitochondria) could have increased an oxidative stress within DAergic terminals. All the animals displayed a significant suppression of behavior following METH regardless of EpoD dose, suggesting the changes in DAergic markers persisting at 3 days post-METH did not affect motor activities.

Together, the locomotor activity data support the hypothesis that EpoD may have acute effects on striatal DAergic signaling. Future studies should focus on measuring DA release in the striatum following EpoD treatment to clarify molecular mechanisms underlying these findings.

The FOB performed 24 h after binge METH revealed that animals treated with EpoD/METH exhibited significantly less activity and alertness than METH-treated animals. The observed abnormal gait, posture, and responsiveness were parkinson-like and are consistent with striatal DA depletion greater than 80%. Indeed, animals in the EpoD/METH group had, on average, 85% reduction in striatal DA 72 h after METH. Therefore, the combination of EpoD and METH seemed to produce a parkinson-like motor deficit. FOB results suggested that EpoD increases the likelihood of poor clinical outcome after METH. Overall, the data support the idea that MT stability has a significant influence on DAergic nerve terminal function and that MT stabilization can have toxic consequences in DAergic neurons in METH-exposed animals.

In summary, we found a deficit in stable MTs, accompanying deficits in DAergic markers, within striatal DAergic axons 3 days following binge METH exposure. Furthermore, treatment with a low dose of MT-stabilizing drug EpoD prevented the METH-mediated loss of stable MTs and loss of striatal DAergic markers. The deficits in MT stability have been implicated in DA signaling-related disorders including schizophrenia, depression, and Parkinson's disease [146, 227, 228, 241, 242]. EpoD has been tested, with some success, to treat these disorders [146, 242, 243]. Our data suggest that EpoD may be effective in restoring striatal axonal transport and DAergic function in

animal models of METH abuse [244-246]and also in human users of the drug, potentially attenuating the risk for development of Parkinson's disease [176]. Further studies are needed to determine the 'therapeutic window' for the treatment of METH neurotoxicity.

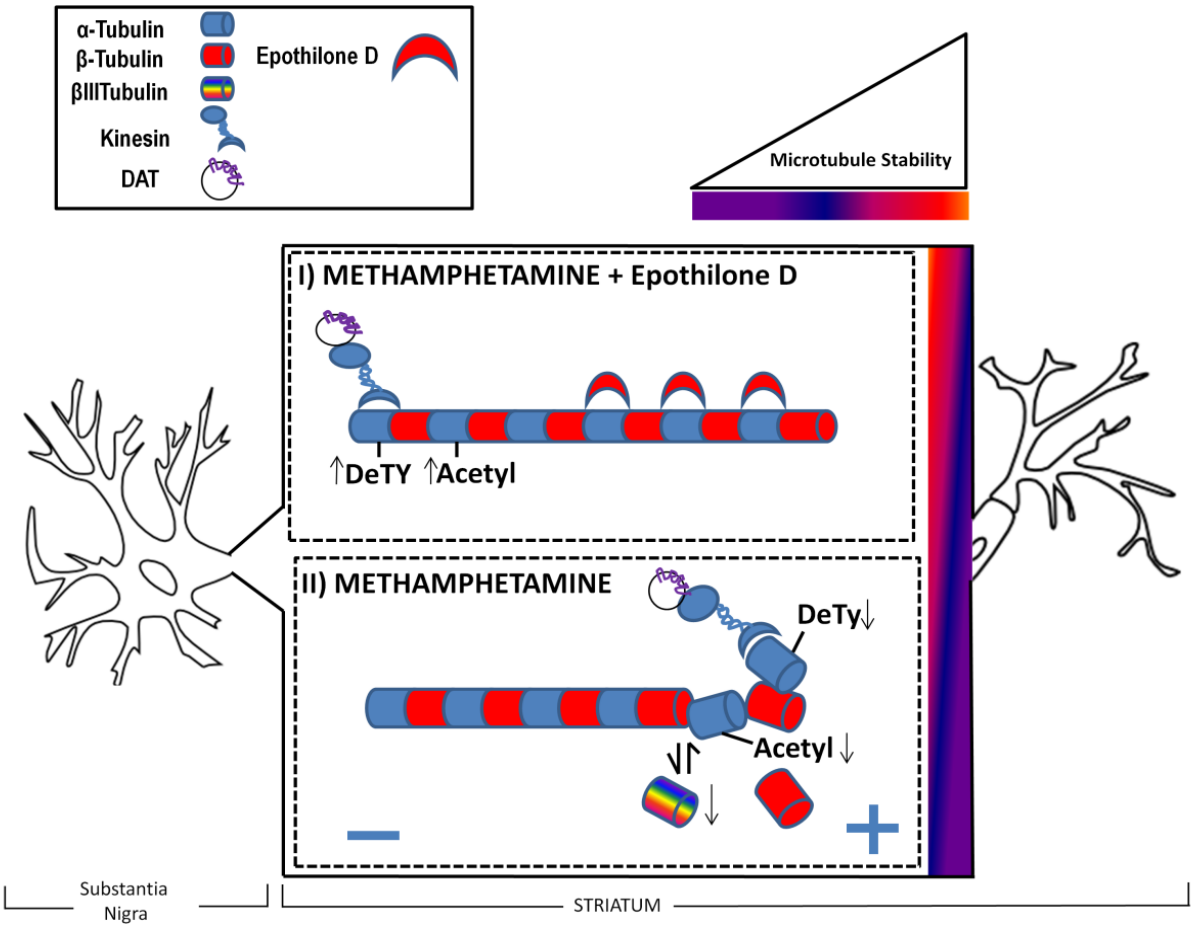

Figure 15. Summary of findings for axonal transport studies. Dopaminergic cell bodys (Left) in the substantia nigra projects to the axon nerve teminals in the striatum (right). Between the cell body and the axon terminals, the process of axonal transport takes place in the axon. Axonal transport is required for the health and maintenance of striatal dopaminergic nerve terminals. Axonal transport requires stable long lived microtubles that are rich in acetylated and detyrosinated α-tubulin. We assessed post-translational modifications of microtubles within the dopaminergic axons. We found a reduction in deytrosinated and acetylated α-tubulin in the striatal axons following binge methamphetamine. We also found a reduction in neuron specific tubulin, β-III tubulin.

Treatment with a microtuble stabilizing drug, epothilone D, was able to inhibit the reduction of these microtubles following methamphetamine. Together, our data here suggests that methamphetamine can impair axonal transport in nigral striatal dopamine neurons. Furthermore, microtuble stabilizing drugs can be used to reverse/prevent this effect of methamphetamine.

CHAPTER 4 PARKIN'S ROLE IN METHAMPHETAMINE NEUROTOXICITY

4 Background

Parkinson's disease (PD) is a progressive neurodegenerative disease affecting dopamine (DA) neurons of the nigrostriatal motor pathway [247, 248]. PD patients develop motor symptoms including rigidity, impaired posture, and abnormal gait.[249] Loss-of-function mutations of PARK2, which encodes the E3 ubiquitin ligase PARKIN, are found in patients with familial PD. [250] Several Park2-/- rodent models (PKO) have been generated but they lack the phenotype or pathology consistent with a PD.[24, 97, 248, 251] It remains unclear why PKO animals lack a robust phenotype considering the proposed vitale role of parkin for DA neuron health and function.

Methamphetamine (METH) exposure may increase the risk of developing PD.[24] METH is a neurotoxic psychostimulant that increases oxidative stress, inactivates parkin, and results in the gross axotomy of striatal DA axons.[25, 27, 55, 252] Following high-dose METH exposure rats display lasting PD-like behaviors [45]. Recently, we determined that METH may impair microtubule stability within DAergic axons of the striatum contribute to its neurontoxicity. Parkin has been shown to be a possible MT stabilizing factor. The neurotoxic effects of METH in PKO rats are unknown.

PKO rodents have abnormal DA signaling and metabolism. PKO mice are insensitive to evoked synaptic potentials [34] and evoked DA release in the striatum.[106, 253, 254] METH potently evokes DA release in the striatum. When challenged with low doses of METH and d-amphetamine PKO rodents display blunted DA release.

Here, we investigated the hypothesis that PKO rats would be hypersensitive to the neurotoxic effects of METH.

4.1 Materials and methods

4.1.1 Parkin knockout animals

Thirty-two age matched (PND 65-75) wildtype (Harlan, Indianapolis, IN) and PARK2 -/- (PKO, SageLabs, St. Louis, MO) male Long-Evans rats were used for all studies. Rats were allowed unrestricted access to food and water. Animals were group housed (four rats per cage) until 24 h prior to testing, when they were separated and singly housed until the end of the study. All procedures were conducted in adherence with the Wayne State University institutional animal care and use committee-approved protocol no. A3310-01.

4.1.2 Drug treatments

Methamphetamine (METH) HCl (Sigma-Aldrich, St. Louis, MO) was diluted in saline (0.9% NaCl) to a final concentration of 6 mg METH / mL. Daily bodyweights were recorded and used to calculate the amount of drug administered. During binge METH treatment animals were administered four successive injections of 6 mg METH / kg bodyweight or 1 mL saline / kg bodyweight each 2 h apart. For the subsequent METH challenge animals received a bolus dose of 2 mg METH / kg BW 24 h following the last injection of binge METH.

4.1.3 Open-field motor behavior measurement

Locomotor measurements were made using Opto-verimax open-field locomotor chamber (Columbus Instruments, Columbus, OH). Two small fans were constantly running to produce sufficient white-noise during behavioral testing. Prior to treatments animals

were placed in the open-field chamber for 1 h and allowed to acclimate. Following acclimation animals were administered binge METH. Animals remained in their open-field chambers except for METH injections and body temperature measurement 1 h following each METH injection. Animals were removed from the chambers 5 h following the last METH injection. Therefore, locomotor behavior was continuously monitored for a total of 12 h. 24 h hollowing binge METH, a brief locomotor behavior session was conducted. During this session animal were placed in the open-field chambers and allowed to acclimate for 10 min. Animals then received a single bolus dose of METH (2 mg METH / kg BW) and their locomotor behavior continuously monitored for 2 h.

Figure 16. Study design summary for parkin studies. Adult male Sprague Dawley rats were treated with binge methamphetamine (Red line). Following binge methamphetamine animals were administered a challenge dose of methamphetamine (blue line). Following treatements animals were allowed to recover for 3 days (black line) and the tissue was harvested (arrow). During each of the three phases of the study open-field behavior was monitored. Following recovery, a functional observation battery was conducted (FOB). Together this study design allowed for the assessment of motor behavior of rats during and following exposure to methamphetamine.

4.1.4 Tissue collection

72 h following the last METH injection animals were euthanized via live decapitation. The brain was removed and immediately placed on ice. Brain regions of interest were collected using blunt dissection methods, placed on dry ice, and stored at -80°C. The left hemisphere of the brain was fixed for 3 days in PBS (10 mM Na2HPO4, 1.8 mM KH2PO4, 2.7 mM KCl, 137 mM NaCl, pH 7.4) containing 4% paraformaldehyde at 4°C. The fixed brain was then processed as previously described.[57]

4.1.5 High-performance liquid chromatography

HPLC procedures are as previously described.[96] Briefly, ~ 10 mg of tissue was sonicated in 0.5 mL 0.3 N perchloric acid (SigmaAldrich). Samples were then centrifuged at 17,000 x g for 30 min at 4°C. 10-80 µl of the supernatant was injected onto a C-18 reverse phase column (ThermoScientific). Analytes were detected using an electrochemical detector (Dionex Coulochem III, E1 = -150 mV, E2 = +220 mV) and compared to known standards of dopamine (DA, Sigma-Aldrich), 3-Methoxytyramine (3-MT, Sigma-Aldrich), 3,4-Dihydroxyphenylacetic acid (DOPAC, Sigma-Aldrich), and Homovanillic acid (HVA, Sigma-Aldrich) diluted in 0.3 N perchloric acid. The resulting peaks were integrated and quantified using chromeleon software (ThermoScientific, Waltham, MA). The remaining pellet was dissolved in 1 M NaOH, overnight, at 4°C. The crude protein content of the dissolved pellet was determined using bicinchoninic acid assay (ThermoScientific). Final values are presented as pg analyte / ng protein.

4.1.6 Tissue fractionation

Tissue was homogenized in 1 mL of ice cold homogenization buffer (0.32M sucrose, PMSF) using 12 strokes in a douce homogenizer. The resulting slurry is then

centrifuged at 800 x g for 17 min at 4°C and the supernatant (S1) retained. The S1 is then centrifuged at 18,000 x g for 24 min at 4°C and the resulting supernatant (S2) fraction retained. The S2 (cytosolic fraction) and P2 (synaptosomal) fractions were then solubilized with the addition of 20 mM tris-HCl pH 8.0 and 2% sodium dodecyl sulphate (SDS). Protein concentration of each sample was determined using the BCA assay (Thermo Fisher Scientific).

4.1.7 Western blot

Western blot procedures are as previously described [57]. Briefly, 15 µg of protein from each fraction was separated on a 12% SDS-PAGE. The proteins were then transferred to a methanol activated PVDF membrane by applying a voltage of 25V for 16 h at 4°C. PVDF membranes were then rinsed with ultrapure water, dried, and reactivated with methanol. The PVDF membranes were then blocked in TBST (50 mM Tris-HCl, 150 mM NaCl, 0.05% Tween-80) containing 5% milk m/vol (blocking buffer) for 1 h at room temperature. PVDF membranes were then incubated in blocking buffer containing primary antibodies (DAT, Santacruz; AcetTUB, Cell Signalling; TH, EMDMillipore; β-actin, EMDMillipore) diluted 1:1000 overnight at 4°C. PVDF membranes are then washed three times in TBST and incubated in horse radish peroxidase conjugated secondary antibodies (Santa Cruz) diluted in blocking buffer for 1 h at room temperature. PVDF membranes were then washed three times in TBST, incubated in ECL substrate (Thermofisher) for 5 min, and imaged using Imagequant (GE). Densiotometry analysis on the resulting images was conducted using ImageJ software (National Institute of Health). Uncut representative images are provided for each experiment.

4.1.8 Immunohistochemistry

Fixed brain tissues were processed as previously described [57]. Citrate buffer antigen retrieval (ThermoFisher) was used for all tissue sections. Coronal tissue sections, 30 μm in thickness, were collected from each animal's striatum. Six sections were harvested from 2.16 mm to -0.2 from bregma according to Paxinos & Watson's rat brain atlas. Sections were incubated overnight at 4°C with TH, AcetTUB, or GFAP antibody all diluted 1:500 in blocking buffer. Sections were then incubated with blocking buffer containing diluted Alexa Fluor® 488 goat anti-mouse (Invitrogen, Carlsbad, CA) and Alexa Fluor 598 goat anti-rabbit (Invitrogen) both diluted 1:400 for 2.5 h at room temperature. DRAQ5 (Invitrogen) was used to stain nuclei. Sections were then mounted using Fluoromount (SouthernBiotech, Birmingham, AL). Slides were imaged using a Leica SP3 laser scanning confocal microscope (Leica, Wetzlar, Germany). Three stacks (consisting of 30+ optical slices per stack) were imaged at high magnification (630X) in the dorsal striatum of each slice. The non-colapsed raw single z-plane images were exported from the Leica Image Analysis Suite (Leica). These images were then analyzed using Imaris co-localization analysis software (Bitplane South Windsor, CT). For each image automatic thresholding and masking functions were used to prevent interference from signal noise and variations in signal intensity. The resulting percent co-occurrence in the TH channel was normalized to non-treated control for ease of graphical comparison. The final value represents the percentage of signal overlap within the TH signal.

4.1.9 Data analysis

All data was graphed and analyzed using graphpad prism software (La Jolla, CA). Clustering analysis was conducted using the heatmap2 package for R statistically programming software. ANOVA with a post hoc test was used on the data. Statistical significance was set at $p < 0.05$.

4.2 Results

4.2.1 PKO rats display atypical locomotor response to binge METH

WT and PKO rats treated with saline displayed normal rodent acclimation behavior characterized by the progressive decrease in locomotor activity from the beginning to the end of the open field session (Figure 17A). WT rats displayed a brief (~20 min) increase in distance traveled after the first METH dose, followed by a prolonged period of decreased locomotion (~8.3 h), and eventual recovery of locomotor activity towards the end of the 12 h binge METH session. In contrast, PKO rats treated with METH displayed an atypical activity pattern across the 12 h binge METH session. Following the fist injection of METH, PKO rats displayed a robust increase in distance traveled, followed by a prolonged period of sporadic locomotor activity (from 140-640 min.), and eventually a loss of locomotor activity at the end of the binge session. Approximately half of the PKO rats were completely immobile (i.e. in a position of lateral recumbency) by the end of the METH-binge session.

PKO rats displayed an apparent abnormal locomotor response to METH. When we conducted an unsupervised clustering analysis of the locomotor activity patterns (i.e. distance traveled), we found three unique clusters (Figure 17B). Most notably, PKO rats treated with METH formed a unique cluster with the exception of 1 animal. Comparing the

heat map between all animals it is apparent the sustained distance traveled throughout the binge session defined the abnormal behavioral phenotype of PKO rats. The cluster analysis highlights the apparent unique locomotor activity pattern displayed by PKO rats following METH. Saline treated WT and PKO were apart of the same cluster, and therefore, the overall behavioral activity between drug naïve WT and PKO were essentially the same. This finding is important because there are conflicting reports in the literature as to the development of behavioral abnormalities in parkin deficient mice [106, 251]. Data here supports previous studies that determined the inactivation of parkin does not result in a behavioral phenotype [251]. Only when PKO rats were exposed to neurotoxic doses of METH was a behavioral phenotypic divergence between WT and PKO rats evident.

PKO rats developed abnormal motor behavior approximately 3 h into the binge METH treatment (Figure 17C). Following the first, second and third dose of METH, PKO rats' movements became highly uncoordinated and PKO animals appeared to have difficulty righting themselves, falling backwards or on the side. They did not move forward, they circled backwards. Following the fourth injection of METH several PKO rats displayed a complete loss of locomotor activity, often lying in a lateral recumbent position. The motor abnormalities lasted for at least 24 h following METH, but in several animals, the motor abnormalities were observable as long as 72 h following METH. At 24 h following METH, PKO rats treated with binge METH had decreased activity, rigid movement, abnormal gait, and moved primarily by walking backwards while their WT counterparts recovered and were moving around.

All METH treated animals displayed hyperthermia 1 h following each METH injection when compared to saline (Figure 17E). The magnitude of hyperthermia during binge METH was indistinguishable between WT and PKO rat. However, some PKO rats (50%) were externally cooled by placing on ice to prevent death. WT animals treated with METH did not require external cooling. Because external cooling lowers body temperature, it is possible that PKO rats in fact had higher temperatures that WT rats in response to METH, but was not observed because of external cooling. Other reports have shown that parkin inactivation results in hypersensitivity to drug induced hyperthermia [255].

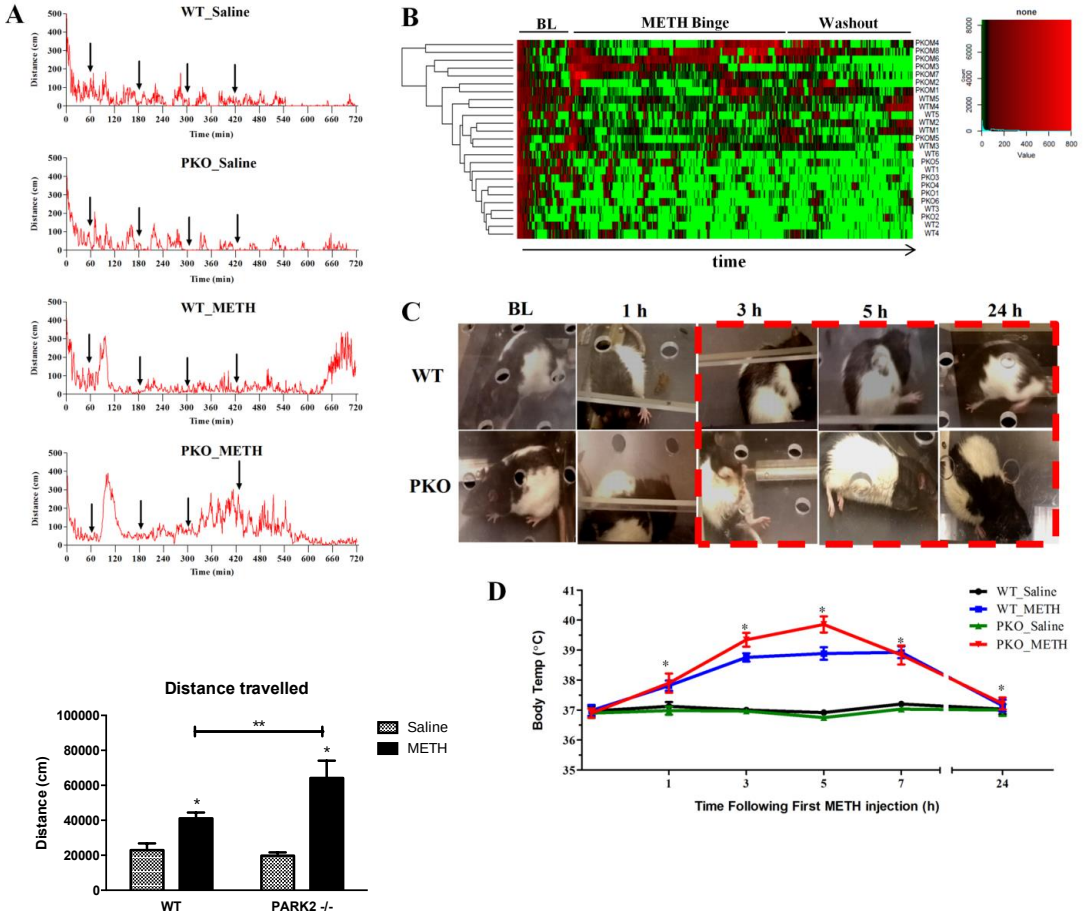

Figure 17. Locomotor activity of parkin knockout (PKO) rats during binge methamphetamine (METH) treatment. Age matched (PND 65-75) wildtype (WT) Long-Evans rats and Park2 -/- (PKO) Long-Evans rats were administered binge (4 injections of 6 mg METH / kg bodyweight, i.p., each 2 hours apart) methamphetamine (METH) while open-field locomotor behavior was continuously monitored. (A) Distance traveled before (≤60 min), during (60-480 min), and after (480-720 min) binge METH treatment. Red lines represent the mean distance traveled (cm/min). Black arrows indicate the time of METH injections. (B) Cluster analysis of the distance traveled for the entire 12 h session. Red shade depicts high behavioral count for the interval and green shade depicts a low behavioral count. The lines to the left of the plot depict the relatedness of each animal's behavioral session. The shorter the line connecting adjacent animals the more similar the behavioral pattern. Treatment conditions are listed to the right of the heatmap; PKO = parkin knockout rat treated with binge saline, PKOM = parkin knockout rat treated with binge METH, WT= WT rat treated with binge saline, WTM= WT rat treated with binge METH. (C) Still-frame images from video recorded during binge METH session. WT and PKO animals. Images from METH treated animals depicted. Red dotted box outlines

images from time-points when impaired motor behavior phenotype is observable in PKO rats. (D) Core-body temperature before, after, and during binge METH treatment. Core-body temperatures were recorded via rectal probe 1 h following each METH injection. ! Acclimation vs. time-point, One-way repeated measures ANOVA, $p<0.05$. *Saline vs. METH, One-way ANOVA, $p<0.05$, Tukey post hoc, $p<0.05$. n=6. Distance = total movement of the animal in the x, y directions. BL= Baseline.

4.2.2 PKO rats have blunted locomotor response to methamphetamine

4.2.2.1 PKO rats' locomotor response to acute high dose METH

Following the first METH injection of the binge treatment (6 mg METH / kg) PKO rats' response displayed a greater in magnitude (+22%) and duration (+48%) in locomotor activity when compared to METH treated WT rats (Figure 18). METH-induced locomotor activity was slightly delayed in PKO rats with peak responses occurring approximately 10 min following WT animals. Increased locomotor activity was not observed in WT and PKO rats treated with saline.

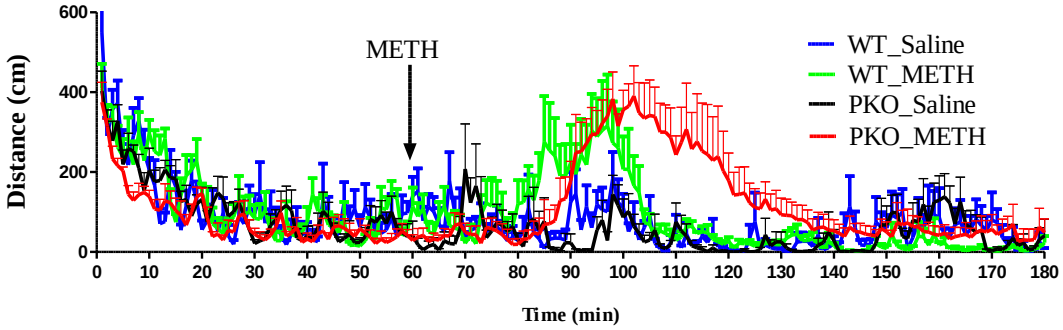

Figure 18. Locomotor response of parkin knockout (PKO) rats to high dose methamphetamine (METH). The line graph depicts locomotor activity (i.e. distance traveled) prior to and following the first METH injection (6 mg METH / kg bodyweight) of the binge METH session. The arrow denotes the time of the METH injection. All measurments were recorded during open-field sessions. Data plotted as the mean (±SEM) distance traveled each minute of the open-field session. WT = Wild-type, PKO = Parkin knockout. n=3-6.

4.2.2.2 PKO rat's locomotor response to low dose METH

All rats received a non-toxic challenge dose of METH (2 mg METH / kg bodyweight) 24 h following binge METH, and open-field activity was measured for 2.1 h. WT rats previously treated with binge saline displayed a significant increase in distance traveled (Figure 19A, top panel) and horizontal counts (19B, bottom panel). In WT drug naive animals, the challenge METH dose resulted in a 10.48-fold greater response than the initial METH dose of the binge session (i.e. 6 mg METH / kg bodyweight). In contrast, drug naïve PKO rats displayed significantly blunted locomotor response to METH challenge. METH exposed WT rats displayed a locomotor response similar to the drug naïve PKO rats. METH exposed PKO rats nearly lacked a discernible response to the METH challenge.

Cluster analysis of the distance traveled during the METH challenge shows three distinct clusters. PKO rats exposed to METH were mostly (83%) clustered together in a low responding group. The second cluster was comprised of animals from all four treatment groups. The third cluster was mostly WT drug naïve animals (86%), which displayed the most robust response to the METH challenge. The lack of response to low-dose METH of the binge METH treated PKO rats can be easily visualized at the top of the heatmap (i.e. dark green color).

Statistical comparison of the total challenge session activity between treatment groups verified the effect seen in figure 19A and 19B (Figure 19C). WT animals treated with binge saline showed the most robust response to the challenge dose with the least time resting and most distance traveled. WT animals treated with binge METH showed slightly

decreased activity during the challenge dose, but this effect was non-significant. The most significant effect can be seen in the PKO rats treated with binge METH. These rats spent a significant amount of time resting and increased distance traveled when compared to WT/Saline and WT/METH. Lack of locomotor response to the METH challenge in the PKO/METH group was not significantly different from the PKO/Saline group.

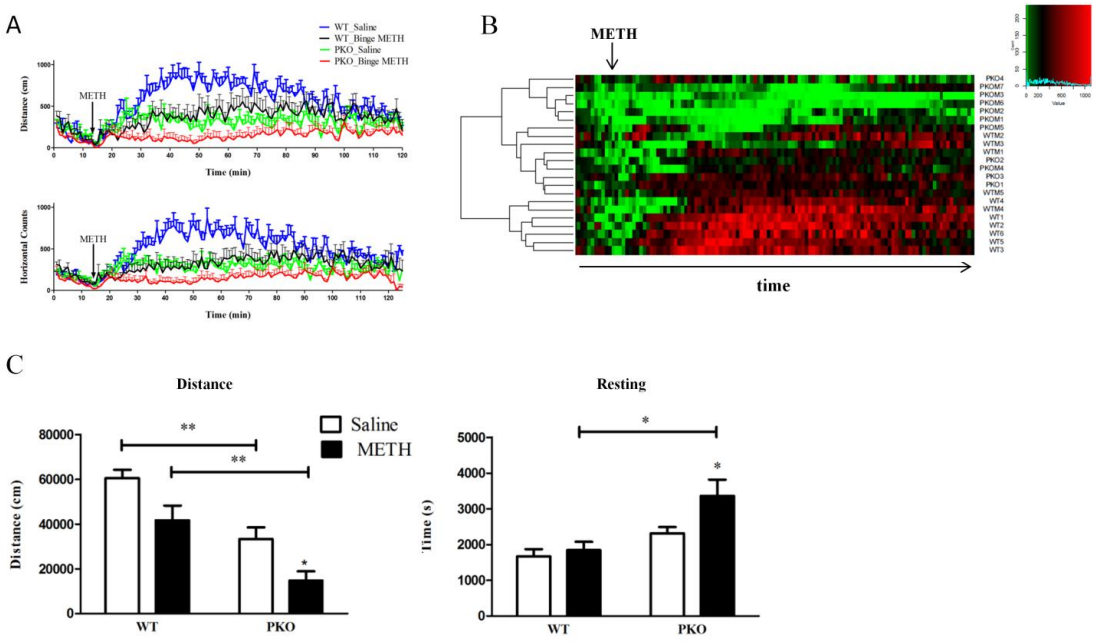

Figure 19. Locomotor response of parkin knockout (PKO) rats to methamphetamine (METH) challenge. WT and PKO animals were first treated with either binge saline or binge METH. 24 hours following the binge session animals were challenged with a single intraperitoneal injection of 2 mg / kg METH. Gross locomotor behavior was recorded for a total of 2 h. (A) Distance traveled and horizontal movements were plotted for each binge treatment group. The means behavior counts were plotted for each minute of the challenge session. (B) Unsupervised cluster analysis was performed on the distance traveled during the challenge session. Red shift depicts high locomotor activity and green depicts lower locomotor activity. Treatment conditions are listed to the right of the heatmap; PKO = parkin knockout rat treated with binge saline, PKOM = parkin knockout rat treated with binge METH, WT= WT rat treated with binge saline, WTM= WT rat treated with binge

METH. (C) Total mean values of distance traveled and resting time for animals during the challenge session. One-way AVOVA, *Dunnets post-hoc test, **Tukey post-hoc test, $p < 0.05$. The data are expressed as mean ± SEM, n = 4-6

4.2.3 Striatal dopamine depletion in PKO rats following binge METH

Binge METH results in long-term depletion of striatal DAergic markers. Here we assessed several DAergic markers in PKO and WT rats treated with binge METH at 3 d after the last injection of the drug. Results show modest reduction in striatal DA of WT rats treated with binge METH (Figure 20A). WT and PKO rats treated with saline show similar striatal DA content. However, PKO rats treated with binge METH had drastically reduced striatal DA contents (-80%) when compared to the saline treated PKO animals. DA metabolites were unchanged in all treatment groups. In addition, binge METH-treated PKO rats displayed augmented 5-HT los as compared to binge METH-treated WT rats (-52% vs. 22%) (not shown).

Dopamine transporter (DAT) levels were significantly reduced in striatal synaptosomes from WT rats following binge METH (Figure 20B). DAT levels were similar to WT saline treated animals for both saline treated and METH treated PKO rats. TH levels were only significantly decreased in METH treated PKO rats, when compared to saline treated WT rats.

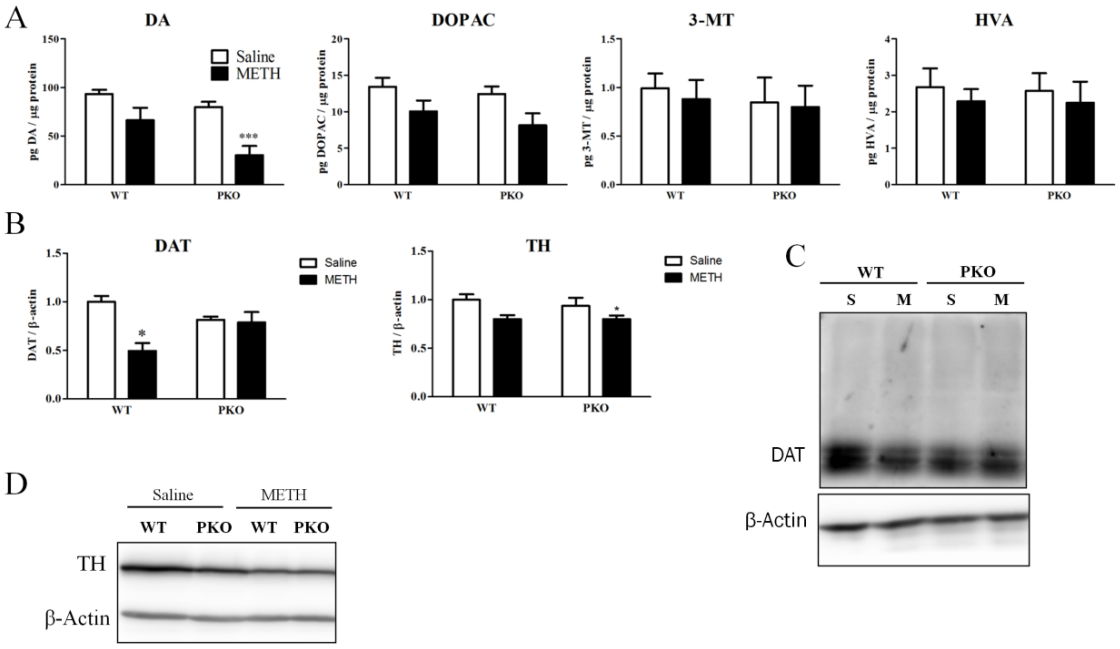

Figure 20. Striatal DAergic markers in parkin knockout (PKO) rats 3 days following binge-methamphetamine (METH). (A) Dopamine and metabolites measured in striatal tissue by HPLC. (B) Dopamine transporter (DAT) and tyrosine hydroxylase (TH) levels in striatal synaptosomes. Protein levels were measured by western blot. β-actin was used as a loading control. Representative western blot images for DAT (C) and TH (D). *, ***One-way ANOVA, Tukey's post hoc test, $p<0.05$, n = 5-8. S= saline, M = METH. The data are expressed as mean ± SEM.

4.2.4 Reactive gliosis in the striatum following binge METH

Damage to the axons of the striatum following binge METH coincides with reactive gliosis. Here we measured the reactive gliosis marker, glial fibrillary acidic protein (GFAP), in fixed striatal brain slices of PKO rats treated with METH. Results show widespread GFAP staining throughout the striatum following binge METH in both WT and PKO rats (Figure 21B). Reactive glia could be seen infiltrating DAergic axons of the striatum (Figure 21C). The induction of GFAP seemed more robust in WT animals treated

with METH (Figure 21D). Both PKO rats treated with saline and METH showed evidence of reactive gliosis. However, when we assessed tissue expression of GFAP in the striata of these animals using WB we did not observe any change between animals (blots not shown). It is unclear as to why the tissue expression of GFAP did not change while reactive glia could be seen in the tissue slices. One possible explanation is the high heterogeneity of the distribution of astrocytes in the brain [256] that can make it difficult to make meaningful quantifications of reactive gliosis by WB or IHC. Therefore, although infiltration of reactive astrocytes into the striatum following METH appears self evident (21B) it is not clear if the quantification (21D) is accurately estimating differences in reactive gliosis between experimental groups. Further complicating the interpretation is the numerous other biological functions of reactive astrocytes, both neuroprotective and neurotoxic [257]. Because we only observed modest reductions in striatal DAergic markers in WT and PKO rats following binge METH (Figure 20) the observed reactive gliosis may not be related to gross DAergic axotomy of the striatum. Studies reporting reactive gliosis following METH utilized much higher doses of METH, and subsequently, observed greater hyperthermia and DAergic marker reduction than reported here [40, 56, 258, 259].

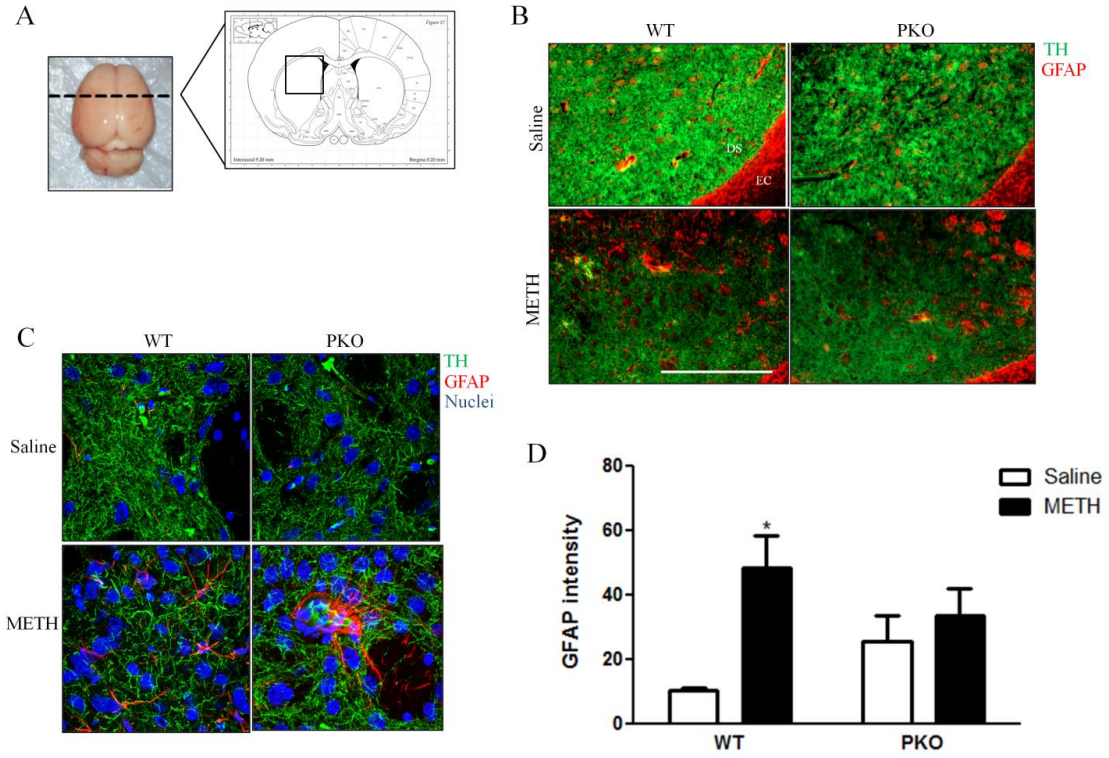

Figure 21. Reactive gliosis in the striatum of parkin knockout (PKO) rats treated with binge methamphetamine (METH). Fixed brain sections from WT and PKO rats treated with binge METH were probed for tyrosine hydroxylase (TH) and Glial Fibilary Glial fibrillary acidic protein (GFAP). (A) Location of the sagital sections taken for staining. (B) Low magnification images of the striatum. EC = external capsule and DS = dorsal striatum. Scale bar = 1 mm (C) High magnification confocal images of the striatum displaying dense clusters of activated glia. (D) Quantification of mean fluorescent intensity of GFAP staining in the dorsal striatum. 3 brain slices per animal. 3 confocal stacks of ~30-60 images each for each brain slice. *One-way ANOVA, Tukey's post-hoc test, $p<0.05$. The data are expressed as mean ± SEM, n = 4.

4.2.5 AcetTUB in the striatum following binge METH

Previously we determined that there are reduced levels of acetylated α-tubulin (AcetTUB) per α-tubulin in striatal DAergic axons following exposure to neurotoxic

METH [57]. Here we measured total levels of AcetTUB in striatal tissue and investigated the amount of AcetTUB in striatal DAergic axons. Results show that administration of binge METH resulted in decreased AcetTUB in the striatum of WT animals (Figure 22A). PKO rats had reduced levels of AcetTUB, regardless of METH treatment, when compared to saline treated WT animals.

Levels of AcetTUB were reduced within striatal DAergic axons of WT rats following binge METH (Figure 22B, C). PKO rats had apparent reductions in AcetTUB within striatal DAergic axons regardless of METH treatment. However, the reduction in AcetTUB was slight, and not statistically significant. Interestingly, in contrast to our previous findings the correlation coefficient measure between TH and AcetTUB was very low (>0.1), suggesting little to no overall correlation between TH and AcetTUB. This observation may hold particular significance because AcetTUB is usually found enriched in axons [260, 261] and overall TH positive axons of the striatum appeared to contain very little AcetTUB. Although this idea is not further explored here, it could potentially help explain why DAergic axons of the striatum are particularly sensitive to MT destabilizing compounds [223]. If DAergic axons are already deficient in stable MT rich in AcetTUB, then destabilization of MT may be particulary difficult for the neuron to recover from.

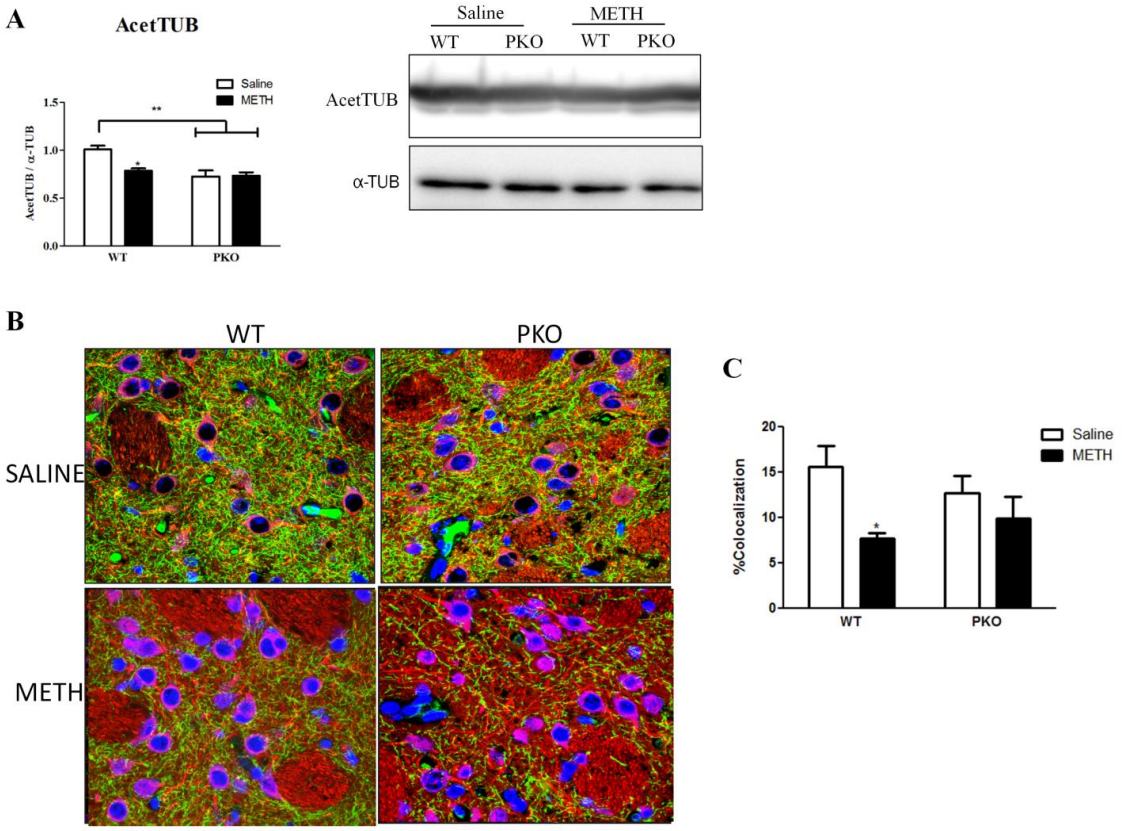

Figure 22. Acetylated α-tubulin in parkin knockout (PKO) rats 3 days following binge METH. Rats were treated with binge METH and a single challenge METH dose 24 following binge METH. (A) Soluble proteins were extracted from striatal tissue and analyzed by western blot. Membranes were probed with antibodies specific for acetylated α-tubulin (AcetTUB) and α-tubulin (α-TUB). (B) Fixed brain tissue was sectioned and probed with antibodies specific for AcetTUB (red) and tyrosine hydroxylase (TH, green). Nuclei were stained with DRAQ5 (blue). Sections were imaged using confocal microscopy. (C) The degree of colocalization was determined using Leica colocalization software. Mean values are represented for each treatment group. Mean values derived from 3 slices per animal. *$p<0.05$. The data are expressed as mean ± SEM.

4.2.6 METH challenge does not result in loss of DAergic markers in the striatum

To indirectly assess DAergic function in the nigrostriatal pathway all animals were given a small challenge dose (2 mg METH / kg body weight) 24 hours following binge

METH. The challenge dose of METH did not likely result in long term (i.e. 7 days or more following METH exposure) DAergic neurotoxicity. Several studies, including our own, have demonstrated that exposure to up to 12-fold the challenge METH dose not robustly produced striatal DA depletion or overt signs of neurotoxicity [165, 262]. 3-times the challenge dose did not change striatal DA content 7 days following METH exposure (Figure 23).

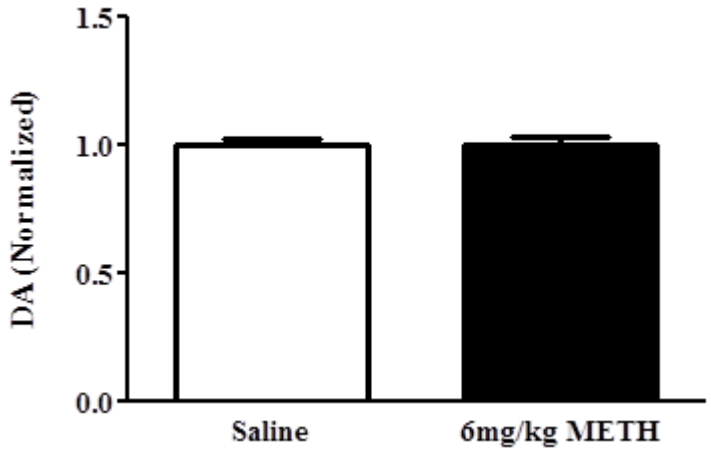

Figure 23. Striatal dopamine (DA) content 7 days following a single intravenous (IV) injection of methamphetamine (METH). Adult male SD rats were injected with 6 mg METH / kg body weight via lateral tail vein. 7 days following METH administration animals were sacrificed and striatal DA content measured by HPLC. All values were normalized to the average DA content of saline treated rats. The data are expressed as mean ± SEM, n = 4-7.

DA content measured in WT and PKO treated with challenge METH was approximately 110 pg DA / µg protein (see figure 20A), in agreement with published striatal DA content of drug naïve rats [263-265]. Furthermore, LE rats and SD rats had similar striatal DA content, therefore strain differences in DA driven behaviors, suggested here and elsewhere [266], are likely not due to striatal DA content.

4.2.7 METH challenge does not alter colocalization of AcetTUB with TH labeled axons in the striatum

The challenge METH dose likely does not produce changes to AcetTUB levels in striatal DAergic axons. Significantly higher doses of METH (12-fold higher) result in relatively modest reduction in AcetTUB in DAergic axons of the striatum [264]. To test whether the challenge METH dose can alter AcetTUB levels in striatal DAergic axons we compared drug naïve WT and PKO rats with WT and PKO treated with challenge METH. Results show that the abundance of AcetTUB within DAergic axons were similar between drug naïve and challenge treated WT and PKO rats (Figure 22). Therefore, the challenge dose cannot account for the differences seen in AcetTUB levels within DAergic axons.

4.3 Discussion

Here, PKO animals displayed a loss of motor control approximately 4 h into binge METH treatment (Figure 17C). The development of this behavioral-phenotype coincided with the peak in METH induced hyperthermia (Figure 17D). Counter-intuitively, the observable loss of motor control was associated with a subsequent increase in total locomotor activity (Figure 17A and 17B). However, the video record of the session revealed that the PKO rats' locomotion was highly abnormal during the METH binge. Specifically, the PKO rats were walking backwards in a circular manner and were losing balance when they tried to stand up. Movements were both sporadic and uncoordinated. Backward walking and circling are mediated by simultaneous release of DA and 5-HT after administration of high doses of METH or other amphetamines [267, 268]. The PKO rats treated with METH had very low DA and 5-HT levels at 7 d after METH binge, confirming

that the release of both neurotransmitters was substantial in these rats. Balance impairment and the associated backward falling in Parkinson's disease do not respond to L-DOPA treatment and, therefore, was suggested to be a result of defective noradrenergic neurotransmission [269]. We did not measure noradrenaline levels in our rats; however, since it is well known that METH releases DA, 5-HT and noradrenaline, it can be speculated that balance impairment and fallings observed in the PKO rats were due to defective noradrenergic neurotransmission. As expected, WT rats remained in stereotypy through the METH binge after the initial increase in locomotor activity and did not display backward walking or circling despite increased release of DA and 5-HT. Most likely, the extent of their release did not reach high enough levels (as in the PKO rats), particularly the extent of 5-HT release [267]. Somewhat smaller (but not statistically significant) stereotypy in the PKO rats than in the WT rats could have been due to decreased levels of striatal postsynaptic D2 receptor in these rats (unpublished results) [270].

Following binge METH, the WT rats' horizontal locomotion recovered whereas PKO rats' locomotion ceased and the uncoordinated movements remained. The behavioral and neurochemical data collectively suggest that binge METH almost entirely depleted striatal monoaminergic stores in the PKO rats and to a lesser extent in the WT rats. The depletions in DA and 5-HT levels were not likely due to degeneration of DAergic and 5-HTergic terminals because they were not accompanied by deficits in the other DAergic/5-HTergic markers. The loss of motor function in the PKO rats was accompanied with 77%-deficit in DA, which is at the level generally required to see obvious motor abnormalities in PD [271]. In stark contrast to parkin PKO rats, WT rats displayed a similar magnitude

of METH induced hyperthermia but with no dramatic loss of motor function during or after binge METH. WT rats tolerate high METH doses without a loss of motor function [272] because the depletion of DA stores is less than 70-80% after 5-8 mg/kg freebase METH [165].

Significantly higher than in the WT rats monoaminergic deficits in the PKO rats suggest higher METH-induced DA release via the DAT or slower uptake of DA back to the terminal in these rats. The first scenario would require increased availability of DAT at striatal presynaptic nerve terminals. Drug-naïve PKO rats, however, had slightly lower levels of the DAT compared to their WT counterparts. As our technique measured DAT in crude synaptosomal fractions, the assessment of distribution of the DAT between purified plasma membrane and endosomal fraction in both phenotypes is warranted. Binge METH did not result in depleted striatal DAT and therefore METH in these animals may have supported greater DA release during the binge and subsequent depletion of DA from presynaptic nerve terminals. Slower uptake of DA back to the terminal in drug-naïve animals or during METH binge could also be due to altered DAT trafficking (endosomes-plasma membrane and axonal) or due to an altered kinetics of DA transport. Drug naïve PKO rats did not significantly differ from drug naïve WT rats in basal locomotor activity. Their exploratory behavior was somewhat decreased compared to the WT rats, which can be indicative of reduced extracellular DA in the striatum [250]. Only when PKO rats were challenged with the DAergic agonist METH the differences in the nigrostriatal DA pathway function were revealed. Thus, the initial locomotor response to 6 mg/kg METH was more robust in the PKO rats than in the WT rats. On the other hand, the initial response

of the PKO rats to the low METH dose (2 mg/kg) was lower than in the WT controls, in agreement with a previous report [106]. This locomotor response of the PKO rats was similar to the WT rats that were previously treated with binge METH. Most drastically, PKO rats previously exposed to binge METH did not display a locomotor response to low dose METH due to almost complete depletion of DA pools. Generally, low doses of METH potently increase horizontal locomotor activity while high doses of METH potently suppress it due to the emergence of stereotypy [273]. Low doses of METH release cytoplasmic pool of newly synthesized DA [274]; therefore, our finding suggests that cytoplasmic DA pool is lower in PKO rats than in WT rats. Alternatively, the pool is not different between the phenotypes but the release of DA via DAT is slower in PKO rats than in WT rats. Interestingly, the increase in locomotor activity after the 6 mg/kg-dose of METH is delayed in the PKO rats compared to the WT controls so is the suppression of locomotor activity, suggesting malfunction of the DAT. Our findings support the growing body of evidence for parkin being an important regulator of DA neuron development, health, and function [275]. Together, this data suggests that drug naïve PKO rats display some hypodopaminergia in the nigrostriatal pathway, which can be highly exacerbated by treatment with binge METH.

Post-synaptic signaling at the striatal DA nerve terminals is greatly influenced by dopamine recetor 2 (D2R) and dopamine receptor 1 (D1R). In the striatum, D1R has important roles in controlling spontaneous motor behavior and the locomotor response to psychostimulants [276, 277]. Interestingly, the AcetTUB pathway appears to excert some control over D2 function [278], and here we found that PKO rats may have reduced levels

of AcetTUB in the striatum. Other preliminary results from our lab (not depicted here) suggest a reduced level of postsynaptic D2 in the striatum of PKO rats, adding credence to the idea that parkin may excert some control of DAergic neuron function in the striatum via signaling pathways affecting the D2 receptor. Of note, mice lacking parkin do not display deficits in either the levels of dopamine receptors or their function [34].

Hyperthermia is crucial in the development of METH induced DAergic toxicity [40, 279] and METH can activate the heatshock pathway [280]. Here hyperthermia was appeared to be necessary to produce PD-like phenotype in the PKO rats. The magnitude of hyperthermia was not statistically different between PKO rats and WT, with slightly higher response thermic response in the PKO rats. However, WT rats did not display any motor deficits. Therefore, we hypothesize that PKO rats are more sensitive to the cellular heatshock of hyperthermia. During heatshock, HDAC6 is recruited to damaged/misfolded proteins in ubiquitin dependent manner [281]. Recently, parkin mediated ubiquitination of damaged misfolded proteins was shown to recruit HDAC6 in response to cell stress [281]. Therefore, it is logical to assume that PKO rats may have a deficient heatshock response and because heatshock response is neuroprotective, this could explain observed neurotoxicity in PKO rats. In support of this interpretation the observed loss of motor function occurred near the time-point when METH induced hyperthermia was the greatest. METH induced hyperthermia did not significantly differ between WT and PKO rats. However, PKO rats would lack the ubiquitination of protein aggregates required for HDAC6 recruitment. This would likely result in the toxic accumulation of aggregated

proteins in the cytosol. The data presented here is insufficient to confirm or reject this hypothesis.

Total levels of AcetTUB were reduced in the striatum of PKO rats, regardless of METH exposure. AcetTUB is a marker for stable long-lived MT required for axonal transport. Therefore, PKO animals may have impaired axonal transport in the striatum, possibly making them sensitive to neurotoxic METH. In further support of this interpretation we observed a similar phenotype as the PKO rats when WT rats were treated with high dose of a MT stabilizing compound EpoD [264]. The high dose of EpoD reduced AcetTUB levels in the striatum and resulted in profound neurotoxicity.

Colocalization analysis revealed that METH decreased AcetTUB within DAergic axons, as we have shown previously [264]. However, PKO rats were insensitive to this effect of METH, as AcetTUB levels with DAergic axons were similar between saline and METH treated PKO rats. This pattern seems to verify the western blot quantification of total soluble AcetTUB. However, the measured decreased AcetTUB in PKO rats was less using colocalization analysis. This is likely due to the non-quantitative nature of IHC [282, 283] when compared to the quantitative validity of western blotting [284]. Furthermore, the loss of AcetTUB measured by western blot, may mostly represent the pool of AcetTUB outside TH axons, and therefore be more indicative of tissue levels of AcetTUB. In this regard, it is possible that the MT of DAergic axons are insensitive to toxic METH insult in PKO rats. On the other hand, glia activation suggest some damage to DAergic axons of the striatum. Reactive gliosis in PKO rats following binge METH was less than that observed in WT rats. Reactive glia can be neuroprotective following some neurotoxic insults via

release of glia cell derived neurotrophic factor, maintenance of blood brain barrier, sequestration of toxic oxidative species, and the release of anti-inflammatory molecules [285]. Therefore, it is possible that the observed sensitivity of PKO to METH neurotoxicity could be due to insufficient reactive gliosis. The data presented here are insufficient to affirm or reject this interpretation.

Fruitful future investigations may look at the role of parkin overexpression, knockout or knockdown on the substrates that are involved in neurotransmitter synthesis, packaging, and release. For example, cell division control related protein 1 (CDCREl-1) may be a likely downstream factor responsible for parkin's influence on DA function [108]. CDCREl-1 appears to have SNARE–like functions that inhibit exocytosis [286]. Parkin-mediated ubiquitination of CDCREl-1 would enhance the turnover of CDCREl-1 in parkin overexpressing rats, possibly inhibiting exocytosis of DA. In the same vein, parkin may be exerting influence on DA function via interactions with K63 of α-synuclein [281]. α-Synuclein overexpression and knockout curiously produce effects DA release similar to that of parkin [287, 288]. The similar effects of parkin and α-synuclein on DA neurotransmission are a tantalizing clue, suggesting convergence of the two pathways during neurodegeneration. However, the possible common pathway between the two proteins in METH neurotoxicity has yet to be elucidated.

4.4 Conclusions

PKO rats are hypersensitive to the neurotoxic effects of METH. Correspondingly, PKO rats develop severe motor impairments during binge METH. Parkin appears have some functional control over DA signaling in the nigrostriatal motor pathway, as suggested

by relative hypolocomotion in PKO rats. Together, the results support the hypothesis that parkin plays a role in maintaining the healthy and proper functioning of nigrostriatal DAergic neurons. In PKO rats, AcetTUB levels in the striatum are not different from WT saline treated controls. Therefore, parkin likely does not influence axonal transport via post-translational modification of MT. If parkin does influence axonal transport in the nigrostriatal pathway it is likely by some other means that MT stabilization. Future studies should focus on unilateral overexpression of parkin and its influence on striatal DAT expression as well as DA synthesis packaging and release.

CHAPTER 5 – MEASURING A-SYNUCLEIN TETRAMER ABUNDANCE IN BRAIN LYSATES

Results in chapter five are transcribed from the peer-reviewed manuscript: Killinger BA, Moszczynska A (2016) Characterization of alpha-Synuclein Multimer Stoichiometry in Complex Biological Samples by Electrophoresis. Killinger B. was responsible for designing, conducting, and reporting transcribed in chapter 3. Moszczynska A. was responsible for editing and reviewing the manuscript prior to acceptance by Analytical Chemistry. This project was initiated as an attempt to address the need for an easy reliable technique to measure protein complex formation in complex biological samples. Although the technique was developed and applied to α-synuclein multimerization, subsequent studies have shown the techniques applicability to other soluble complexes [289].

5 Background

Parkinson's disease (PD) is a neurodegenerative disease characterized by the formation of proteinaceous inclusions, termed "Lewy bodies" that contain large amounts of α-synuclein, a small cytosolic protein for which the biological function is still unclear [109, 290]. In vivo α-synuclein occurs as a variety of multimers including a dimer, tetramer, and octomer which appear to be biologically important and possibly resistant to toxic aggregation [127, 291, 292]. New therapeutic strategies for treating PD may involve the use of drugs to stabilize soluble multimeric α-synuclein to prevent the formation of higher order soluble toxic multimers [293].

Soluble monomeric α-synuclein is an intrinsically disordered protein and behaves like a larger protein of ~50-60 kDa when assessed using a number of techniques including size-exclusion chromatography and blue native gel electrophoresis (BN-PAGE) [127]. The unusual behavior of α-synuclein makes the separation of native multimers from the monomer, according to mass, particularly challenging. Chemical crosslinking can be used to preserve α-synuclein multimers allowing their separation from the monomer by traditional sodium dodecylsulphate polyacrylamide electrophoresis (SDS-PAGE) [291, 293, 294]. α-Synuclein multimerizes upon binding to phospholipid membranes, but it remains unclear whether free soluble α-synuclein can form stable soluble multimers. Upon binding to phospholipid membranes α-synuclein adopts defined secondary structure and subsequently multimerize [290, 295]. Although the interaction between α-synuclein with phospholipid membranes is intimately involved in the multimerization process and biological function of α-synuclein, the molecular details of this interaction remain unclear.

Here, we developed a new technique, termed "multimer-PAGE," to quantify the multimerization of α-synuclein in complex biological samples. Using this technique, it is possible to compare the ratio of α-synuclein multimers between 14 brain tissue samples without the need for specialized equipment.

5.1 Materials and Methods

5.1.1 Animals

20 adult male Sprague Dawley (SD) rats (250-350g) were pair housed in polycarbonate cages at approximately 70°F. Rats were euthanized via live decapitation. Following euthanasia, the brain was removed and dissected on ice. All collected brain

tissue was placed on dry ice, and frozen at -80°C until assayed. All procedures were conducted in accordance with the Wayne State University institutional care and use committee approved protocol #A3310-01.

5.1.2 Sample preparation

All procedures were conducted on ice and in a cold room. Frozen brain tissue samples weighing approximately 25-200 mg were homogenized in 1 mL 1 X BN-PAGE sample buffer (Invitrogen, Waltham, MA) for native separation or phosphate buffered saline pH 7.4 (PBS) for in-solution crosslinking experiments. All solutions contained EDTA free protease inhibitor cocktail (Sigma-Aldrich, St. Louis, MO). Tissue was disrupted using 30 strokes in a 7 mL dounce homogenizer. Following homogenization, samples were briefly vortexed and incubated on ice for 30 min. For some experiments, 0.5% m/vol NP40 (Boston Bioproducts, St. Ashland, MA) or 1% m/vol digitonin (Sigma) was added to the lysate prior to the 30 min incubation on ice. The sample was then centrifuged at 18,000 x g for 30 min. Following centrifugation the supernatant (S1) was carefully transferred to a pre-chilled 1.5 mL eppendorf tube. To determine protein concentration of the sample, 8 µl of the S1 was transferred to a separate eppendorf tube containing 2 µl of 10% m/vol SDS, mixed well, and incubated at room temperature for 10 min. This delipidated sample was then used to determine the protein content using bicinchoninic acid assay (BCA assay, Thermofisher, Waltham, MA). Samples were diluted to a final concentration of 0.1-4 mg protein / mL, depending on the experiment. The insoluble pellet (P1) was resuspended in 1.5 mL RIPA buffer (10mM Tris-HCl pH 8.0, 1% Triton X-100, 0.1%m/v sodium dodecyl sulphate, and 140 mM NaCl) mixed thoroughly,

and incubated on ice for 1h. The P1 sample was then centrifuged at 18,000 x g for 30 min at 4°C, and the supernatant retained (S2). The S2 was then processed for lipid and protein quantification. α-Synuclein was purified as previously described [296]. Relative purity of α-synuclein was determined by SDS-PAGE and subsequent Coomassie Blue G-250 staining. The lyophilized purified α-synuclein was dissolved in 1 x BN-PAGE sample buffer for native separation or PBS for in-sample crosslinking experiments to a final concentration of 4 mg protein / mL.

5.1.3 Lipid and protein isolation

Bulk lipid extraction was performed essentially as previously described [297]. Briefly, 20 mL of a chloroform and methanol mixture (2:1) was added to 1 g of rat brain tissue. The tissue was homogenized via sonication for 2 min. The homogenate was vortexed well, 4 mL of PBS added, and the sample vortexed again. The sample was then allowed to sit for 5 min to allow the solution to separate into two phases. The organic phase containing the purified lipids at the bottom of the tube was carefully removed and dried under vacuum using a Centrivap DNA Concentrator (Labconco, Kansas City, MO). The purified lipids were then resuspended in 200 µl 1 X BN-PAGE sample buffer containing 10% m/vol NP40, bath sonicated for 30 min, and centrifuged at 18,000 x g to remove any insoluble lipids not incorporated into the NP40 micelles. Isolated lipids were used within 24 h to avoid excessive lipid oxidation. Extracted brain lipids were used for generating a lipid standard for total lipid determination and to generate mixed micelles only (Figure 25A and D).

To extract lipid and proteins from individual lysates we first diluted the samples to 2 mg protein / mL using the appropriate buffer in a 1.5 mL eppendorf tube. The dilution was conducted to yield a final sample volume of 150 µl. Then 600 µl methanol and 150 µl chloroform were added to each sample. Samples were mixed well, 450 µl of dH20 added to each sample and mixed well again. Samples were then centrifuged at 14,000 x g for 5 min. The upper aqueous phase was then carefully discarded, making sure not to disturb the precipitated proteins between the lower and upper phase. 450 µl of methanol was then added to each sample, vortexed, and centrifuged at 14,000 x g for 5 min. The methanol chloroform mixture contained the lipids and precipitated proteins are found in the pellet. The extracted lipids from individual samples were used to quantify the amount of soluble lipids (Figure 25D). The precipitated proteins from individual samples were used for mixed micelles experiments (Figure 25A).

The precipitated proteins (300 µg) were dissolved in 100 µl 1 X BN-PAGE sample buffer containing either 0.5% NP40 or 0.5% NP40 brain lipid mixture. Samples were mixed thoroughly, allowed to sit on ice for 30 min, and mixed thoroughly again. All samples were then centrifuged 18,000 x g for 30 min to remove any remaining insoluble lipids or proteins. Protein content of each mixture was then determined using BCA assay.

5.1.4 Blue native polyacrylamide gel electrophoresis

Procedures were conducted as previously described[298]. Briefly, linear gradient 2.8-13%T and non-gradient 6%T gels were used for all BN-PAGE separations. All gradient gels were poured by hand using a linear gradient former built as previously described [299]. A 2.8%T gel was used for the sample wells. 0-0.5% m/v Coomassie Blue G-250 (Sigma-

Aldrich, St. Louis, MO) was added to all samples immediately prior to electrophoresis and 4-50 µg of brain tissue lysate protein or 50-200 ng purified α-synuclein were loaded into each sample well of the BN-PAGE gel. Either native page marker (Invitrogen) or 1 µg of bovine serum albumin (BSA, Santa Cruz Biotechnology, Dallas, TX) diluted in 1 X BN-PAGE buffer was used as a protein standard. Electrophoresis was conducted using running buffer (100mM bis-tris, 100 mM tricine) containing either 0.001% (for non-detergent samples) or 0.01% (for detergent samples) G-250 at 100 V until the samples entered the gel, and then 180 V for approximately 3 h (until the dye front reached the end of the gel) at 4°C. When detergent samples were resolved, the running buffer containing 0.01% G-250 was replaced by the running buffer containing 0.001% G-250, approximately half-way through the run. 6%T BN-PAGE gels were run under the same conditions but stopped once samples had migrated about 2 cm into the resolving gel. Once electrophoresis was complete the lanes of the gel were either excised for 2D electrophoresis or electroblotted onto methanol activated polyvinylidene fluoride (PVDF) membranes. Electroblotting of BN-PAGE gels was performed at 20 V for 3 h at 4°C using the BN-PAGE running buffer. Following electroblotting, PVDF membranes were fixed for 20 min in 10% acetic acid, rinsed with ultrapure water, and then dried.

5.1.5 In-gel crosslinking

Excised gel pieces were washed with PBS three times for 10 min at 4°C to remove excess bis-tris and 6-aminocaproic acid because could compete with crosslinking reactions. Gel lanes were then incubated for 5-30 min at 4°C in PBS containing either 1% paraformaldehyde (PFA), 1% glutaradehyde, 0.1-2 mM Dithiobis

(succinimidylpropionate) (DSP, ThermoFisher Scientific, Waltham, MA), 0.1-2 mM 3,3'-dithiobis (sulfosuccinimidyl propionate) (DTSSP, Thermofisher Scientific), or 0.1-2mM disuccinimidyl glutarate (DSG, ThermoFisher Scientific). DSP, DTSSP, and DSG must first be dissolved in DMSO to a concentration of 25 mM before adding drop-wise to the PBS. Gels were then incubated in 375 mM Tris-HCl pH 8.8 buffer (when resolving by SDS-PAGE gradient gel) or 125 mM Tris-HCl pH 6.8 (when resolving by non gradient SDS-PAGE gel), both containing 2% SDS for 1 h at room temperature.

5.1.6 2D-Sodium dodecyl sulfate gel electrophoresis

Excised gel strips were placed in-between Mini PROTEAN® system glass plates with a 1 mm spacer (Biorad, Hercules, CA). Each gel strip was positioned with the lowest percentage gel facing down (to ensure proteins leave the gel strip during electrophoresis). When 6%T BN-PAGE gel was used the orientation of the gel strip wasn't crucial. Approximately 30 mm space is needed on the end of the gel strip for comb placement to form 2 wells. The glass plates containing the gel strip were then locked into the Bio-Rad gel stand and checked for leaks. Then a 3-16%T linear gradient or 12%T gel was poured between the glass plates leaving approximately 10 mm space under the excised gel piece for the sample gel. For 12%T gel, a 1 cm space was left for the stacking gel to ensure sufficient band focusing. Butanol was gently layered over the top of the gradient and the gel was allowed to polymerize at room temperature for ~1 h. Once the gel was polymerized, the butanol was removed and a sample gel of 3%T was poured around the gel strip. Tilting the gel stand slightly prevented bubbles from forming under the gel strip bubbles. The 2-well comb was placed in between the glass plates and 30 min was allowed for

polymerization. Alternatively, 2D-SDS-PAGE gels can also be precast (without the excised gel strip). However this requires custom well comb, which can be fashioned out of polystyrene sheets purchased from most hobby stores. Reduction in band resolution, due to uneven migration of the sample out of excised gel, was observed when using precast gels and therefore the method should generally be avoided. Gels were then run at 125 V until the dye front reached the end and gels were then transferred to PVDF membrane in Towbin transfer buffer (25mM Tris-HCl, 192mM glycine, and 20% methanol) using the constant of 20 V for ~16 h at 4°C.

5.1.7 Immunodection

Dried membranes were reactivated in 100% Methanol for 1 min and then rinsed with ultrapure water. To confirm even transfer, all membranes were stained using Ponceau S (Sigma-Aldrich). Membranes were incubated in blocking buffer which consisted of 5% m/vol milk diluted in TBST (50 mM Tris-HCl, 150 mM NaCl, 0.05% Tween-80, pH 8.0) for 1 h at room temperature. Then membranes were incubated in blocking buffer containing either monoclonal (BD Biosciences) or polyclonal (Santa-Cruz) anti-α-synuclein antibodies diluted 1:1000, overnight at 4°C. Parkin monoclonal and polyclonal antibodies were diluted 1:1000 in blocking buffer and incubated with membranes over-night at 4°C. Membranes were then washed 2 X 10 min with TBST before incubating in the appropriate HRP conjugated anti-body diluted 1:5,000 in blocking buffer for 1 h at RT. Membranes were then washed 2 X 10 min with TBST, incubated 5 min in ECL substrate, and imaged using GE Imagequant LAS 4000 (GE Health Care, Little Chalfont, United Kingdom).

5.1.8 In-sample crosslinking

Brain tissue lysates in PBS (see section 2.2) were diluted to concentrations ranging between 0.1-4 mg protein / mL. DSP or DSG (1 mM) were added to each sample and incubated at 4°C for 10 min. The reaction was quenched with 50 mM Tris-HCl pH 8.0 for 15 min. 1 X SDS-PAGE sample buffer (50 mM Tris-HCl pH 6.8, 2% SDS, 10% glycerol, and 0.1% bromophenol blue) was then added to each sample, mixed well, and heated at 90°C for 5 min. 10 µg protein from each sample was added to each well. DSP crosslinker arm was cleaved by adding 5 mM dithiothreitol (DTT) prior to heating the sample. Purified α-synuclein was dissolved in PBS to a concentration of 4 mg / mL and crosslinked with 2 mM DSP for 10 min at 4°C. The reaction was quenched with 50 mM Tris-HCL pH 8.0 for 15 min.

5.1.9 Determination of total lipid content

Total sample lipid content was determined essentially as previously described [300]. Specifically, lipids isolated from the samples were dissolved in 100 µl chloroform. The chloroform solution was then placed into a disposable 12 X 75mm borosilicate glass tube (Corning Inc., Corning, NY) and allowed to dry completely. Standards were generated by dissolving a known mass of isolated rat brain lipids (see section 2.4) or canola oil (local grocery store) in chloroform. Standard solutions were then pipetted into 6 glass tubes to yield 5-400 µg total lipid, and dried completely. Then, 100 µl of concentrated sulfuric acid (Sigma-Aldrich) was placed in each tube and incubated at 90°C for 20 min. The tubes are then cooled immediately using an ice water bath, and solutions transferred to a clear polystyrene 96-well plate (Thermofisher). Light absorbance was measured at wavelength 540 nm, then 50 µl of phosphor-vanillin solution (0.2 mg vanillin dissolved in 1 mL 17%

phosphoric acid) was added, and the plate incubated at room temperature for 10 min. The plate was then read at 540 nm again, and the background (i.e. first absorbance measurement) was subtracted from sulfo-phospho-vanillin absorbance (i.e. second absorbance measurement). Detection limit was determined to be approximately 5 µg lipid.

5.1.10 Polyacrylamide gel-solutions

All gels were formed using two stock polyacrylamide solutions. The first 40%T acrylamide stock solution that can be purchased (Biorad) was used for all SDS-PAGE gels. The second 40%T acrylamide stock solution is made by mixing 48 g acrylamide (Fisher Scientific) and 1.5 g N,N-Methylenebisacrylamide (Fisher Scientific) in 100 mL ultrapure water (heating to 40°C required to dissolve completely). This second acrylamide solution was used only for BN-PAGE gels. BN-PAGE gel buffers were prepared as previously described[301]. Stacking gel buffer (125mM Tris-HCl pH 6.8, 0.1% m/vol SDS) and resolving gel buffer (375mM Tris-HCl pH 8.8, 0.1% m/vol SDS) were used for all SDS-PAGE gels. 0.1% m/vol ammonium persulphate (Sigma) and 0.05% vol/vol N,N,N′,N′-Tetramethylethylenediamine (Sigma) were used to the intiate polymerization of SDS-PAGE polyacrylamide gels.

5.1.11 Blot Quantification

Densitometry analysis was conducted on all images using Imagej software (National Institutes of Health). Linear regression analysis and repeated measures ANOVA were conducted using Graphpad Prism software (La Jolla, CA). All images are uncut (unless depicted by a black line) and representative of each experiment conducted. Several

overexposed images are presented to display banding pattern, but these images were not used for any quantification.

5.2 Results/Discussion

5.2.1 Separation of α-synculein by blue native Page

To develop the multimer-PAGE protocol we first needed to describe, in detail, the migration pattern of α-synuclein during BN-PAGE (Figure 24). Extraction of proteins from rat brain tissue using 0.5% NP40, 1% digitonin, or in the absence of detergent under typical lysis concentrations (25 mg tissue / mL buffer) showed efficient tissue solubilization, an absence of abundant high molecular weight (>150kDa) α-synuclein interactions, and allowed for the separation of soluble α-synuclein via BN-PAGE (Figure 24A). Monoclonal and polyclonal antibodies against the c-terminus of α-synuclein produced similar band patterns for tissue lysates. α-Synulcein migrated to the gel position of approximately 50-146 kDa on the 2.8-13%T BN-PAGE gel. The addition of up to 50 µg lysate protein still produced one major band at 50 kDa. A mass shift to approximately ~100 kDa was observed following the extraction with digitonin and NP40. The overall protein distribution on BN-PAGE appeared similar between extraction conditions, with the exception of an increased abundance of observable protein complexes with digitonin and NP40 (Figure 24A, Ponseau S stain). Together, these results show that under typical BN-PAGE conditions soluble α-synuclein from rat brain tissue was separated as a single species, predominantly migrating between the 50-146 kDa position on BN-PAGE, in agreement with several reports [127, 294].

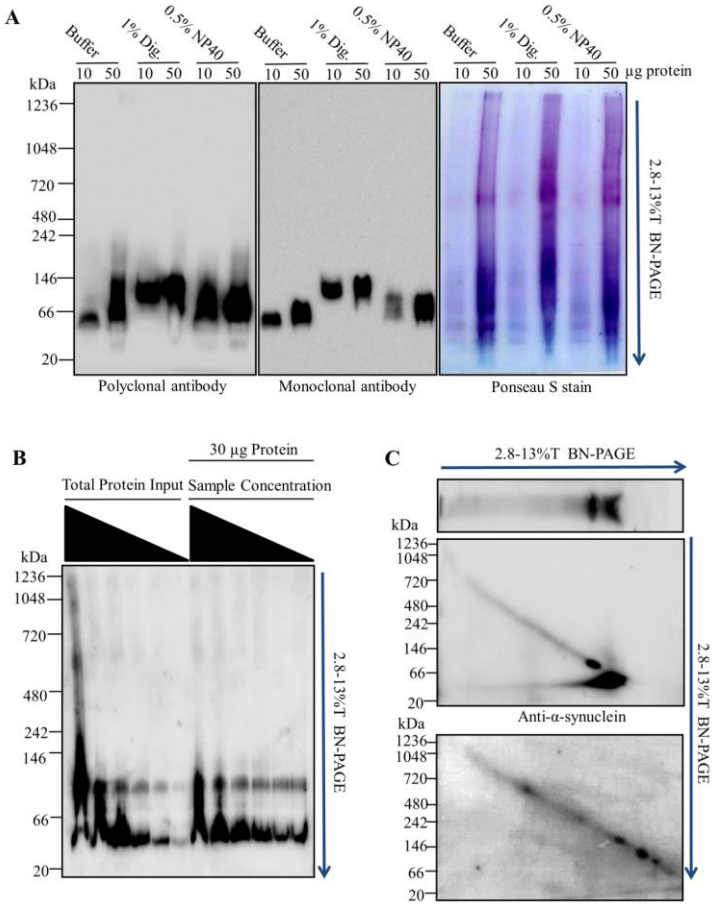
A
Buffer
1% Dig.
0.5% NP40
10 50
µg protein
kDa
1236
1048
720
480
242
146
66
20
2.8-13%T BN-PAGE
Polyclonal antibody
Monoclonal antibody
Ponseau S stain
B
30 µg Protein
Total Protein Input
Sample Concentration
C
2.8-13%T BN-PAGE
Anti-α-synuclein

Figure 24. Migration of α-synuclein on BN-PAGE. (A) Rat brain tissue lysates were resolved under typical blue native polyacrylamide gel electrophoresis (BN-PAGE) conditions. A total of 25 mg of rat brain tissue was homogenized in 1 mL of blue native page (BN-PAGE) sample buffer (50 mM BisTris, 6 N HCl, 50 mM NaCl, 10% vol/vol glycerol, 0.001% m/vol Ponceau S, pH ~ 7.2). Then either 1% m/vol digitonin (Dig.) or 0.5% vol/vol NP40 was added to the sample and incubated at 4 °C for 30 min. Samples were then centrifuged at 18 000g for 30 min at 4 °C, and the supernatant (S1) was retained. Protein concentration of the S1 was determined using bicinchoninic acid (BCA) assay (ThermoFisher). In total, 10 μg and 50 μg of brain tissue lysate protein were resolved using BN-PAGE. Proteins were then immunoblotted onto polyvinylidene fluoride (PVDF) membranes and blue dye removed by washing the membrane with 100% methanol. PVDF membranes were then stained with ponseau S, imaged, and subsequently probed with both polyclonal and monoclonal anti-α-synuclein antibodies. (B) Rat brain tissue was then disrupted under high tissue to buffer ratio (m/vol) and separated by BN-PAGE. To do this, 200 mg rat brain tissue was homogenized, as described above, in 1 mL of BN-PAGE sample buffer in the absence of detergents. A total of 5–50 μg of total protein input of the undiluted S1 fraction was loaded into the first six wells of BN-PAGE gel. The S1 sample was then serial diluted from 0.8 to 4 mg protein/mL and 30 μg of protein loaded into the remaining wells (last six lanes). (C) Rat brain tissue lysates separated by BN-PAGE in two dimensions. A total of 200 mg of rat brain tissue was homogenized as described above. In total, 30 μg of the lysate was then resolved on a 2.8–13%T BN-PAGE gel. The gel lane was then excised and cast into a 2.8–13%T BN-PAGE gel perpendicular to the first dimension direction of migration. The sample was separated again via 2.8–13%T BN-PAGE. Top panel represents the immunoblot of first dimension BN-PAGE and the middle panel depicts immunoblot following the second dimension BN-PAGE. Bottom panel depicts ponseau S staining of the blotted proteins from the second dimension BN-PAGE. All membranes were probed with anti-α-synuclein antibodies and the appropriate HRP conjugated secondary antibodies. All separations shown were conducted using 2.8–13%T linear gradient BN-PAGE gels. Blue arrows indicate the direction of migration during BN-PAGE electrophoresis. All data representative of 3–10 experiments.

Previous reports demonstrate high lysis concentrations preserve α-synuclein multimers. Therefore, we then resolved high concentration rat brain tissue lysates (200 mg tissue / 1 mL buffer) in the absence of detergents, and observed several α-synuclein species migrating to 50 kDa, ~100 kDa, 600 kDa, and 1048 kDa following BN-PAGE (Figure 24B). The mass shift of α-synuclein was sensitive to both total protein input, and to some extent, sample dilution. Under conditions of high sample concentration and/or high total protein input α-synuclein preferentially migrates to the 100 kDa BN-PAGE gel position.

At the highest total protein input (50 µg protein) the predominant species of α-synuclein had an apparent mass of 100 kDa and two other massive species, at 600 kDa and 1048 kDa, could clearly be observed, albeit far less abundant than the 100 kDa position. The mass shift of α-synuclein during BN-PAGE was not completely lost following dilution of the sample, suggesting that the sample concentration at initial tissue lysis was also a crucial factor for the observed BN-PAGE mass shift. Interestingly, once the majority of α-synuclein had shifted to 100 kDa, several minor bands remained at the original position (more clearly seen in Figure 25B, bottom panel) suggesting the original band may be comprised of several species with distinct masses. Together, these results show that α-synuclein migrates to several positions on BN-PAGE depending on how the sample is prepared and that an unknown dilution sensitive factor was responsible for this apparent mass shift.

Next, we tested whether the observed α-synuclein mass-shift was a progressive process (i.e. a product of electrophoresis) by separating tissue lysates via BN-PAGE in 2 dimensions. Following the first dimension separation of 30 µg brain lysate by BN-PAGE one main band at 50 kDa and a minor band just above ~100 kDa, were observed (Figure 24C, top panel), as was shown previously in figure 24B. When we subsequently separated the BN-PAGE gel lane by BN-PAGE perpendicular to the original migration direction we again observed two distinct α-synuclein species at 50 kDa and ~100 kDa (25C, middle panel), both at the original positions of the 1D-BN-PAGE. This suggests that the mass shift of α-synuclein during BN-PAGE was either due to a saturable process (i.e. non-progressive) or the observed massive species existed in the original sample. The lack of a

progressive mass shift during the second dimension BN-PAGE makes it highly unlikely that buffer components (i.e. coomassie blue g-250, Bis-Tris, aminocaporic acid, and tricine) were responsible for the observed mass shift.

5.2.2 Endogenous lipids determine α-synuclein migration distance during BN-PAGE.

An unknown biological factor or factors, lost upon dilution of the lysate and influenced the initial lysis concentration, were causing a mass shift of α-synuclein during BN-PAGE. Endogenous phospholipids are nearly insoluble amphiphiles that have the potential to form small soluble aggregates, termed micelles. Micelles form at threshold concentrations and are sensitive to dilution [302]. Since α-synuclein is known to multimerize upon phospholipid membrane binding [291], endogenous lipid micelle-α-synuclein complex could be responsible for the α-synuclein mass shift during BN-PAGE. To test whether endogenous lipids were responsible for the apparent mass shift of α-synuclein, we removed lipids from the brain tissue lysates and then resolved the lipid free proteins by BN-PAGE. We found α-synuclein formed one distinct 50 kDa species in the absence of endogenous lipids (Figure 25A) similar to what was observed in low-lysis concentration detergent free samples (See figure 24A). When 0.5% NP40 was added to lipid free proteins we observed a mass shift too approximately of ~100 kDa with only a small amount of the 50 kDa α-synuclein species remaining (visualized a small spots towards the perimeter of the lane). The mass shift was similar to that observed with BN-PAGE of NP40 tissue extracts (Figure 24A). NP40/brain-lipid mixed micelles were then added to the lipid free proteins and another mass shift was observed, with α-synuclein now

running at ~50, ~100, and ~200 kDa, similar to that observed in the detergent free high concentration samples (refer to figure 24B). Therefore, lipid and detergent micelles alone could produce a substantial apparent mass shift (+400% mass) during 1D-BNP. Interestingly, the micelles and endogenous lipids could be observed on the back of PVDF blots of the BN-PAGE following transfer, mostly stacked at the bottom of the membrane (Figure 25A, middle panel). Strikingly, the α-synuclein migration pattern was identical to the observed micelle migration pattern on the PVDF membrane. Ponceau S staining confirmed that the observed micelle positions were not highly proteinaceous (i.e. below ponseau S detection threshold, ~10 µg protein per lane). Taken together this data demonstrates that α-synuclein was migrating with endogenous lipids and/or detergent micelles during BN-PAGE, and this effect was likely responsible for mass shifts observed when tissue was disrupted at high concentrations.

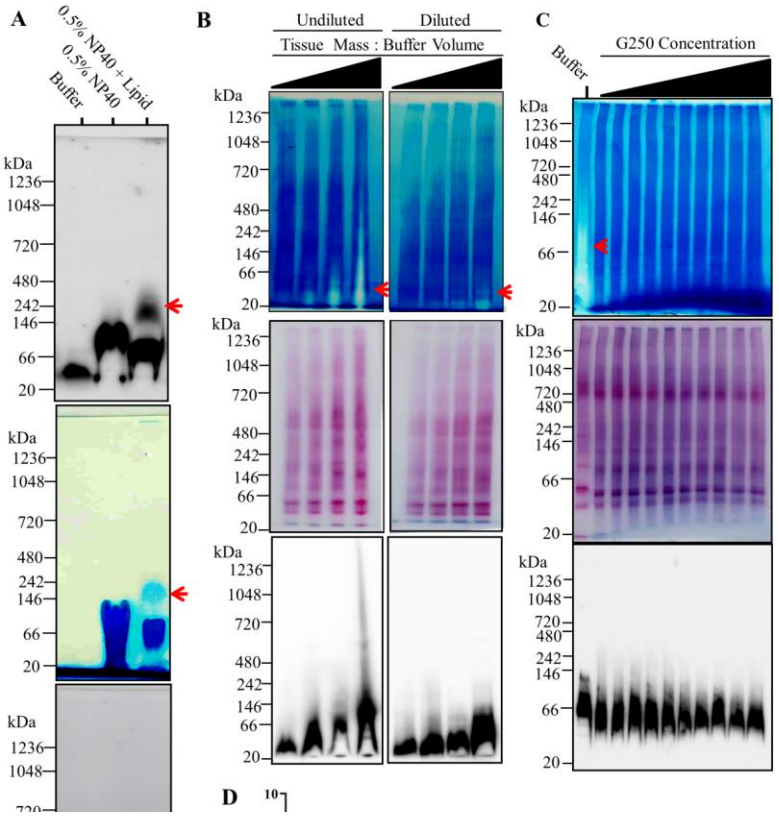
A
Buffer
0.5% NP40
0.5% NP40 + Lipid
kDa
1236
1048
720
480
242
146
66
20
B
Undiluted
Diluted
Tissue Mass : Buffer Volume
C
Buffer
G250 Concentration
D
10

Figure 25. Lipids determine α-synuclein migration pattern on BN-PAGE. Sample lipid content determines the migration of α-synuclein during BN-PAGE. (A) 200 mg rat brain tissue was homogenized in 1 mL of blue native page (BN-PAGE) sample buffer (50 mM BisTris, 6 N HCl, 50 mM NaCl, 10% vol/vol glycerol, 0.001% m/vol Ponceau S, pH ~ 7.2) and incubated on ice for 30 min. The sample was centrifuged then at 18 000g for 30 min, S1 retained, and protein content determined using bicinchoninic acid (BCA) assay. Samples were then adjusted to a final concentration of 2 mg protein/mL. A volume of 150 μL of the samples were mixed with 600 μL of methanol and 150 μL of chloroform. A volume of 450 μL of ultrapure water was then added to the sample and mixed thoroughly. Following centrifugation at 18 000g for 5 min, the upper aqueous phase was discarded and the lower phase resuspended in 600 μL of methanol. The sample was centrifuged at 18 000g for 5 min. The liquid was discarded and precipitate (proteins) retained. Separately, bulk lipids were isolated by homogenizing 1 g of rat brain tissue in a mixture of chloroform and methanol (2:1). Following sonication for 2 min, the homogenate was vortexed well, 4 mL of PBS added, and vortexed again. The sample was then allowed to sit for 5 min to allow the solution to separate into two phases. The organic phase containing the purified lipids was removed and dried under vacuum. The lipid pellet was then completely dissolved in 200 μL of 10% NP40. The precipitated lipid free proteins were dissolved in BN-PAGE sample buffer, BN-PAGE sample buffer containing 0.5% w/v NP40, or BN-PAGE sample buffer containing 0.5% w/v NP40 mixed lipid micelles. Samples were mixed thoroughly, incubated on ice for 30 min, and mixed thoroughly again. All samples were then centrifuged at 18 000g and the resulting 10 μg of protein of the soluble fraction resolved by BN-PAGE. Top panel depicts immunobloting of samples with anti-α-synuclein antibody. Middle panel depicts the white light image of polyvinylidene fluoride (PVDF) membrane immediately following transfer of the BN-PAGE gel. Bottom panel depicts ponseau S staining of PVDF membrane following the removal of G250 from the membrane by washing in 100% methanol for ~5 min. (B) 25, 50, 100, and 200 mg of rat brain tissue was homogenized in 1 mL of BN-PAGE sample buffer as described above and resolved via BN-PAGE. A total of 30 μg of total proteins were resolved in each lane without sample dilution (left column panels) and following dilution of samples to 2 mg protein/mL (right column panels). Top row depicts white light image of PVDF membrane immediately following transfer. Middle row depicts subsequent ponseau S staining of the PVDF membrane following removal of G-250. Bottom row depicts the immunoreactivity of α-synuclein. (C) Increasing concentrations of G-250 (0–2%) was added to rat brain tissue lyates from high concentration homogenization conditions (200 μg tissue/mL buffer). A total of 30 μg of protein was then resolved via BN-PAGE. Top panel depicts white light image of PVDF membrane. Middle row depicts ponseau S staining of PVDF membrane following removal of G-250. Bottom row dipicts the immunoreactivity of alpha-synuclein. (D) Lipid to protein content of insoluble fraction following tissue homogenization at different tissue to buffer ratios.

When we resolved brain lipid/detergent mixed micelles by BN-PAGE we noticed that they could be clearly visualized following transfer to PVDF membranes (Figure 25A,

middle panel). Next we asked whether a similar pattern could be observed when tissue was lysed at high concentrations. Such a pattern would presumably confirm the hypothesis of endogenous lipid micelles being responsible for the observed mass shift during BN-PAGE. Results show that indeed the same type of pattern was observable most noticeably when tissue was lysed at high concentrations (Figure 25B, top panel). As with the lipid/detergent micelles, α-synuclein migration patterned mirrored the apparent endogenous lipid structures (Figure 25B, bottom panel) following BN-PAGE. Dilution of the samples did not abolish the visualization of the lipids, but instead resulted in their shift to lower, discrete bands. Again, α-synuclein migration mirrored the position shift of the endogenous lipid micelles upon sample dilution. Gross protein distribution was relatively unaffected by the lipid structures migrating on BN-PAGE (Figure 25B, Middle panel). Together, these observations demonstrate that α-synuclein was co-migrating with soluble endogenous lipid structures.

Coomassie G-250 incorporates into detergent micelles [303], imparting a net negative charge, carrying them to the dye front during BN-PAGE, ultimately preventing distortion of protein [298]. We wanted to determine whether G-250 could alter the distribution of the apparent endogenous lipid micelles and produce a corresponding mass shift in α-synuclein. When 0.01-1% G250 was added directly to samples from high concentration lysis conditions, the original lipid smear on the PVDF membrane was no longer observable (Figure 25C, Top Panel). Gross protein migration appeared unaffected by G-250 treatments, but α-synuclein migration became more focused to a position of 50

kDa as the G-250 concentration increased. Therefore, excess G-250 added directly to the sample prevents the lipid mediated mass shift during BN-PAGE.

Lipids extracted under high concentration lysis conditions determined the electrophoretic mobility of α-synuclein during BN-PAGE; however it was unclear whether high concentration tissue lysis resulted in increased lipid extraction from tissue. To directly address this we measured the lipid and protein content in the remaining insoluble pellet (P1) at several lysis concentrations (Figure 25D). Results showed a sharp decrease in the lipid/protein ratio in the insoluble pellet when tissue was disrupted at high concentrations (i.e. 50-200 mg tissue / mL buffer). Interestingly, all lysis conditions above 50 mg tissue / mL buffer had similar lipid extraction efficacy. We attempted to directly measure the lipid content in S1 fractions but the lipid concentration was near the assay's threshold for detection (~5 µg lipid) and we were unable to obtain quantitative results. Even without the S1 lipid concentration it was clear that high lysis concentrations were increasing ratio of lipid to protein extracted from tissue.

Mass shift of a protein during BN-PAGE electrophoresis is commonly interpreted as a formation of protein complexes. However, as we have demonstrated here, the electrophoretic mobility of α-synuclein during BN-PAGE can vary drastically depending on sample preparation (specifically sample lipid content). A previous report demonstrated a similar effect for the mitochondrial protein carrier protein AAC319 [304]. Therefore, BN-PAGE alone is insufficient to accurately detect and describe soluble α-synuclein multimers.

5.2.3 α-Synuclein multimers can be resolved via SDS-PAGE following in-gel chemical crosslinking

Chemical crosslinking methods can be used to selectively capture protein-protein interactions. Once protein-protein interactions are captured the samples can be separated in the presence of SDS micelles via traditional SDS-PAGE. SDS solubilizes lipids [305], denatures proteins [306], thereby avoiding complications involved with BN-PAGE when separating lipid binding proteins, in this case α-synuclein. Therefore, following separation of tissue lysates via BN-PAGE, we incubated BN-PAGE gel lanes in several crosslinking solutions and then resolved them using 2D-SDS-PAGE (Figure 26A). Results showed that crosslinking with 0.1 mM DSP, 0.1 mM DTSSP (not shown), 1% Glutaraldehyde, 0.1 mM DSG, but not 1% PFA, produced several high molecular weight α-synuclein products in addition to the monomer detected following 2D-SDS-PAGE. We also observed two massive α-synuclein species of low abundance that were only captured and detectable with DSG or DSP. These elute from the BN-PAGE positions corresponding to the two high molecular weight species (~600 kDa and ~1048 kDa) clearly seen following BN-PAGE in figure 25B. Both species were far less massive on the SDS-PAGE (~80 kDa, and 170 kDa, respectively). Because DSP and DSG crosslinking is relatively specific for protein-protein interactions, the 600 kDa and 1048 kDa apparent masses on BN-PAGE were like due to processes other than true multimerization (e.g. lipid/detergent binding), as opposed to true multimers of 600 and 1048 kDa. PFA was ineffective at capturing α-synuclein multimers most likely because the spacer-arm length of PFA is relatively short (2Å) while the effective crosslinkers had much longer spacer arm length (≥7Å). Several other reports have

also demonstrated the successful capture of α-synuclein multimers using crosslinkers with similar spacer-arm length [127, 292-294]

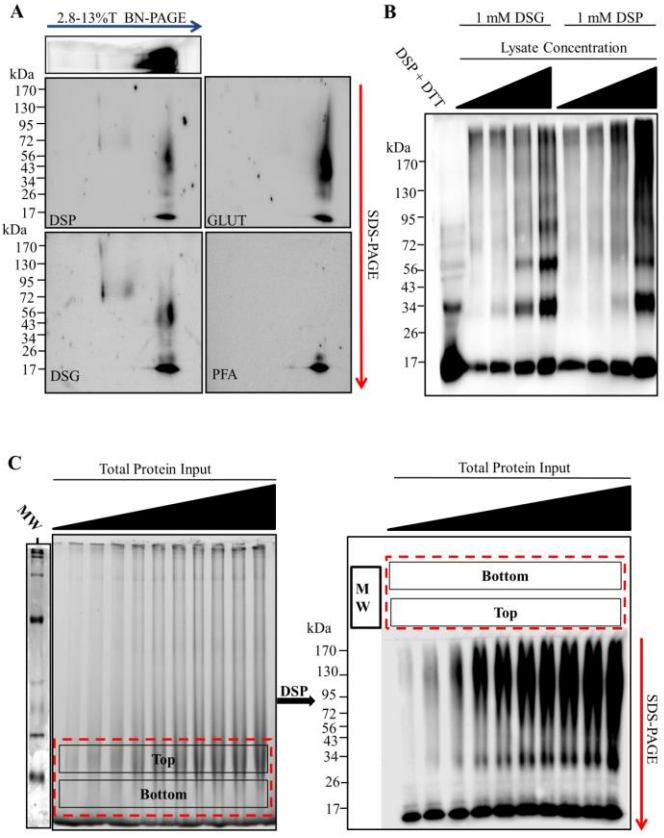
A
2.8-13%T BN-PAGE
kDa
170
130
95
72
56
43
34
26
17
DSP
GLUT
DSG
PFA
SDS-PAGE
B
1 mM DSG
1 mM DSP
Lysate Concentration
DSP + DTT
C
Total Protein Input
MW
Top
Bottom
DSP
Total Protein Input
M
W
Bottom
Top
SDS-PAGE

Figure 26. Multimer-PAGE format. Rat brain tissue was homogenized in blue native page (BN-PAGE) sample buffer (50 mM Bis-Tris, 6N HCl, 50 mM NaCl, 10% vol/vol glycerol, 0.001% m/vol Ponceau S, pH 7.2) at a ratio of 200 mg of wet tissue to 1 mL of buffer. Following centrifugation at 18 000g for 30 min at 4 °C, the protein content of the S1 fraction was determined by bicinchoninic acid (BCA) assay. (A) 30μg protein per lane was resolved via BN-PAGE. Individual lanes were then excised, washed with phosphate buffered saline pH 7.4 (PBS), and incubated in PBS solutions containing 0.1 mM dithiobis(succinimidyl propionate) (DSP), 0.1 mM disuccinimidyl glutarate (DSG), 1% glutaraldehyde (GLUT), or 1% paraformaldehyde (PFA) for 30 min at 4 °C. The excised gel pieces were then cast into SDS-PAGE and run perpendicular to the original migration direction. (B) Rat brain tissue was homogenized in PBS at a ratio of 200 mg wet tissue/1 mL buffer. Samples were centrifuged at 18 000g for 30 min at 4 °C. The sample was then diluted from 4 to 1 mg protein/mL. Following dilution, 1 mM DSG or 1 mM DSP was added to the samples and incubated for 10 min at 4 °C. The reaction was then quenched with 100 mM Tris- HCl pH 8.0 for 15 min at 4 °C. The 5× SDS-PAGE sample buffer was added to each sample, mixed well, and 10 μg of protein loaded into each lane of a 3–16%T SDS-PAGE gel. The 5 mM DTT was added to the 4 mg protein/mL DSP cross-linked sample to cleave the cross-linker (lane 1). (C) Increasing concentrations of total soluble protein were resolved via BN-PAGE (from the left; 4, 8, 12, 16, 20, 24, 28, 32, 36, and 40 μg of protein). BN-PAGE gel was cut above and below the 66 kDa molecular weight marker (red dotted box), washed with PBS, incubated with 0.1 mM DSP, and cast into a SDS-PAGE gel. Left panel depicts white light image of gel following BN-PAGE. Right panel depicts immunoblotting of the second dimension SDS-PAGE. All blots probed with rabbit polyclonal anti-α-synuclein antibody and appropriate horse radish peroxidase (HRP) conjugated secondary antibody. Images are representative of 3–5 separate experiments.

It remained unclear whether any α-synuclein multimers existed in solution prior to electrophoresis or were products of BN-PAGE. To address this, we directly crosslinked the soluble brain extracts using 1 mM DSP or DSG, and resolved them via 4-16% SDS-PAGE (Figure 26B). Results show that α-synuclein multimers could be detected in lystates using both DSP and DSG crosslinkers. These multimers ranged from 34 kda to >170 kDa, and appeared to be formed predominantly by diffusion mediated crosslinking. Serial dilution of the sample prior to crosslinking prevented the capture of multimeric species, and for unclear reasons, also resulted in reduced immunodetection of the monomer (i.e. 17 kDa). Because directly crosslinking the sample did not produce α-synuclein multimers

comparable to the in-gel crossslinking of BN-PAGE, the α-synuclein multimers observed following BN-PAGE were most likely, to some extent, products of electrophoresis.

Once we had determined that several multimers were found at the 50-100 kDa positions of the BN-PAGE gel, we then "scaled up" and optimized the procedure to make comparisons of many samples more reliable and less time consuming. To do this we exploited the observation that under most sample conditions nearly all native α-synuclein migrated to the ~50-100 kDa position on the BN-PAGE gel, and simply cut the gel just below the 66 kDa marker and just at the 146 kDa marker and ran the 2D-SDS-PAGE parallel to the BN-PAGE lanes (Figure 26C). The excised gel should encompass the 40-146 kDa positions, to ensure all α-synuclein is resolved by 2D-SDS-PAGE. This technique allowed the experimental conditions to be nearly identical between samples. Using this "scaled up" procedure would allow the crosslinked α-synuclein products to form more discrete bands when separated by 2D-SDS-PAGE, as opposed to smeared blebs observed with running the entire excised lanes, making them easier to visualize and compare. Several experimental conditions could now be run on single gel making comparisons between the extracts simple and reproducible. Furthermore, several multimers at the gel position could be quantified simultaneously, as opposed to only the typically two α-synuclein species observed following BN-PAGE. For simplicity, we termed the entire process as "multimer-PAGE," with the presented blots representing the blotted 2D-SDS-PAGE of crosslinked native complexes.

5.2.4 Optimization of in-gel chemical crosslinking

Diffusion based chemical crosslinking can randomly covalently bind proteins forming progressively massive products only limited by the diffusion of the protein in solution. Protocols using chemical crosslinking of proteins should be carefully validated to avoid diffusion based products, unless the product is desired, as was later exploited here to produce the α-synuclein multimer molecular weight "standard" (see figure 27E). Generally, crosslinker concentration, time of crosslinking, and the molecular structure of the crosslinker are manipulated to determine true products (i.e. those that existed prior to crosslinking) vs. diffusion based (i.e. those that formed during crosslinking). Here we tested two crosslinking molecules DSP and DSG, both of which have been used in tissue and solution to stabilize α-synuclein multimers 6. Crosslinking the excised BN-PAGE gel with as little as 0.1 mM DSP (Figure 27A) or DSG (Figure 27B) was sufficient to capture α-synuclein multimers. For reasons that are unclear, increasing DSG concentrations appeared to reduce the detection of both multimeric and monomeric α-synuclein. Because of the unusual behavior of DSG during in-gel crosslinking, we chose to use 0.1 mM DSP for the remaining studies. The main α-synuclein species observed following in-gel crosslinking was smeared between 34-130 kDa on the SDS-PAGE. Next we tested what crosslinker incubation time was optimal to capture the multimers (Figure 28C). Gels incubated with 0.1 mM DSP for 5 min preferentially capture αS80. The crosslinking time to capture multimers was so rapid it strongly suggested that diffusion based crosslinking was not a main driving factor of α-synuclein multimers detection following multimer-PAGE protocol. Crosslinking produced nearly equal multimer abundance at 30 and 45 min, and therefore 30 min was chosen for the remaining studies.

During validation of the multimer-PAGE protocol we observed that optimal resolution of crosslinked products during SDS-PAGE requires that excised gel pieces be cast directly into the SDS-PAGE gel as described in the methods. Alternatively, when gel pieces were placed directly on top of a preformed SDS-PAGE gel (also mentioned in methods) lane distortion became evident (See Figure 27C) but did not appear to effect quantification. Therefore, this method can be used when sample processing speed is crucial, as it is more time intensive to cast excised gels directly into SDS-PAGE gels. We also observed that using a 12%T SDS-PAGE with a stacking layer ultimately provided superior band resolution to 3-16%T SDS-PAGE gels.

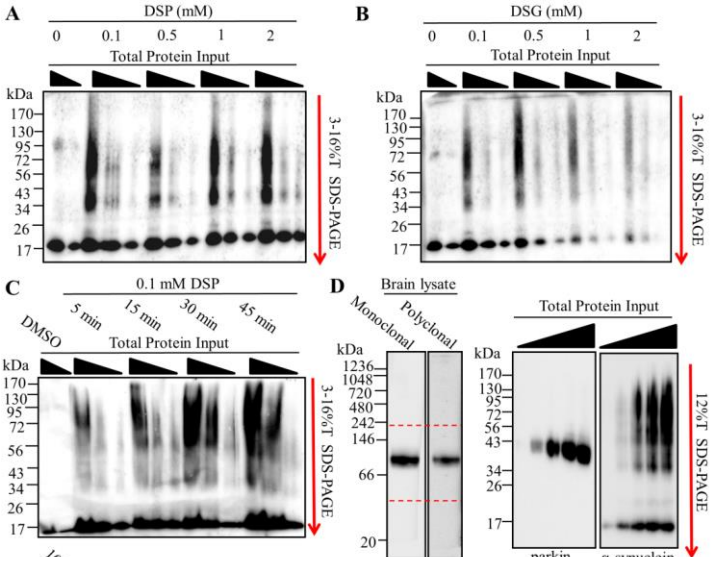
A
DSP (mM)
0
0.1
0.5
1
2
Total Protein Input
kDa
170
130
95
72
56
43
34
26
17
3-16%T SDS-PAGE
B
DSG (mM)
0
0.1
0.5
1
2
Total Protein Input
kDa
170
130
95
72
56
43
34
26
17
3-16%T SDS-PAGE
C
0.1 mM DSP
DMSO
5 min
15 min
30 min
45 min
Total Protein Input
kDa
170
130
95
72
56
43
34
26
17
3-16%T SDS-PAGE
D
Brain lysate
Monoclonal
Polyclonal
kDa
1236
1048
720
480
242
146
66
20
Total Protein Input
kDa
170
130
95
72
56
43
34
26
17
12%T SDS-PAGE

.Figure 27. Optimization of in-gel chemical cross-linking and multimer-PAGE gel format. 10, 20, and 40 μg of rat soluble brain tissue lysate were resolved by blue native polyacrylamide electrophoresis (BN-PAGE). 2.8–13% linear BN-PAGE gels were cut just above and below the 66 kDa molecular weight marker following electrophoresis. The excised gel pieces were washed in phosphate buffered saline pH 7.4 (PBS) for 30 min at 4 °C. Excised BN-PAGE gel pieces were incubated with cross-linking solution and cast directly to SDS-PAGE gels. The cross-linked proteins were resolved by SDS-PAGE perpendicular to the original direction of sample migration. SDS-PAGE gels were then immunoblotted. Excised gel pieces incubated with either (A) 0.1–2 mM dithiobis (succinimidyl propionate) (DSP) (B) or 0.1–2 mM disuccinimidyl glutarate (DSG). (C) Excised gel pieces incubated with 0.1 mM DSP for 5–45 min. (D) 30 μg of rat brain tissue lysate separated by BN-PAGE, blotted, and probed for parkin (Left panel). 10, 20, 30, and 40 μg of lysate protein resolved by BN-PAGE. BN-PAGE gel was excised between 40 and 242 kDa positions, incubated with 0.1 mM DSP for 30 min at 4 °C, and resolved via SDS-PAGE. Immunoblotting for parkin and α-synuclein shown (Right panels). (E) Purified α-synuclein was dissolved in PBS and diluted to a concentration of 5 mg protein/mL. The 2 mM DSP was added to the sample and incubated for 10 min at 4 °C. The reaction was quenched with 100 mM Tris-HCl pH 8.0. 200 ng of α-synuclein resolved on 12%T SDS-PAGE. (F) Increasing protein input resolved by 2.8–13%T BN-PAGE and 6%T BN-PAGE. Samples were allowed to migrate the length of the 2.8–13%T BN-PAGE and the 66 kDa gel position excised as before. In contrast, samples were allowed to migrate on approximately 2 cm into the resolving gel on the 6%T BN-PAGE, and this 2 cm gel piece excised. In-gel cross-linking was performed and both excised gel pieces resolved via SDS-PAGE. Bands are labeled with their apparent corresponding species according the standard (E). Dotted red lines indicate position of gel excision. All blots probed with rabbit polyclonal anti-α-synuclein antibody and appropriate horse radish peroxidase (HRP) conjugated secondary antibody. Images are representative of three separate experiments.

Next we tested the specificity of multimer-PAGE for α-synuclein. To do this we ran the multimer-PAGE protocol and probed for the E3 ligase parkin, a small globular soluble protein not known to interact with lipids or form progressively massive multimers. We found that parkin also migrates to approximately the same BN-PAGE gel position as α-synuclein (Figure 27D), making it a good internal control. Following ultimer-PAGE we observed no detectable crosslinked parkin multimers following multimer-PAGE protocol. Instead we saw one species located at ~43 kDa. This position is slightly below the 50 kDa

position where parkin is normally found. The slight discrepancy in MW of parkin is likely due to the stabilization of a compact tertiary structure of parkin by chemical crosslinking, which can increase proteins mobility on SDS-PAGE [307, 308]. The migration of parkin during multimer-PAGE was in stark contrast to α-synuclein, which under the same experimental conditions produced abundant multimers. This finding demonstrates that multimer-PAGE is relatively specific for α-synuclein and gross diffusion based protein crosslinking was not a key factor.

To determine stoichiometry of α-synuclein multimers following multimer-PAGE we generated a molecular weight "standard" by crosslinking concentrated purified α-synuclein (5 mg purified α-synuclein / 1 mL) with 2 mM DSP and separated the resulting products by SDS-PAGE (Figure 27E). Results show five species at gel positions corresponding to the molecular weights of 17 (αS17), 35 (αS35), 50 (αS56), 80 (αS80), and 100 kDa (αS100). α-Synuclein was detected above 130 kDa position but was poorly resolved by SDS-PAGE, and therefore was disregarded as a undefined α-synuclein multimers species. The observed multimers were likely captured primarily via diffusion controlled crosslinking because there was an inverse relationship between multimers abundance and the observed molecular weight, which likely occurs if multimers were crosslinked in a step-wise fashion.

We next wanted to determine the optimal polyacrylamide gel format for multimer-PAGE (Figure 27F). We found that 6%T BN-PAGE gel followed by 12%T SDS-PAGE gel provided the greatest resolution of α-synuclein multimers with the least effort. We simply ran the 6%T BN-PAGE gel (with 2.8%T well gel) at 100V until all soluble proteins

had migrated ~2 cm into the resolving gel. The gel was excised as before and cast into the 12%T SDS-PAGE. The new gel format had several key advantages; 1) avoided hand pouring linear gradient polyacrylamide gels which can be time-consuming and have poor reproducibility 2) ensured all α-synuclein (and other proteins) in the sample were resolved by multimer-PAGE 3) crosslinked products migrated out of a single 6%T BN-PAGE gel to the SDS-PAGE gel more consistently allowing for increased band resolution 4) allowed for investigation of protein complexes other that α-synuclein without extensive validation of BN-PAGE migration (i.e. do not need to know a BN-PAGE migration pattern) 5) faster BN-PAGE run times (~30 min at 100V).

5.2.5 Optimization of brain tissue sample preparation and separation

Once in-gel crosslinking and electrophoresis conditions were optimized we then tested the influence of sample preparation on multimer-PAGE output. First, we investigated whether lipid content of the sample would alter the observed multimer pattern. We had already observed that α-synuclein migrated with endogenous brain lipids during BN-PAGE (Figure 25A, B, and C) however when we assessed these samples using multimer-PAGE we found little evidence of any multimeric α-synuclein species in any of the samples (Figure 28A). Neither proteins alone nor proteins reconstituted into lipid/detergent micelles produced detectable multimers. This suggests that although α-synuclein was strongly interacting with lipid/detergent mixed micelles the binding to these micelles alone was insufficient to produce multimers. Furthermore, multimers observed following multimer-PAGE of tissue lysates were likely not due to protein-lipid crosslinking, as these products would then be predicted to be in abundance in the presence

of excess brain lipids. However, phosphatidalserine and phosphatidylethanolamine both contain primary amines so protein-lipid crosslinked products cannot be conclusively ruled

out.

Figure 28. Effect of sample preparation on observed multimer abundance. Sample preparation determines observed multimer abudance and pattern. Rat brain tissue was

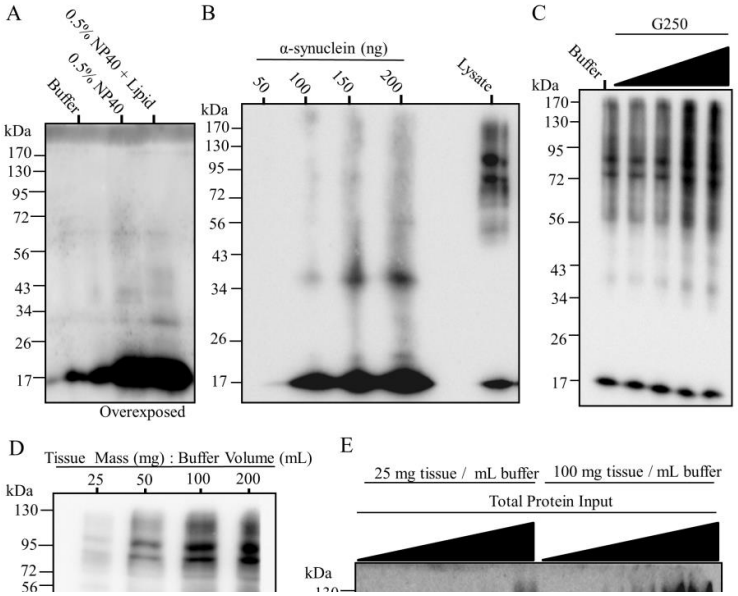

homogenized in blue native page (BN-PAGE) sample buffer (50 mM BisTris, 6 N HCL, 50 mM NaCl, 10% vol/vol glycerol, 0.001% m/vol Ponseau S, pH 7.2) at a ratio of 200 mg wet tissue/1 mL buffer. Following centrifugation at 18 000g for 30 min at 4 °C, the protein content of the S1 fraction was determined by the bicinchoninic acid (BCA) assay. (A) 300 μg proteins from the sample was precipitated and resusupended in either BN-PAGE sample buffer containing either 0.5% NP40 or 0.5% NP40 mixed lipid micelles. Protein (10 μg) was resolved by multimer-PAGE. (B) 50–200 ng of purified α-synuclein and 30 μg of brain tissue lysate were resolved via multimer-PAGE. (C) 0–1% G250 directly added to S1 samples. 30 μg of these samples was separated by multimer-PAGE. (D) Rat brain tissue was disrupted in BN-PAGE sample buffer at a tissue mass to buffer ratio of 25, 50, 100, and 200. A total of 30 μg of protein from each lysis condition was resolved via multimer-PAGE. SDS-PAGE of S1 and P1 found in the bottom two panels. (E) Rat brain tissue was homogenized in a tissue mass to a buffer ratio of 25 and 100. Increasing total protein input was then resolved via multimer-PAGE. (From the left: 5, 10, 20, 30, and 40 μg protein). All samples were centrifuged at 18,000g for 30 min prior to BN-PAGE. All blots probed with rabbit polyclonal anti-α-synuclein antibody and appropriate horse radish peroxidase (HRP) conjugated secondary antibody. Images are representative of 2–4 separate experiments.

Since recombining separated components (i.e. lipids and proteins) of complex biological samples did not produce detectable multimers by BN-PAGE, we wanted to determine whether α-synuclein alone could assembly into multimers during multimer-PAGE. To test this, we resolved increasing α-synuclein input (50-200 ng) by multimer-PAGE and found multimers, to a limited extent, could be detected (Figure 28B). However, multimers from purified α-synuclein required excess protein input, and were qualitatively distinct from those found in tissue lysates. High molecular weight α-synuclein multimers (i.e. αS56, αS80, and αS100) are preferentially detected in lysates while αS35 is the primary multimer detected when using purified α-synuclein. The multimer pattern when using purified α-synuclein was indicative of diffusion based crosslinking and distinct from multimers from lysates, as previously reported [294]. Therefore, α-synuclein was insufficient to produce the observed multimers in complex biological samples.

G-250 incorporates into micelles and can form micelle like structures in water, and therefore we wanted to know whether G-250 could affect multimer detection (Figure 28C). G-250 added directly to the sample produced increased multimer abundance only when G-250 concentrations were relatively high (0.5% and 1%). G-250 concentrations below 0.5% (first three lanes) were similar in multimer abundance and distribution. Because samples are not typically exposed to G-250 concentrations above 0.5% during multimer-PAGE protocol, this effect is likely minimal.

Previously we demonstrated that disruption of brain tissue at high concentrations increased relative lipid extraction and altered the migration of α-synuclein during BN-PAGE (See Figure 26D, B), so we explored whether the ratio of tissue to lysis buffer influenced the abundance of observed multimers. Results showed that when tissue was disrupted at increasing concentrations multimers in the S1 fraction were in greater abundance but the pattern was relatively unchanged (Figure 28D). αS80 and αS100 appeared to be particularly abundant with αS56 being lower in abundance. Interestingly, the total amount of α-synuclein extracted (i.e. S1 fraction) per protein was similar when 50 mg tissue per mL buffer or greater was used for tissue lysis. Despite the similar extraction efficacy, multimers were clearly more abundant. Both the 100 and 200 mg tissue per mL buffer showed nearly the same multimer abundance, and therefore 100 mg tissue per mL buffer condition was selected for multimer quantification.

Few multimers were detected at typical tissue lysis concentration (i.e. 25 mg tissue/ mL buffer) when 20 µg total protein was input into multimer-PAGE (See figure 28D). However, our previous data suggested that, to some extent, α-synuclein multimers were

being formed during electrophoresis (See Figure 26C and B). Therefore, we next asked whether increasing sample input of from low and high lysis concentrations would produce observable multimers. Results show that as sample input increased, multimers became more abundant in both the low and high concentration tissue lysis samples (Figure 28E). α-Synuclein multimers were detectable with 10 µg protein in the high concentration lysis but required 15 µg following low concentration tissue lysis. Multimer-abundance increased disproportionally to monomer abundance following both lysis concentrations. This observation, as seen previously (Figure 26C), seems to support the idea that multimers were forming during multimer-PAGE and do not exist in the original sample. Therefore, although lysis at high concentration allows for ease of multimer detection, it doesn't seem absolutely necessary to produce multimers given sample input into the multimer-PAGE is sufficiently high.

5.2.6 Using multimer-PAGE to measure the stoichiometry of α-synuclein multimers in biological samples

Next we wanted to determine a standardized method to analyze the data produced by multimer-PAGE. To do this we exploited the observation that the ratio of αS80 to αS17 increases linearly with increasing protein input into multimer-PAGE (see figure 26C). This phenomenon allowed the assessment of multimerization while avoiding variability from factors such as relative α-synuclein abundance in the sample.

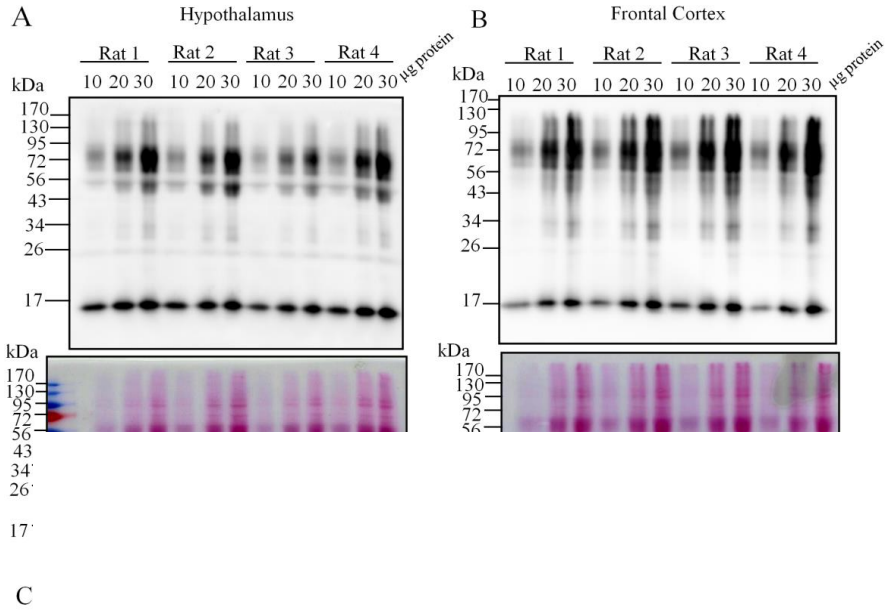

Figure 29. Quantification of α-synuclein multimers using multimer-PAGE. Multimer-PAGE can be used to compare many complex biological samples. Brain tissue from 4 male Sprague–Dawley rats was weighed and homogenized in BN-PAGE sample buffer (100 mg tissue/mL buffer). Samples were centrifuged at 18 000g for 30 min at 4 °C. The supernatant was retained and 10, 20, and 30 μg of protein separated by multimer-PAGE. Multimer-PAGE of samples from the hypothalamus (A) and cortex (B). Top panels depict immunoblotting for α-synuclein. Bottom panels depict ponseau S stain of multimer-PAGE blots prior to immunoprobe. (C) The ratio of 17 kDa (αS17) to 80 kDa (αS80) α-synuclein was calculated using ImageJ software and values are plotted for each protein input. The R2 for each line is depicted on the graph. (D) Bar graph comparing the multimer curve slopes between the two brain regions. ("Rate of multimer formation" = slope of multimer curves. *students t test, $t(6) = 11.29$, $p < 0.0001$, $n = 4$).

We generated a multimer curve by separating 10, 20, and 30 μg protein of lysates from the rat hypothalamus (Figure 29A) and frontal cortex (Figure 29B) via multimer-PAGE. Care was taken to ensure tissue was disrupted in 1 mL BN-PAGE sample buffer per 100 mg tissue. Once the multimer curve was generated (Figure 29C) we could plot the ratio of αS80 to αS17 at each protein input. The corresponding slope of the multimer curve could then be calculated and compared. We refer to the calculated slope as the rate of multimer formation because the line likely represents the propensity of α-synuclein to form multimers during multimer-PAGE. We then compared multimer formation between two distict brain regions (29D). Results show, that within each brain region, animals had similar rate of multimer formation, resulting in very little variability. However, when we compared the two brain regions there was significant (Students t-test, $t(6) = 11.29$, $p<0.0001$, $n = 4$) reduction in the rate of multimer formation in the hypothalamus when compared to the frontal cortex. The significance the regional difference in multimer formation is not realized here, but the method appears to provide reproducible and accurate measurement of the α-synuclein multimer abundance between different biological samples.

5.2.7 Final optimized protocol for α-synuclein multimer-PAGE

The final optimized protocol for α-synuclein multimer-PAGE involves four key steps and takes approximately 1 day to complete (Figure 30). With this protocol we could routinely measure and compare several high molecular weight α-synuclein species across complex biological samples. Effort was taken to ensure the process wasn't overly complicated and could be conducted using common lab equipment. Although this protocol was optimized for α-synuclein detection it should be emphasized that experimentation with protein separation, crosslinking, and sample handing conditions could potentially help answer questions about numerous other protein complexes. This technique likely has broad applicability to the study of the stoichiometry of numerous other protein-complexes. Although the current protocol is limited to measuring "low-n" multimers consisting of ~10 or less α-synuclein molecules, the SDS-PAGE gel format could be easily adjusted to study ever more massive multimeric species.

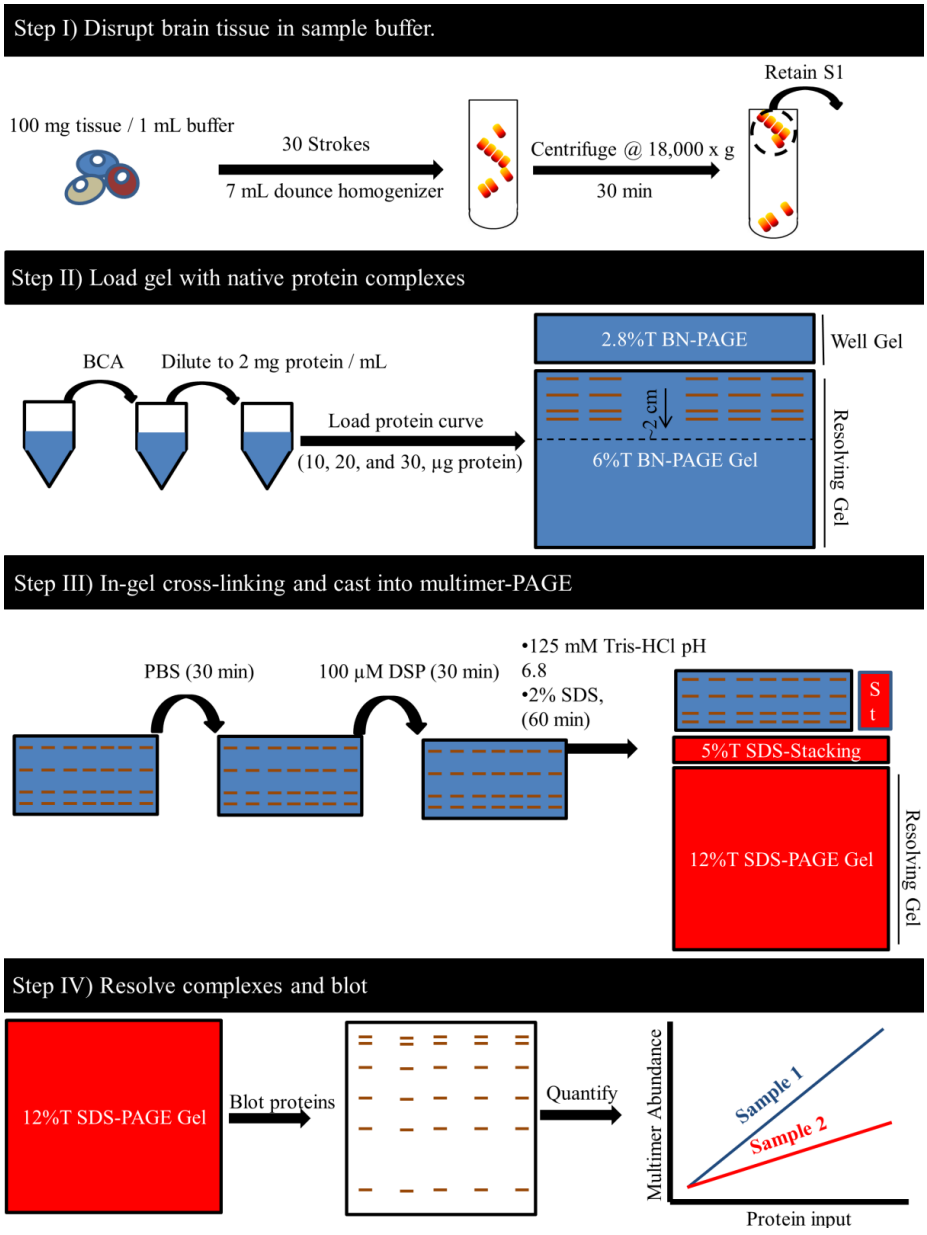
Step I) Disrupt brain tissue in sample buffer.
100 mg tissue / 1 mL buffer
30 Strokes
7 mL dounce homogenizer
Centrifuge @ 18,000 x g
30 min
Retain S1
Step II) Load gel with native protein complexes
BCA
Dilute to 2 mg protein / mL
Load protein curve
(10, 20, and 30, µg protein)
2.8%T BN-PAGE
Well Gel
~2 cm
6%T BN-PAGE Gel
Resolving Gel
Step III) In-gel cross-linking and cast into multimer-PAGE
PBS (30 min)
100 µM DSP (30 min)
•125 mM Tris-HCl pH 6.8
•2% SDS,
(60 min)
St
5%T SDS-Stacking
12%T SDS-PAGE Gel
Resolving Gel
Step IV) Resolve complexes and blot
12%T SDS-PAGE Gel
Blot proteins
Quantify
Multimer Abundance
Sample 1
Sample 2
Protein input

Figure 30. Final optimized protocol for α-synuclein multimer-PAGE. First, rat brain tissue was homogenized in blue native page electrophoresis (BN-PAGE) sample buffer (50 mM BisTris, 6 N HCl, 50 mM NaCl, 10% vol/vol glycerol, 0.001% m/vol Ponseau S, pH ~7.2) at a specific buffer to tissue ratio (100 mg of wet tissue per 1 mL of buffer) (top panel). Homogenization was conducted on ice and consisted of 30 gentle strokes in a 7 mL glass dounce homogenizer. Samples were then centrifuged for 30 min at 18 000g, and the supernatant (S1) containing the soluble biological molecules was retained. Samples were then prepared to load into a BN-PAGE gel (see Step II). To do this, protein content of this sample was then determined using bicinchoninic acid (BCA) assay and the S1 diluted to 2 mg protein/mL using BN-PAGE sample buffer. In order to compare samples, 10, 20, and 30 μg of each sample was loaded into a 6%T BN-PAGE gel. A 100 V potential was applied to the gel until the sample had migrated to approximately 2 cm into the resolving layer of the 6%T BN-PAGE gel. The gel was then removed, well gel discarded, and the 2 cm section of gel containing the samples was excised. The excised gel piece was then washed in phosphate buffered saline pH 7.4 (PBS) for approximately 30 min at 4 °C (see step III). The PBS solution should be changed at least 3 times during the washing. Then the gel piece is placed in 10 mL of PBS and 40 μL of 25 mM dithiobis(succinimidyl propionate) (DSP) dissolved in DMSO added to the PBS. The gel is incubated in this cross-linking solution for 30 min at 4 °C, then the solution is discarded and replaced with quenching solution (125 mM Tris-HCL pH 6.8, 2% SDS) and incubated for 60 min at room temperature. The excised gel piece is then placed between glass plates and cast into 12%T SDS-PAGE gel. A constant voltage of 100 V is then applied to the gel using SDS-PAGE running buffer until coomassie dye has left the end of the gel. The 12%T SDS-PAGE gel was then electroblotted onto polyvinylidene fluoride (PVDF) membranes and probed with several α-synuclein antibodies (see Step IV). Densitometry analysis can then be conducted on the observed bands using imageJ software. The slope of the lines plotting multimer abundance and total protein input could be used to compare samples. ("ST" = well for molecular weight standard).

5.3 Conclusions

α-Synuclein formed several soluble multimers during BN-PAGE provided that lipid interactions were preserved during tissue lysis. Preservation of lipid interactions likely stabilized α-synuclein secondary structure [295, 309] subsequently "seeding" multimer formation [291] and/or stabilizing existing multimers. We found that a practical method to preserve lipid interactions involved disrupting the tissue in small buffer volumes (i.e. 50-200 mg tissue / mL buffer) in the absence of detergents. The high ratio of tissue to buffer increased the extraction of lipids from tissue. Extracted lipids behaved like endogenous

micelles. Although we did not provide a direct description of these micelles, they are logically consistent with the fact that free phospholipids are almost completely insoluble in water and the lipid structures migrated on BN-PAGE as complexes (i.e. above the dye front) and not monomers (i.e. with the dye front). The α-synuclein species observed following the multimer-PAGE, once optimized, were in general agreement with the previously reported α-synuclein multimers [290, 292-294] , and distinct from those produced by diffusion mediated protein crosslinking.

Future studies are needed to explore the applicability of the multimer-PAGE technique. Studies that may be fruitful should focus on the possible heterogeneity (e.g. differences in protein folding, post-translational modification etc.) of the observed α-synuclein multimers and how this may confer/abolish stability. Liquid chromatography Mass Spectrometry (LC-MS) would be particularly useful in identifying possible heterogeneity post-translational modifications between multimers; although mass adjustments to account for the crosslinker would need to be applied, as has been done numerous reports [310]. LC-MS may also allow for the identification of the specific lipid(s) interacting with α-synuclein [311] . It is also important to further validate multimer-PAGE across several PD models to determine its usefulness in describing the pathology of the disease.

Multimer-PAGE provides several unique advantages over in-solution crosslinking or native-PAGE alone. Kinetics of the chemical crosslinking reaction could be controlled precisely making the comparison between many samples easily reproducible. The pre-separation of proteins appeared to reduce diffusion based crosslinking, probably because

the movement of complexes in the sample was restricted to the immediate vicinity of their position in the polyacrylamide gel, making chance interactions with other proteins unlikely. Multimer-PAGE seemed useful in detecting stable protein complexes other that α-synuclein multimers. In this regard, multimer-PAGE may be a particularly valuable supplemental technique for BN-PAGE, to verify true protein complexes, as protein mobility on BN-PAGE alone clearly isn't sufficient [304]. For example, multimer-PAGE detected parkin as a monomer (50 kDa) in contrast to a previous report that found parkin to be exclusively a tetramer, based on BN-PAGE experiments [312]. Multimer-PAGE format also allows the simultaneous comparison of many biological samples, so that, relative protein complex abundance can be compared on a single blot. Although not reported here, gels could also be incubated with solutions containing experimental molecules to assess their influence on complex stability.

Lipid-protein crosslinking could occur between α-synuclein and phosphatidalserine or phosphatidylethanolamine. This interpretation of the data has the advantage of explaining the seemingly anomalous behavior of α-synuclein following sample dilution prior to chemical crosslinking (seen in figure 26B). DSP treatment enhances α-synuclein detection on PVDF membranes as described previously [313]. The enhancement is lost upon sample dilution. Because we observed that α-synuclein association with endogenous lipids was sensitive to dilution, it could be that upon dilution α-synuclein disassociates from endogenous lipids, reverting to an unstable intrinsically dynamic protein in solution. Crosslinking of free α-synuclein would then likely form a more compact structure as adjacent lysine residues of α-synuclein cross-link to each other. In contrast, if lipid-protein

crosslinking occurred between α-synuclein and several phospholipids, α-synuclein would not only have a larger molecular radius but would presumably be more hydrophobic, allowing for enhanced PVDF binding. Data provided here is insufficient to conclusively affirm or reject this interpretation and future studies should aim to address this potentially important molecular behavior of soluble α-synuclein.

Overall, multimer-page is a useful technique to study protein complexes in great detail. Multimer-PAGE was used successfully to describe and compare soluble α-synuclein multimers across complex biological samples.

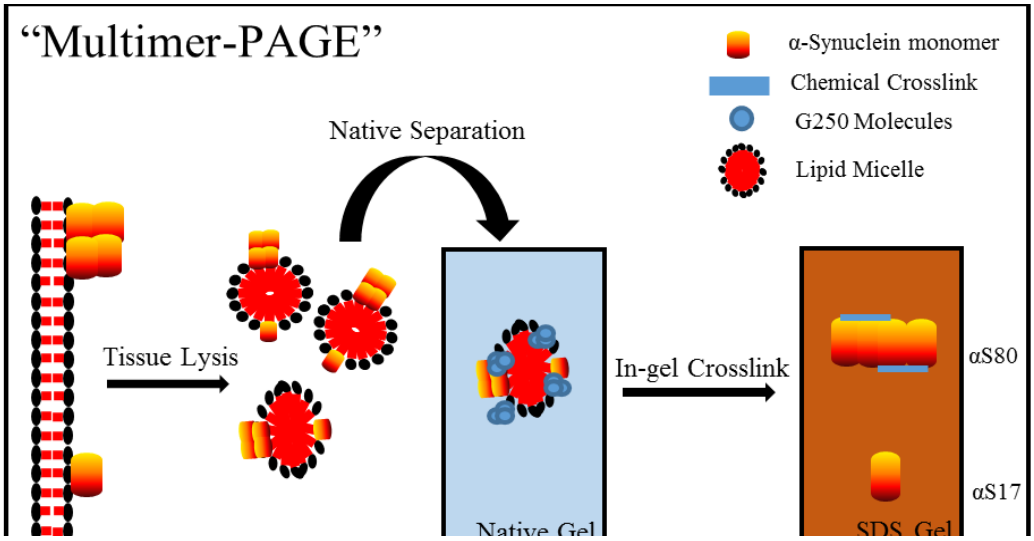

Figure 31. Summary of multimer-PAGE technique. Depicted is a conceptual process underlying the multimer-PAGE technique. First tissue is disrupted taking care to preserve intact protein complexes. During native extraction α-synuclein likely is in dynamic interaction with lipid/detergent micelles. The micelles containing α-synuclein are separated by blue native gel electrophoresis. Subsequent chemical crosslinking stabilizes the separated protein complexes. These complexes can then be resolved using SDS-PAGE. The technique can be setup to resolve and compare α-synuclein multimers between 14 samples. Ultimately, this technique is usuful in the measurement of α-synuclein multimer abundance in biological samples.

CHAPTER 6: SUMMARY AND FUTURE DIRECTIONS

6 Self-administration model of neurotoxicity

6.1.1 Key findings

Adult male Long-Evans can be trained to readily self-administered 0.1 mg / kg / infusion of METH using an FR5 schedule of reinforcement. Long-Evans rats self-administered approximately 2 mg METH / kg bodyweight per 4 h session. Following 14 consequetive days of METH self-administration degeneration in striatal TH labeled axons or perbutation in striatal dopamine were not observed.

6.1.2 Conclusions

Long-Evans rats readily self-administer METH, albeit, less robustly than that reported for Sprague-Dawley rats. Furthermore, short-access METH self-administration investigated here does not produce robust striatal DAergic neurotoxicity. Therefore, short-access METH self-administration is not a robust rodent model of METH neurotoxicity.

6.1.3 Future Directions

Future investigations into the etiology and treatment of METH neurotoxicity should focus on either a binge METH or extended access METH self-administration models. Extended access METH self-administration neurotoxicity models have been demonstrated elsewhere [65, 160]. Extended access models allow for exposure to higher doses of METH, and potentially, can better mimic human use.

Here we did not observe reductions in striatal DAergic markers 21 days following METH self-administration. Long-term (>7 days) depletion of striatal DA can be indicative of physical damage and loss of striatal DAergic axons. Because we did not observe

reductions in striatal DA 21 days following METH, physical damage to striatal DAergic axons is unlikely. Future studies should address the possibility that damage to striatal axons occurs at low levels, and closer to the time of METH exposure. Studies looking at striatal health and function at an earlier timepoint (ie 24-48h) following METH exposure will help clarify if any neurotoxicity is taking place, which may not be obvious 21 days following METH self-administration. For example it may be fruitful to assess reactive gliosis and microglia activation in the striatum in animals who recently have self-administered METH. Because activated microglia activation is observed in the brains of human METH users, the confirmation of this effect a rodent self-administration paradigm would lend clinical validity to the model. Acute microglia activation together with a lack of long-term striatal DAergic deficits would help confirm the models validity as approximating human METH use.

METH administration in rodents tends to be highly variable, and the cause remains unclear. This is in contrast to other drugs of abuse like cocaine and opiates which produce robust operant responding in most rats. Because suseptiblility to drug taking is a central issue to METH abuse, investions into the root causes are particularly important. Future fruitful studies should explore the contribution of genetics and environment on variable responding of rats for METH. To assess the genetic contribution to METH self-administration animals should be first categorized into high and low responders based on performance during the METH self-administration session. Exome sequencing of these two groups could give insight into functional genetic contributions to the phenotype. Once

potential functional targets are identified, then knockdown and/or knockout models can be explored to verify the contribution of the identified target to self-administration.

6.2 Role of axonal transport in METH neurotoxicity

6.2.1 Key findings

Immunoreactivity of AcetTUB is decreased in the striatum 3 days following binge METH. Co-localization between AcetTUB and TH labled axons decreaseed in the striatum 3 days following binge METH. Treatment with EpoDL prevented the METH-induced loss of striatal AcetTUB, TH, and DAT. EpoDL prevented METH-induced reactive gliosis. Immunoreactivity of DAT is increased in the striatum 3 days following EpoDL treatment.

6.2.2 Conclusions

METH exposure results in destabilized MT of striatal DAerigic axons. EpoD can be used to prevent the METH-induced destabilization of MT in DAergic axons. EpoD may influence DA neurotransmission in the striatum and could serve as a novel therapeutic intervention for METH neurotoxicity.

6.2.3 Future Directions

Future investigations should focus on the neuroprotective effects of EpoD. To do this, an optimal dosing regimen should be determined, using the dose range presented here as a guide. High doses of EpoD can be neurotoxic, as suggested here, and elsewhere. The effect of EpoD on striatal DAT and DA levels should also be investigated. Because EpoDL increased both striatal DAT and DA, EpoD could possibly be used as a novel DA enhancing therapy for diseases such as PD.

The role of MT in METH neurotoxicity should be further investigated. Here we found evidence that stable MT were lost in DAergic axons following METH. However, this evidence is based on the indirect measure of MT PTM. Future investigations should attempt to verify the loss of stable MT through other methods than those used here. For example, the conditional deletion or overexpression of FLOXED Hdac6 (gene encoding HDAC6) in DA neurons of the nigralstriatal pathway could potentially clarify the role of AcetTUB in METH neurotoxicity. HDAC6 is a required enzyme for the deacetylation of MT. Measuring the METH neurotoxicity in these animals would help clarify the role of AcetTUB in METH neurotoxicity. Our results suggest that HDAC6 may serve a neurotoxic role in nigrostriatal DAergic neurons. However, HDAC6 could also be neuroprotective because of its known functions in the removal of toxic/misfolded protein aggregates.

Impaired axonal transport following binge METH should be verified. Measuring axonal transport in vivo is technically challenging and therefore we chose to measure PTM of MT. However, these PTM are a relatively indirect measure of axonal transport, and therefore, do not necessarily indicate impaired transport. Deficits in axonal transport could be verified in primary neuron culture using fluorescent quantum dots (QDOT) as the transported cargo [314]. We had explored the microinjection of QDOT in the substantia nigra to measure axonal transport in vivo but found extensive transport throughout the brain (data not shown here) and therefore the technique was not particularly useful to study axonal transport selectively in nigrostrial DA neurons. An alternative to QDOT based cargo would be the use of labeling strategies for a cell specific cargo for example DAT. This method would have the advantage of being DA neuron specific and sensitive. However,

collecting meaningful live images of tagged-DAT in vivo would be difficult with currently available technologies (i.e. cannot penetrate deep tissue structures and resolution is limited). Therefore, the examination of axonal transport via post-mortem analysis of brain tissue slices (i.e. IHC) would still be necessary.

6.3 Role of Parkin in METH neurotoxicity

6.3.1 Key findings

PKO rats are hyposensitive to the acute locomotor activating effects of METH. PKO rats develop PD-like phenotype following exposure to high dose METH. PKO rats are hypersensitive to METH induced DA depletion in the striatum but not METH-induced reduction of striatal DAT or TH. PKO rats have reduced levels of striatal AcetTUB, but are insensitive to the AcetTUB lowering effects of binge METH.

6.3.2 Conclusions

Parkin plays a role in maintaining function of the nigrostriatal dopamine pathway. Parkin does not play a role in maintating striatal AcetTUB levels.

6.3.3 Future directions

Several studies have suggested a role of parkin for the turnover and stability of MT [315-319]. Here we present evidence that parkin appears to play a role in METH induced neurotoxicity in the striatum. Behavioural data seems to suggest that parkin may have an important role in maintaining proper DA function in the nigrostriatal system. We hypothesized that parkin may maintain DAergic neuron health through the maintance of axonal transport, but when we measured AcetTUB levels in the striatum following parkin overexpression, we saw no alteration in the striatal AcetTUB levels. This is despite the

apparent reduction in AcetTUB levels in PKO rats, as measured by western blot and IHC. Using a PTM of α-tubulin (ie AcetTUB) as a marker of axonal transport is fraught with interpretational difficulties. Future studies should focus on assessing the process of axonal transport directly via either primary neuron cultures or in vivo imaging techniques. Current in vivo imaging techniques are relatively insensitive and technically challenging. Imaging in primary neuron culture is a more sensitive and allows for easy experimental manipulation. Parkin overexpression and knockdown in these types of models will likely yield more direct answers to the question of what is parkins role in axonal transport.

We demonstrate that PKO rats develop a distinct motor impairment phenotype upon the toxic insult of binge METH. It's still not clear why PKO rats are sensitive to METH. Fruitful future studies should focus the possible exaggerated hyperthermia response in the rats. Because we externally cooled rat in these studies we can not accurately determine any sensitivity to METH-induced hyperthermia. Another important study to help determine the molecular causes of PKO sensistivity is to investigate ubiquitination targets downstream of parkin. Newer proteomic approaches allow for the large scale identification of differentially ubiquitinated protiens [320]. Running this type of this large scale unbiased analysis could help discover regulatory targets downstream of parkin that may be important for the observed phenotype.

6.4 Measuring α-Synuclein tetramers

6.4.1 Key findings

BN-PAGE was insufficient to determine α-synuclein multimer stoichiometry in brain lysates. This was partially due to soluble α-synuclein migrating within a

lipid/detergent structure during BN-PAGE to a position of 66-200 kDa. The limitation of BN-PAGE could be circumvented by using in-gel chemical crosslinking of native proteins. Using this new technique, termed multimer-PAGE, we observed predominately three α-synuclein species of 17, 56, and 80 kDa. Multimer-PAGE, has potential to be used to measure protein stoichiometry of many other protein complexes in biological samples.

6.4.2 Conclusions

α-Synuclein forms several stable soluble multimers in the brain. Using multimer-PAGE the stoichiometry of α-synuclein multimers can be determined and compared between many complex biological samples.

6.4.3 Future Directions

Future studies should determine if binge METH treatment alters the ratio of α-synuclein monomer to tetramer in the striatum. Preliminary studies in our lab suggest that directly treating gels with DA and METH can inhibit endogenous α-synuclein tetramer stability (data not shown). This finding is preliminary, but it seems to suggest that METH directly and indirectly (via DA) promotes the shift from the α-synuclein tetramer to the disordered monomer (i.e. the aggregation prone species). To investigate this hypothesis multimer-PAGE should be conducted in striatal lysates of rats treated with binge METH.

Further studies should employ multimer-PAGE to investigate role of α-synuclein multimers in DA vesicle transport. Numerous studies show that α-synuclein is primarily involved in neurotransmitter packaging, exocytosis, and vesicle trafficking [321]. The exact role of α-synuclein in the axonal transport of DA containing vesicles is unknown. What is known is the multimerization of α-synuclein on vesicle membranes is intimately

tied to the vesicle trafficking function of α-synuclein. Therefore, the measured ratio of α-synuclein monomer to tetramer may be indicative of impaired axonal transport of DA vesicles. In this scenario, METH and/or excess cytosolic DA would impair the formation of α-synuclein multimers on the surface of vesicles. The inhibition of multimer formation would increase monomeric α-synuclein (i.e. the species associated with aberrant aggregation). The net result would be the toxic aggregation of α-synuclein and impaired vesicular transport.

The absolute ratio of soluble α-synuclein monomer to tetramer in the striatum should be determined. To do this, future studies need to investigate the lipid binding role of α-synuclein. The interaction of α-synuclein with an unknown soluble lipid (s) is strongly implicated here and elsewhere. The interaction with α-synuclein and the free lipid pool likely determines the measured α-synuclein stoichiometry by multimer-PAGE. By determining the exact nature of α-synuclein interaction with free lipids will result in a much deeper understanding of α-synuclein function. The lipid (s) could be easily determined by mass spectrometry of the lipids isolated from purified α-synuclein. Once it is determined which lipids α-synuclein is binding, and more importantly, how many molecules of lipid α-synuclein binds endogenously, it could be determined the stoichiometry of the hypothesized α-synuclein-lipid particle.

6.5 General Discussion

6.5.1 The role of axonal transports role in clinical METH neurotoxicity

Currently there is a lack of direct evidence for axonal transport deficits in the brain of human METH users. However, there are several reasons to believe that heavy METH

use could impair axonal transport in the nigralstriatal dopamine pathway. First there is an accumulation of oxidative products and reduction of antioxidant molecules in the striatum of heavy METH users [321]. This observation suggest that oxidative stress plays a role in damage to the striatal DAergic nerve teminals. Clearance of oxidativily damaged cellular components, and the restoration of homeostatsis at striatal DAergic nerve terminals, would likely involve the processes of axonal transport. Accumulation of cytoskeletal associtated protein tau and plasma membrane associtated cytoskeletal filament protein spectrin II are cleaved in the hippocampus and cortex of rats treated with METH [322]. Cleaved tau can inhibit kinesin mediated axonal transport [323] and therefore axonal transport maybe inhibited following toxic doses of METH. Inhibition of retrograde transport would presumably be important to remove oxidatively damage organelles and other cellular components. Oxidative stress in METH users could disrupt axonal transport by damaging the necessary components such as MT's and motoroproteins. Indeed damage to the axonal transport machinery has been observed in animal models of several other neurodegenerative disorder [324, 325].

DAergic axon components, such as DAT and DA, recover following abstinence from METH [326, 327]. Axonal transport is required specifically for DAT which is not locally synthesized in the striatal nerve terminals. Therefore, to some extent anterograde axonal transport is required for the observed restoration of striatal DAT. Restoration of DAergic nerve terminal components by enhancing axonal transport would presumably help restore normal DAergic nerve terminal function. However, increasing the availability of

DAT at the nerve terminal could result in undesirable results such as increasing the addictive properties of METH [51].

Addressing the role of axonal transport dysfunction in human METH users is experimentally challenging. In vivo monitoring of axonal transport remains beyond current technologies limiting the direct observation of axonal transport in human METH users. However, several of the tubulin PTM's explored here may allow for the assessment of axonal transport fidelity in METH users. The use of AcetTUB and DeTyTUB may be particularly useful, in that both of these PTM's were altered in our rat model of METH neurotoxicity. There assessment would be limited to post-mortem tissue samples, which subsequently limits the conclusions of such studies.

Induced pluripotent stem cells (iPSC) technology may allow for the assessment of axonal transport in neurons derived from METH users [328]. iPSCs can be cultured from fibroblast cells of patients currently using METH, which can in turn be differentiated into DAergic cells[329]. Axonal transport could then be directly monitored in these neurons using labeling strategies and microscopy [330]. Although this model has the advantage of directly measuring axonal transport in human patient's neurons, the phenotype of the neurons would poorly recapitulate METH exposed neurons in the brain.

6.5.2 EpoD as a treatment for METH neurotoxicity

EpoD was originally developed as an anticancer treatment[331]. Subsequent development for neurodegenerative disease was explored because EpoD selectively accumulates in the brain, in contrast to other MT stabilizing componds that do not cross the blood brain barrier. Clinical trials of EpoD were conducted by Bristol-Myers Squibb

for the treatment of alzhiemers disease but were discontinued in 2013. There are currently no ongoing clinical trials investigating the use of EpoD for treatment of Alzeimer's diseases.

Development of EpoD as a treatment for axonal transport dysfunction in the CNS is impeded by potential off target effects. Known taxol compounds, such as paclitaxel, can induce peripheral neuropathy, but they do not cross the blood brain barrier [332]. EpoD, readily crosses the blood brain barrier [152] and could induce neuropathly in the CNS. Our data seems to suggest, at least with the highest does tested, some adverse neurotoxicity is occurring the central nervous system. Chronic stabilization of MT's in cells of the central nervous system likely have widesweeping effects because MTs are involved in many cellular functions. For this reason, treatment with EpoD may be most beneficial if done acutely following injury, for example, following overdose of METH. In this situation, EpoD may increase axonal transport and allow for neurons to more efficiently clear damaged cellular components and restore function cellular compoents to the striatal nerve terminals. In this vein, studies that explore the use of low dose EpoD following neural injury may be more successful than pretreatement. Furthermore, treatment following neuronal injury is more clinically applicable as neuronal injury (METH overdose) is unpredicatable.

6.5.3 Modeling METH neurotoxicity in rodents

METH self-administration models have been used for many years to study addictive properties of METH. Self-administration models have been under-utilized for METH neurotoxicity studies. The primary reason is that drug responding in rodents does

not mimic human users. Because the half-life of METH in rodents is short (~2 h) they administer METH continuously over a period of many hours. Human users will often administer single large doses of METH 1-2 times a day because the half-life of METH is ~12 h. Determining an accurate model of human use is very important, because depending on the model used METH exposure can lead to very different outcomes [333].

6.5.4 α-Synuclein and METH neurotoxicity

α-Synuclein's possible role in METH neurotoxicity remains obscure. Several studies have suggested that METH may increase α-synuclein expression in the brain[118]. Overexpression of α-synuclein can lead to neurodegeneration in DAergic neruons [334]. Therefore, it is possible that the effect of METH on α-synuclein expression may impact the health and function of DAergic neurons. However, this hypothesis remains to be directly assessed.

REFERENCES

[1] T. Nagai, S. Kamiyama, Forensic toxicologic analysis of methamphetamine and amphetamine optical isomers by high performance liquid chromatography, Zeitschrift fur Rechtsmedizin. Journal of legal medicine, 101 (1988) 151-159.

[2] D.A. Wolkoff, Methamphetamine abuse: an overview for health care professionals, Hawaii medical journal, 56 (1997) 34-36, 44.

[3] A.L. Guerrero, [Parkinson's disease of Adolf Hitler and its influence in the development of World War Second], Neurologia, 18 (2003) 66-69.

[4] D. Werb, K. Hayashi, N. Fairbairn, K. Kaplan, P. Suwannawong, C. Lai, T. Kerr, Drug use patterns among Thai illicit drug injectors amidst increased police presence, Substance abuse treatment, prevention, and policy, 4 (2009) 16.

[5] K.P. Shaw, Human methamphetamine-related fatalities in Taiwan during 1991-1996, Journal of forensic sciences, 44 (1999) 27-31.

[6] M.L. Brecht, L. Greenwell, M.D. Anglin, Methamphetamine treatment: trends and predictors of retention and completion in a large state treatment system (1992-2002), Journal of substance abuse treatment, 29 (2005) 295-306.

[7] K.C. Brouwer, P. Case, R. Ramos, C. Magis-Rodriguez, J. Bucardo, T.L. Patterson, S.A. Strathdee, Trends in production, trafficking, and consumption of methamphetamine and cocaine in Mexico, Substance use & misuse, 41 (2006) 707-727.

[8] National Survey on Drug Abuse and Health, DOI (2015).

[9] V.U.N.O.o.D.a. Crime, United Nations Office of Drugs and Crime, World drug report 1(2007).

[10] L.R. Dye, Recipe for disaster: Mexican methamphetamine, Journal of medical toxicology : official journal of the American College of Medical Toxicology, 2 (2006) 81-82.

[11] C.C. Cruickshank, K.R. Dyer, A review of the clinical pharmacology of methamphetamine, Addiction, 104 (2009) 1085-1099.

[12] N.I.o.D. Abuse, National Survey on Drug Use and Health, DOI (2012).

[13] A.Y. Chan, S.A. Storck, D.U. Stone, Ocular injuries from shake and bake methamphetamine labs, The Journal of the Oklahoma State Medical Association, 104 (2011) 409-412.

[14] A. Giovanni, L.P. Liang, T.G. Hastings, M.J. Zigmond, Estimating hydroxyl radical content in rat brain using systemic and intraventricular salicylate: impact of methamphetamine, Journal of neurochemistry, 64 (1995) 1819-1825.

[15] A. Ghuran, J. Nolan, The cardiac complications of recreational drug use, The Western journal of medicine, 173 (2000) 412-415.

[16] A. Ghuran, J. Nolan, Recreational drug misuse: issues for the cardiologist, Heart, 83 (2000) 627-633.

[17] T.T. Bashour, Acute myocardial infarction resulting from amphetamine abuse: a spasm-thrombus interplay?, American heart journal, 128 (1994) 1237-1239.

[18] J. Lynch, M.A. House, Cardiovascular effects of methamphetamine, The Journal of cardiovascular nursing, 6 (1992) 12-18.

[19] L.J. Schep, R.J. Slaughter, D.M. Beasley, The clinical toxicology of metamfetamine, Clin Toxicol (Phila), 48 (2010) 675-694.

[20] L.J. Liang, D. Huang, M.L. Brecht, Y.I. Hser, Differences in Mortality among Heroin, Cocaine, and Methamphetamine Users: A Hierarchical Bayesian Approach, J Drug Issues, 40 (2010) 121-140.

[21] A.C. Dean, S.M. Groman, A.M. Morales, E.D. London, An evaluation of the evidence that methamphetamine abuse causes cognitive decline in humans, Neuropsychopharmacology : official publication of the American College of Neuropsychopharmacology, 38 (2013) 259-274.

[22] C.K. Chen, S.K. Lin, Y.C. Chen, M.C. Huang, T.T. Chen, S.C. Ree, L.J. Wang, Persistence of psychotic symptoms as an indicator of cognitive impairment in methamphetamine users, Drug and alcohol dependence, 148 (2015) 158-164.

[23] R.S. Durvasula, C.H. Hinkin, Neuropsychological Dysfunction among HIV Infected Drug Abusers, American journal of infectious diseases, 2 (2006) 67-73.

[24] K. Curtin, A.E. Fleckenstein, R.J. Robison, M.J. Crookston, K.R. Smith, G.R. Hanson, Methamphetamine/amphetamine abuse and risk of Parkinson's disease in Utah: a population-based assessment, Drug Alcohol Depend, 146 (2015) 30-38.

[25] I.N. Krasnova, J.L. Cadet, Methamphetamine toxicity and messengers of death, Brain Res Rev, 60 (2009) 379-407.

[26] M.Y. J Sian, P Riederer, and M Gerlach, Basic Neurochemistry: Molecular, Cellular and Medical Aspects. 6th edition, American Society for Neurochemistry, DOI (1999).

[27] U.D. McCann, D.F. Wong, F. Yokoi, V. Villemagne, R.F. Dannals, G.A. Ricaurte, Reduced striatal dopamine transporter density in abstinent methamphetamine and methcathinone users: evidence from positron emission tomography studies with

[11C]WIN-35,428, The Journal of neuroscience : the official journal of the Society for Neuroscience, 18 (1998) 8417-8422.

[28] J.M. Wilson, K.S. Kalasinsky, A.I. Levey, C. Bergeron, G. Reiber, R.M. Anthony, G.A. Schmunk, K. Shannak, J.W. Haycock, S.J. Kish, Striatal dopamine nerve terminal markers in human, chronic methamphetamine users, Nat Med, 2 (1996) 699-703.

[29] G.A. Ricaurte, R.W. Guillery, L.S. Seiden, C.R. Schuster, R.Y. Moore, Dopamine nerve terminal degeneration produced by high doses of methylamphetamine in the rat brain, Brain research, 235 (1982) 93-103.

[30] S. Ares-Santos, N. Granado, I. Espadas, R. Martinez-Murillo, R. Moratalla, Methamphetamine causes degeneration of dopamine cell bodies and terminals of the nigrostriatal pathway evidenced by silver staining, Neuropsychopharmacology : official publication of the American College of Neuropsychopharmacology, 39 (2014) 1066-1080.

[31] Y. Sekine, Y. Ouchi, G. Sugihara, N. Takei, E. Yoshikawa, K. Nakamura, Y. Iwata, K.J. Tsuchiya, S. Suda, K. Suzuki, M. Kawai, K. Takebayashi, S. Yamamoto, H. Matsuzaki, T. Ueki, N. Mori, M.S. Gold, J.L. Cadet, Methamphetamine causes microglial activation in the brains of human abusers, The Journal of neuroscience : the official journal of the Society for Neuroscience, 28 (2008) 5756-5761.

[32] M. Kawabori, M.A. Yenari, The role of the microglia in acute CNS injury, Metab Brain Dis, 30 (2015) 381-392.

[33] S. Rivest, Regulation of innate immune responses in the brain, Nat Rev Immunol, 9 (2009) 429-439.

[34] M.S. Goldberg, S.M. Fleming, J.J. Palacino, C. Cepeda, H.A. Lam, A. Bhatnagar, E.G. Meloni, N. Wu, L.C. Ackerson, G.J. Klapstein, M. Gajendiran, B.L. Roth, M.F. Chesselet, N.T. Maidment, M.S. Levine, J. Shen, Parkin-deficient mice exhibit nigrostriatal deficits but not loss of dopaminergic neurons, J Biol Chem, 278 (2003) 43628-43635.

[35] N.D. Volkow, L. Chang, G.J. Wang, J.S. Fowler, D. Franceschi, M. Sedler, S.J. Gatley, E. Miller, R. Hitzemann, Y.S. Ding, J. Logan, Loss of dopamine transporters in methamphetamine abusers recovers with protracted abstinence, The Journal of neuroscience : the official journal of the Society for Neuroscience, 21 (2001) 9414-9418.

[36] T.E. Albertson, R.W. Derlet, B.E. Van Hoozen, Methamphetamine and the expanding complications of amphetamines, The Western journal of medicine, 170 (1999) 214-219.

[37] S. Darke, S. Kaye, R. McKetin, J. Duflou, Major physical and psychological harms of methamphetamine use, Drug and alcohol review, 27 (2008) 253-262.

[38] J.A. Perez, Jr., E.L. Arsura, S. Strategos, Methamphetamine-related stroke: four cases, The Journal of emergency medicine, 17 (1999) 469-471.

[39] J. Yuan, G. Hatzidimitriou, P. Suthar, M. Mueller, U. McCann, G. Ricaurte, Relationship between temperature, dopaminergic neurotoxicity, and plasma drug concentrations in methamphetamine-treated squirrel monkeys, The Journal of pharmacology and experimental therapeutics, 316 (2006) 1210-1218.

[40] J.F. Bowyer, D.L. Davies, L. Schmued, H.W. Broening, G.D. Newport, W. Slikker, Jr., R.R. Holson, Further studies of the role of hyperthermia in methamphetamine neurotoxicity, J Pharmacol Exp Ther, 268 (1994) 1571-1580.

[41] A.E. Fleckenstein, D.G. Wilkins, J.W. Gibb, G.R. Hanson, Interaction between hyperthermia and oxygen radical formation in the 5-hydroxytryptaminergic response to a single methamphetamine administration, The Journal of pharmacology and experimental therapeutics, 283 (1997) 281-285.

[42] D.A. Tata, J. Raudensky, B.K. Yamamoto, Augmentation of methamphetamine-induced toxicity in the rat striatum by unpredictable stress: contribution of enhanced hyperthermia, The European journal of neuroscience, 26 (2007) 739-748.

[43] R.R. Matsumoto, M.J. Seminerio, R.C. Turner, M.J. Robson, L. Nguyen, D.B. Miller, J.P. O'Callaghan, Methamphetamine-induced toxicity: an updated review on issues related to hyperthermia, Pharmacology & therapeutics, 144 (2014) 28-40.

[44] S.E. Stephans, B.K. Yamamoto, Methamphetamine-induced neurotoxicity: roles for glutamate and dopamine efflux, Synapse, 17 (1994) 203-209.

[45] T.L. Wallace, G.A. Gudelsky, C.V. Vorhees, Methamphetamine-induced neurotoxicity alters locomotor activity, stereotypic behavior, and stimulated dopamine release in the rat, The Journal of neuroscience : the official journal of the Society for Neuroscience, 19 (1999) 9141-9148.

[46] P.H. Kelly, P.W. Seviour, S.D. Iversen, Amphetamine and apomorphine responses in the rat following 6-OHDA lesions of the nucleus accumbens septi and corpus striatum, Brain research, 94 (1975) 507-522.

[47] D.S. Segal, R. Kuczenski, In vivo microdialysis reveals a diminished amphetamine-induced DA response corresponding to behavioral sensitization produced by repeated amphetamine pretreatment, Brain research, 571 (1992) 330-337.

[48] I. Creese, S.D. Iversen, The role of forebrain dopamine systems in amphetamine induced stereotyped behavior in the rat, Psychopharmacologia, 39 (1974) 345-357.

[49] J.B. Lucot, G.C. Wagner, C.R. Schuster, L.S. Seiden, The effects of dopaminergic agents on the locomotor activity of rats after high doses of methylamphetamine, Pharmacology, biochemistry, and behavior, 13 (1980) 409-413.

[50] B. Giros, M. Jaber, S.R. Jones, R.M. Wightman, M.G. Caron, Hyperlocomotion and indifference to cocaine and amphetamine in mice lacking the dopamine transporter, Nature, 379 (1996) 606-612.

[51] A. Salahpour, A.J. Ramsey, I.O. Medvedev, B. Kile, T.D. Sotnikova, E. Holmstrand, V. Ghisi, P.J. Nicholls, L. Wong, K. Murphy, S.R. Sesack, R.M. Wightman, R.R. Gainetdinov, M.G. Caron, Increased amphetamine-induced hyperactivity and reward in mice overexpressing the dopamine transporter, Proc Natl Acad Sci U S A, 105 (2008) 4405-4410.

[52] S.D. Friedman, E. Castaneda, G.K. Hodge, Long-term monoamine depletion, differential recovery, and subtle behavioral impairment following methamphetamine-induced neurotoxicity, Pharmacology, biochemistry, and behavior, 61 (1998) 35-44.

[53] L.E. Halpin, W.T. Gunning, B.K. Yamamoto, Methamphetamine causes acute hyperthermia-dependent liver damage, Pharmacol Res Perspect, 1 (2013) e00008.

[54] M.L. Miller, B.D. Vaillancourt, M.J. Wright, Jr., S.M. Aarde, S.A. Vandewater, K.M. Creehan, M.A. Taffe, Reciprocal inhibitory effects of intravenous d-methamphetamine self-administration and wheel activity in rats, Drug Alcohol Depend, 121 (2012) 90-96.

[55] J.F. Bowyer, L.C. Schmued, Fluoro-Ruby labeling prior to an amphetamine neurotoxic insult shows a definitive massive loss of dopaminergic terminals and axons in the caudate-putamen, Brain research, 1075 (2006) 236-239.

[56] T.R. Guilarte, M.K. Nihei, J.L. McGlothan, A.S. Howard, Methamphetamine-induced deficits of brain monoaminergic neuronal markers: distal axotomy or neuronal plasticity, Neuroscience, 122 (2003) 499-513.

[57] A.B. Killinger, A. Moszczynska, Epothilone D Prevents Binge Methamphetamine-Mediated Loss of Striatal Dopaminergic Markers, Journal of neurochemistry, DOI 10.1111/jnc.13391(2015).

[58] K.P. Ritchie, B.M. Keller, K.M. Syed, J.R. Lepock, Hyperthermia (heat shock)-induced protein denaturation in liver, muscle and lens tissue as determined by differential scanning calorimetry, International journal of hyperthermia : the official journal of European Society for Hyperthermic Oncology, North American Hyperthermia Group, 10 (1994) 605-618.

[59] L.V. Panlilio, S.R. Goldberg, Self-administration of drugs in animals and humans as a model and an investigative tool, Addiction, 102 (2007) 1863-1870.

[60] J.R. Weeks, Experimental morphine addiction: method for automatic intravenous injections in unrestrained rats, Science, 138 (1962) 143-144.

[61] R. Stefanski, S.H. Lee, S. Yasar, J.L. Cadet, S.R. Goldberg, Lack of persistent changes in the dopaminergic system of rats withdrawn from methamphetamine self-administration, European journal of pharmacology, 439 (2002) 59-68.

[62] J.D. Shepard, D.T. Chuang, Y. Shaham, M. Morales, Effect of methamphetamine self-administration on tyrosine hydroxylase and dopamine transporter levels in mesolimbic and nigrostriatal dopamine pathways of the rat, Psychopharmacology, 185 (2006) 505-513.

[63] K.A. Brennan, J. Colussi-Mas, C. Carati, R.A. Lea, P.S. Fitzmaurice, S. Schenk, Methamphetamine self-administration and the effect of contingency on monoamine and metabolite tissue levels in the rat, Brain research, 1317 (2010) 137-146.

[64] M. Schwendt, A. Rocha, R.E. See, A.M. Pacchioni, J.F. McGinty, P.W. Kalivas, Extended methamphetamine self-administration in rats results in a selective reduction of dopamine transporter levels in the prefrontal cortex and dorsal striatum not accompanied by marked monoaminergic depletion, The Journal of pharmacology and experimental therapeutics, 331 (2009) 555-562.

[65] I.N. Krasnova, Z. Justinova, B. Ladenheim, S. Jayanthi, M.T. McCoy, C. Barnes, J.E. Warner, S.R. Goldberg, J.L. Cadet, Methamphetamine self-administration is associated with persistent biochemical alterations in striatal and cortical dopaminergic terminals in the rat, PloS one, 5 (2010) e8790.

[66] D.J. Eyerman, B.K. Yamamoto, A rapid oxidation and persistent decrease in the vesicular monoamine transporter 2 after methamphetamine, Journal of neurochemistry, 103 (2007) 1219-1227.

[67] D.S. Segal, R. Kuczenski, M.L. O'Neil, W.P. Melega, A.K. Cho, Prolonged exposure of rats to intravenous methamphetamine: behavioral and neurochemical characterization, Psychopharmacology, 180 (2005) 501-512.

[68] D.M. Kuhn, D.M. Francescutti-Verbeem, D.M. Thomas, Dopamine disposition in the presynaptic process regulates the severity of methamphetamine-induced neurotoxicity, Annals of the New York Academy of Sciences, 1139 (2008) 118-126.

[69] F. Fumagalli, R.R. Gainetdinov, Y.M. Wang, K.J. Valenzano, G.W. Miller, M.G. Caron, Increased methamphetamine neurotoxicity in heterozygous vesicular monoamine transporter 2 knock-out mice, The Journal of neuroscience : the official journal of the Society for Neuroscience, 19 (1999) 2424-2431.

[70] V. Sandoval, E.L. Riddle, G.R. Hanson, A.E. Fleckenstein, Methylphenidate alters vesicular monoamine transport and prevents methamphetamine-induced dopaminergic deficits, The Journal of pharmacology and experimental therapeutics, 304 (2003) 1181-1187.

[71] F. Fumagalli, R.R. Gainetdinov, K.J. Valenzano, M.G. Caron, Role of dopamine transporter in methamphetamine-induced neurotoxicity: evidence from mice lacking the transporter, The Journal of neuroscience : the official journal of the Society for Neuroscience, 18 (1998) 4861-4869.

[72] G.J. Marek, G. Vosmer, L.S. Seiden, Dopamine uptake inhibitors block long-term neurotoxic effects of methamphetamine upon dopaminergic neurons, Brain research, 513 (1990) 274-279.

[73] O. Acikgoz, S. Gonenc, B.M. Kayatekin, N. Uysal, C. Pekcetin, I. Semin, A. Gure, Methamphetamine causes lipid peroxidation and an increase in superoxide dismutase activity in the rat striatum, Brain research, 813 (1998) 200-202.

[74] J.F. Cubells, S. Rayport, G. Rajendran, D. Sulzer, Methamphetamine neurotoxicity involves vacuolation of endocytic organelles and dopamine-dependent intracellular oxidative stress, J Neurosci, 14 (1994) 2260-2271.

[75] M.J. LaVoie, T.G. Hastings, Dopamine quinone formation and protein modification associated with the striatal neurotoxicity of methamphetamine: evidence against a role for extracellular dopamine, The Journal of neuroscience : the official journal of the Society for Neuroscience, 19 (1999) 1484-1491.

[76] T. Kita, M. Takahashi, K. Kubo, G.C. Wagner, T. Nakashima, Hydroxyl radical formation following methamphetamine administration to rats, Pharmacology & toxicology, 85 (1999) 133-137.

[77] D.M. Thomas, D.M. Francescutti-Verbeem, D.M. Kuhn, Increases in cytoplasmic dopamine compromise the normal resistance of the nucleus accumbens to methamphetamine neurotoxicity, Journal of neurochemistry, 109 (2009) 1745-1755.

[78] S. Amor, F. Puentes, D. Baker, P. van der Valk, Inflammation in neurodegenerative diseases, Immunology, 129 (2010) 154-169.

[79] D.M. Thomas, P.D. Walker, J.A. Benjamins, T.J. Geddes, D.M. Kuhn, Methamphetamine neurotoxicity in dopamine nerve endings of the striatum is associated with microglial activation, The Journal of pharmacology and experimental therapeutics, 311 (2004) 1-7.

[80] V. Coelho-Santos, J. Goncalves, C. Fontes-Ribeiro, A.P. Silva, Prevention of methamphetamine-induced microglial cell death by TNF-alpha and IL-6 through activation of the JAK-STAT pathway, Journal of neuroinflammation, 9 (2012) 103.

[81] S. Ares-Santos, N. Granado, R. Moratalla, The role of dopamine receptors in the neurotoxicity of methamphetamine, Journal of internal medicine, 273 (2013) 437-453.

[82] M. Pekny, M. Nilsson, Astrocyte activation and reactive gliosis, Glia, 50 (2005) 427-434.

[83] M. Belanger, P.J. Magistretti, The role of astroglia in neuroprotection, Dialogues in clinical neuroscience, 11 (2009) 281-295.

[84] M. Toborek, M.J. Seelbach, C.S. Rashid, I.E. Andras, L. Chen, M. Park, K.A. Esser, Voluntary exercise protects against methamphetamine-induced oxidative stress in brain microvasculature and disruption of the blood-brain barrier, Molecular neurodegeneration, 8 (2013) 22.

[85] J.P. Hansen, E.L. Riddle, V. Sandoval, J.M. Brown, J.W. Gibb, G.R. Hanson, A.E. Fleckenstein, Methylenedioxymethamphetamine decreases plasmalemmal and vesicular dopamine transport: mechanisms and implications for neurotoxicity, The Journal of pharmacology and experimental therapeutics, 300 (2002) 1093-1100.

[86] J.L. Cadet, C. Brannock, Free radicals and the pathobiology of brain dopamine systems, Neurochemistry international, 32 (1998) 117-131.

[87] C.W. Olanow, W.G. Tatton, Etiology and pathogenesis of Parkinson's disease, Annual review of neuroscience, 22 (1999) 123-144.

[88] Y. Sun, A.N. Pham, T.D. Waite, Elucidation of the interplay between Fe(II), Fe(III), and dopamine with relevance to iron solubilization and reactive oxygen species generation by catecholamines, Journal of neurochemistry, 137 (2016) 955-968.

[89] B. Halliwell, Role of free radicals in the neurodegenerative diseases: therapeutic implications for antioxidant treatment, Drugs Aging, 18 (2001) 685-716.

[90] H. Shimura, N. Hattori, S. Kubo, Y. Mizuno, S. Asakawa, S. Minoshima, N. Shimizu, K. Iwai, T. Chiba, K. Tanaka, T. Suzuki, Familial Parkinson disease gene product, parkin, is a ubiquitin-protein ligase, Nature genetics, 25 (2000) 302-305.

[91] D.P. Huynh, D.R. Scoles, T.H. Ho, M.R. Del Bigio, S.M. Pulst, Parkin is associated with actin filaments in neuronal and nonneural cells, Annals of neurology, 48 (2000) 737-744.

[92] P.K. Kurup, J. Xu, R.A. Videira, C. Ononenyi, G. Baltazar, P.J. Lombroso, A.C. Nairn, STEP61 is a substrate of the E3 ligase parkin and is upregulated in Parkinson's disease, Proceedings of the National Academy of Sciences of the United States of America, 112 (2015) 1202-1207.

[93] H. Jiang, Q. Jiang, J. Feng, Parkin increases dopamine uptake by enhancing the cell surface expression of dopamine transporter, The Journal of biological chemistry, 279 (2004) 54380-54386.

[94] A. Moszczynska, B.K. Yamamoto, Methamphetamine oxidatively damages parkin and decreases the activity of 26S proteasome in vivo, J Neurochem, 116 (2011) 1005-1017.

[95] L. Pasquali, G. Lazzeri, C. Isidoro, S. Ruggieri, A. Paparelli, F. Fornai, Role of autophagy during methamphetamine neurotoxicity, Annals of the New York Academy of Sciences, 1139 (2008) 191-196.

[96] B. Liu, R. Traini, B. Killinger, B. Schneider, A. Moszczynska, Overexpression of parkin in the rat nigrostriatal dopamine system protects against methamphetamine neurotoxicity, Exp Neurol, 247 (2013) 359-372.

[97] F.A. Perez, W.R. Curtis, R.D. Palmiter, Parkin-deficient mice are not more sensitive to 6-hydroxydopamine or methamphetamine neurotoxicity, BMC Neurosci, 6 (2005) 71.

[98] F.P. Manfredsson, C. Burger, L.F. Sullivan, N. Muzyczka, A.S. Lewin, R.J. Mandel, rAAV-mediated nigral human parkin over-expression partially ameliorates motor deficits via enhanced dopamine neurotransmission in a rat model of Parkinson's disease, Experimental neurology, 207 (2007) 289-301.

[99] M. Bian, J. Liu, X. Hong, M. Yu, Y. Huang, Z. Sheng, J. Fei, F. Huang, Overexpression of parkin ameliorates dopaminergic neurodegeneration induced by 1-methyl-4-phenyl-1,2,3,6-tetrahydropyridine in mice, PloS one, 7 (2012) e39953.

[100] T. Yasuda, H. Hayakawa, T. Nihira, Y.R. Ren, Y. Nakata, M. Nagai, N. Hattori, K. Miyake, M. Takada, T. Shimada, Y. Mizuno, H. Mochizuki, Parkin-mediated protection of dopaminergic neurons in a chronic MPTP-minipump mouse model of Parkinson disease, Journal of neuropathology and experimental neurology, 70 (2011) 686-697.

[101] C. Lo Bianco, B.L. Schneider, M. Bauer, A. Sajadi, A. Brice, T. Iwatsubo, P. Aebischer, Lentiviral vector delivery of parkin prevents dopaminergic degeneration in an alpha-synuclein rat model of Parkinson's disease, Proceedings of the National Academy of Sciences of the United States of America, 101 (2004) 17510-17515.

[102] L. Vercammen, A. Van der Perren, E. Vaudano, R. Gijsbers, Z. Debyser, C. Van den Haute, V. Baekelandt, Parkin protects against neurotoxicity in the 6-hydroxydopamine rat

model for Parkinson's disease, Molecular therapy : the journal of the American Society of Gene Therapy, 14 (2006) 716-723.

[103] K. Tieu, A guide to neurotoxic animal models of Parkinson's disease, Cold Spring Harbor perspectives in medicine, 1 (2011) a009316.

[104] J.C. Paterna, A. Leng, E. Weber, J. Feldon, H. Bueler, DJ-1 and Parkin modulate dopamine-dependent behavior and inhibit MPTP-induced nigral dopamine neuron loss in mice, Molecular therapy : the journal of the American Society of Gene Therapy, 15 (2007) 698-704.

[105] H. Jiang, Y. Ren, E.Y. Yuen, P. Zhong, M. Ghaedi, Z. Hu, G. Azabdaftari, K. Nakaso, Z. Yan, J. Feng, Parkin controls dopamine utilization in human midbrain dopaminergic neurons derived from induced pluripotent stem cells, Nature communications, 3 (2012) 668.

[106] J.M. Itier, P. Ibanez, M.A. Mena, N. Abbas, C. Cohen-Salmon, G.A. Bohme, M. Laville, J. Pratt, O. Corti, L. Pradier, G. Ret, C. Joubert, M. Periquet, F. Araujo, J. Negroni, M.J. Casarejos, S. Canals, R. Solano, A. Serrano, E. Gallego, M. Sanchez, P. Denefle, J. Benavides, G. Tremp, T.A. Rooney, A. Brice, J. Garcia de Yebenes, Parkin gene inactivation alters behaviour and dopamine neurotransmission in the mouse, Hum Mol Genet, 12 (2003) 2277-2291.

[107] S. Sato, T. Chiba, S. Nishiyama, T. Kakiuchi, H. Tsukada, T. Hatano, T. Fukuda, Y. Yasoshima, N. Kai, K. Kobayashi, Y. Mizuno, K. Tanaka, N. Hattori, Decline of striatal dopamine release in parkin-deficient mice shown by ex vivo autoradiography, Journal of neuroscience research, 84 (2006) 1350-1357.

[108] M. Periquet, O. Corti, S. Jacquier, A. Brice, Proteomic analysis of parkin knockout mice: alterations in energy metabolism, protein handling and synaptic function, Journal of neurochemistry, 95 (2005) 1259-1276.

[109] J.T. Bendor, T.P. Logan, R.H. Edwards, The function of alpha-synuclein, Neuron, 79 (2013) 1044-1066.

[110] B.R. Lee, T. Kamitani, Improved immunodetection of endogenous alpha-synuclein, PloS one, 6 (2011) e23939.

[111] F. Fornai, P. Lenzi, M. Gesi, P. Soldani, M. Ferrucci, G. Lazzeri, L. Capobianco, G. Battaglia, A. De Blasi, F. Nicoletti, A. Paparelli, Methamphetamine produces neuronal inclusions in the nigrostriatal system and in PC12 cells, Journal of neurochemistry, 88 (2004) 114-123.

[112] H. Shimura, M.G. Schlossmacher, N. Hattori, M.P. Frosch, A. Trockenbacher, R. Schneider, Y. Mizuno, K.S. Kosik, D.J. Selkoe, Ubiquitination of a new form of alpha-synuclein by parkin from human brain: implications for Parkinson's disease, Science, 293 (2001) 263-269.

[113] K.K. Chung, Y. Zhang, K.L. Lim, Y. Tanaka, H. Huang, J. Gao, C.A. Ross, V.L. Dawson, T.M. Dawson, Parkin ubiquitinates the alpha-synuclein-interacting protein, synphilin-1: implications for Lewy-body formation in Parkinson disease, Nat Med, 7 (2001) 1144-1150.

[114] D. Kirik, C. Rosenblad, C. Burger, C. Lundberg, T.E. Johansen, N. Muzyczka, R.J. Mandel, A. Bjorklund, Parkinson-like neurodegeneration induced by targeted

overexpression of alpha-synuclein in the nigrostriatal system, The Journal of neuroscience : the official journal of the Society for Neuroscience, 22 (2002) 2780-2791.

[115] E. Lauwers, Z. Debyser, J. Van Dorpe, B. De Strooper, B. Nuttin, V. Baekelandt, Neuropathology and neurodegeneration in rodent brain induced by lentiviral vector-mediated overexpression of alpha-synuclein, Brain Pathol, 13 (2003) 364-372.

[116] C. Lo Bianco, J.L. Ridet, B.L. Schneider, N. Deglon, P. Aebischer, alpha -Synucleinopathy and selective dopaminergic neuron loss in a rat lentiviral-based model of Parkinson's disease, Proceedings of the National Academy of Sciences of the United States of America, 99 (2002) 10813-10818.

[117] M. Yamada, T. Iwatsubo, Y. Mizuno, H. Mochizuki, Overexpression of alpha-synuclein in rat substantia nigra results in loss of dopaminergic neurons, phosphorylation of alpha-synuclein and activation of caspase-9: resemblance to pathogenetic changes in Parkinson's disease, Journal of neurochemistry, 91 (2004) 451-461.

[118] B. Butler, J. Gamble-George, P. Prins, A. North, J.T. Clarke, H. Khoshbouei, Chronic Methamphetamine Increases Alpha-Synuclein Protein Levels in the Striatum and Hippocampus but not in the Cortex of Juvenile Mice, J Addict Prev, 2 (2014).

[119] W. Jiang, J. Li, Z. Zhang, H. Wang, Z. Wang, Epigenetic upregulation of alpha-synuclein in the rats exposed to methamphetamine, European journal of pharmacology, 745 (2014) 243-248.

[120] E.H. Norris, B.I. Giasson, H. Ischiropoulos, V.M. Lee, Effects of oxidative and nitrative challenges on alpha-synuclein fibrillogenesis involve distinct mechanisms of protein modifications, The Journal of biological chemistry, 278 (2003) 27230-27240.

[121] Y. Tai, L. Chen, E. Huang, C. Liu, X. Yang, P. Qiu, H. Wang, Protective effect of alpha-synuclein knockdown on methamphetamine-induced neurotoxicity in dopaminergic neurons, Neural regeneration research, 9 (2014) 951-958.

[122] L. Chen, E. Huang, H. Wang, P. Qiu, C. Liu, RNA interference targeting alpha-synuclein attenuates methamphetamine-induced neurotoxicity in SH-SY5Y cells, Brain research, 1521 (2013) 59-67.

[123] G. Ronzitti, G. Bucci, M. Emanuele, D. Leo, T.D. Sotnikova, L.V. Mus, C.H. Soubrane, M.L. Dallas, A. Thalhammer, L.A. Cingolani, S. Mochida, R.R. Gainetdinov, G.J. Stephens, E. Chieregatti, Exogenous alpha-synuclein decreases raft partitioning of Cav2.2 channels inducing dopamine release, The Journal of neuroscience : the official journal of the Society for Neuroscience, 34 (2014) 10603-10615.

[124] E. Illes-Toth, C.F. Dalton, D.P. Smith, Binding of Dopamine to Alpha-Synuclein is Mediated by Specific Conformational States, Journal of the American Society for Mass Spectrometry, 24 (2013) 1346-1354.

[125] H.J. Lee, S.M. Baek, D.H. Ho, J.E. Suk, E.D. Cho, S.J. Lee, Dopamine promotes formation and secretion of non-fibrillar alpha-synuclein oligomers, Experimental & molecular medicine, 43 (2011) 216-222.

[126] O. Tavassoly, J.S. Lee, Methamphetamine binds to alpha-synuclein and causes a conformational change which can be detected by nanopore analysis, FEBS letters, 586 (2012) 3222-3228.

[127] T. Bartels, J.G. Choi, D.J. Selkoe, alpha-Synuclein occurs physiologically as a helically folded tetramer that resists aggregation, Nature, 477 (2011) 107-110.

[128] U. Dettmer, A.J. Newman, F. Soldner, E.S. Luth, N.C. Kim, V.E. von Saucken, J.B. Sanderson, R. Jaenisch, T. Bartels, D. Selkoe, Corrigendum: Parkinson-causing alpha-synuclein missense mutations shift native tetramers to monomers as a mechanism for disease initiation, Nature communications, 6 (2015) 8008.

[129] K.A. Conway, J.C. Rochet, R.M. Bieganski, P.T. Lansbury, Jr., Kinetic stabilization of the alpha-synuclein protofibril by a dopamine-alpha-synuclein adduct, Science, 294 (2001) 1346-1349.

[130] C.L. Pham, R. Cappai, The interplay between lipids and dopamine on alpha-synuclein oligomerization and membrane binding, Biosci Rep, 33 (2013).

[131] M.Y. Lin, Z.H. Sheng, Regulation of mitochondrial transport in neurons, Experimental cell research, 334 (2015) 35-44.

[132] J.E. Vance, R.B. Campenot, D.E. Vance, The synthesis and transport of lipids for axonal growth and nerve regeneration, Biochimica et biophysica acta, 1486 (2000) 84-96.

[133] S. Roy, G. Yang, Y. Tang, D.A. Scott, A simple photoactivation and image analysis module for visualizing and analyzing axonal transport with high temporal resolution, Nature protocols, 7 (2012) 62-68.

[134] J. Block-Galarza, K.O. Chase, E. Sapp, K.T. Vaughn, R.B. Vallee, M. DiFiglia, N. Aronin, Fast transport and retrograde movement of huntingtin and HAP 1 in axons, Neuroreport, 8 (1997) 2247-2251.

[135] A. Rao, T.L. Richards, D. Simmons, N.R. Zahniser, A. Sorkin, Epitope-tagged dopamine transporter knock-in mice reveal rapid endocytic trafficking and filopodia

targeting of the transporter in dopaminergic axons, FASEB journal : official publication of the Federation of American Societies for Experimental Biology, 26 (2012) 1921-1933.

[136] S. Roy, Seeing the unseen: the hidden world of slow axonal transport, The Neuroscientist : a review journal bringing neurobiology, neurology and psychiatry, 20 (2014) 71-81.

[137] C. Conde, A. Caceres, Microtubule assembly, organization and dynamics in axons and dendrites, Nature reviews. Neuroscience, 10 (2009) 319-332.

[138] K.A. James, J.J. Bray, I.G. Morgan, L. Austin, The effect of colchicine on the transport of axonal protein in the chicken, The Biochemical journal, 117 (1970) 767-771.

[139] B. Zhang, A. Maiti, S. Shively, F. Lakhani, G. McDonald-Jones, J. Bruce, E.B. Lee, S.X. Xie, S. Joyce, C. Li, P.M. Toleikis, V.M. Lee, J.Q. Trojanowski, Microtubule-binding drugs offset tau sequestration by stabilizing microtubules and reversing fast axonal transport deficits in a tauopathy model, Proceedings of the National Academy of Sciences of the United States of America, 102 (2005) 227-231.

[140] S. Westermann, K. Weber, Post-translational modifications regulate microtubule function, Nat Rev Mol Cell Biol, 4 (2003) 938-947.

[141] C.A. Arce, J.A. Rodriguez, H.S. Barra, R. Caputo, Incorporation of L-tyrosine, L-phenylalanine and L-3,4-dihydroxyphenylalanine as single units into rat brain tubulin, Eur J Biochem, 59 (1975) 145-149.

[142] A.S. Infante, M.S. Stein, Y. Zhai, G.G. Borisy, G.G. Gundersen, Detyrosinated (Glu) microtubules are stabilized by an ATP-sensitive plus-end cap, J Cell Sci, 113 (Pt 22) (2000) 3907-3919.

[143] J.S. Akella, D. Wloga, J. Kim, N.G. Starostina, S. Lyons-Abbott, N.S. Morrissette, S.T. Dougan, E.T. Kipreos, J. Gaertig, MEC-17 is an alpha-tubulin acetyltransferase, Nature, 467 (2010) 218-222.

[144] Y. Zhang, N. Li, C. Caron, G. Matthias, D. Hess, S. Khochbin, P. Matthias, HDAC-6 interacts with and deacetylates tubulin and microtubules in vivo, EMBO J, 22 (2003) 1168-1179.

[145] B.J. North, B.L. Marshall, M.T. Borra, J.M. Denu, E. Verdin, The human Sir2 ortholog, SIRT2, is an NAD+-dependent tubulin deacetylase, Mol Cell, 11 (2003) 437-444.

[146] G.A. Morfini, M. Burns, L.I. Binder, N.M. Kanaan, N. LaPointe, D.A. Bosco, R.H. Brown, Jr., H. Brown, A. Tiwari, L. Hayward, J. Edgar, K.A. Nave, J. Garberrn, Y. Atagi, Y. Song, G. Pigino, S.T. Brady, Axonal transport defects in neurodegenerative diseases, The Journal of neuroscience : the official journal of the Society for Neuroscience, 29 (2009) 12776-12786.

[147] S. Millecamps, J.P. Julien, Axonal transport deficits and neurodegenerative diseases, Nature reviews. Neuroscience, 14 (2013) 161-176.

[148] L.S. Goldstein, Axonal transport and neurodegenerative disease: can we see the elephant?, Progress in neurobiology, 99 (2012) 186-190.

[149] E. Perlson, S. Maday, M.M. Fu, A.J. Moughamian, E.L. Holzbaur, Retrograde axonal transport: pathways to cell death?, Trends in neurosciences, 33 (2010) 335-344.

[150] S. Fernandes, S. Salta, T. Summavielle, Methamphetamine promotes alpha-tubulin deacetylation in endothelial cells: the protective role of acetyl-l-carnitine, Toxicology letters, 234 (2015) 131-138.

[151] B. Zhang, J. Carroll, J.Q. Trojanowski, Y. Yao, M. Iba, J.S. Potuzak, A.M. Hogan, S.X. Xie, C. Ballatore, A.B. Smith, 3rd, V.M. Lee, K.R. Brunden, The microtubule-stabilizing agent, epothilone D, reduces axonal dysfunction, neurotoxicity, cognitive deficits, and Alzheimer-like pathology in an interventional study with aged tau transgenic mice, The Journal of neuroscience : the official journal of the Society for Neuroscience, 32 (2012) 3601-3611.

[152] K.R. Brunden, B. Zhang, J. Carroll, Y. Yao, J.S. Potuzak, A.M. Hogan, M. Iba, M.J. James, S.X. Xie, C. Ballatore, A.B. Smith, 3rd, V.M. Lee, J.Q. Trojanowski, Epothilone D improves microtubule density, axonal integrity, and cognition in a transgenic mouse model of tauopathy, J Neurosci, 30 (2010) 13861-13866.

[153] D. Cartelli, F. Casagrande, C.L. Busceti, D. Bucci, G. Molinaro, A. Traficante, D. Passarella, E. Giavini, G. Pezzoli, G. Battaglia, G. Cappelletti, Microtubule alterations occur early in experimental parkinsonism and the microtubule stabilizer epothilone D is neuroprotective, Sci Rep, 3 (2013) 1837.

[154] R.J. Kowalski, P. Giannakakou, E. Hamel, Activities of the microtubule-stabilizing agents epothilones A and B with purified tubulin and in cells resistant to paclitaxel (Taxol(R)), The Journal of biological chemistry, 272 (1997) 2534-2541.

[155] C. Ballatore, K.R. Brunden, D.M. Huryn, J.Q. Trojanowski, V.M. Lee, A.B. Smith, 3rd, Microtubule stabilizing agents as potential treatment for Alzheimer's disease and

related neurodegenerative tauopathies, Journal of medicinal chemistry, 55 (2012) 8979-8996.

[156] U.D. McCann, H. Kuwabara, A. Kumar, M. Palermo, R. Abbey, J. Brasic, W. Ye, M. Alexander, R.F. Dannals, D.F. Wong, G.A. Ricaurte, Persistent cognitive and dopamine transporter deficits in abstinent methamphetamine users, Synapse, 62 (2008) 91-100.

[157] Y. Sekine, Y. Minabe, Y. Ouchi, N. Takei, M. Iyo, K. Nakamura, K. Suzuki, H. Tsukada, H. Okada, E. Yoshikawa, M. Futatsubashi, N. Mori, Association of dopamine transporter loss in the orbitofrontal and dorsolateral prefrontal cortices with methamphetamine-related psychiatric symptoms, Am J Psychiatry, 160 (2003) 1699-1701.

[158] N.D. Volkow, L. Chang, G.J. Wang, J.S. Fowler, M. Leonido-Yee, D. Franceschi, M.J. Sedler, S.J. Gatley, R. Hitzemann, Y.S. Ding, J. Logan, C. Wong, E.N. Miller, Association of dopamine transporter reduction with psychomotor impairment in methamphetamine abusers, Am J Psychiatry, 158 (2001) 377-382.

[159] J.D. Jones, S.D. Comer, A review of human drug self-administration procedures, Behavioural pharmacology, 24 (2013) 384-395.

[160] R. Le Cozannet, A. Markou, R. Kuczenski, Extended-access, but not limited-access, methamphetamine self-administration induces behavioral and nucleus accumbens dopamine response changes in rats, The European journal of neuroscience, 38 (2013) 3487-3495.

[161] J.J. Anker, T.R. Baron, N.E. Zlebnik, M.E. Carroll, Escalation of methamphetamine self-administration in adolescent and adult rats, Drug Alcohol Depend, 124 (2012) 149-153.

[162] A.K. Cho, W.P. Melega, R. Kuczenski, D.S. Segal, Relevance of pharmacokinetic parameters in animal models of methamphetamine abuse, Synapse, 39 (2001) 161-166.

[163] R. Stefanski, B. Ladenheim, S.H. Lee, J.L. Cadet, S.R. Goldberg, Neuroadaptations in the dopaminergic system after active self-administration but not after passive administration of methamphetamine, European journal of pharmacology, 371 (1999) 123-135.

[164] J.R. Hollerman, W. Schultz, Dopamine neurons report an error in the temporal prediction of reward during learning, Nature neuroscience, 1 (1998) 304-309.

[165] B. Killinger, M. Shah, A. Moszczynska, Co-administration of betulinic acid and methamphetamine causes toxicity to dopaminergic and serotonergic nerve terminals in the striatum of late adolescent rats, J Neurochem, 128 (2014) 764-775.

[166] S.L. Walsh, G.C. Wagner, Motor impairments after methamphetamine-induced neurotoxicity in the rat, The Journal of pharmacology and experimental therapeutics, 263 (1992) 617-626.

[167] M. Shoaib, C.W. Schindler, S.R. Goldberg, Nicotine self-administration in rats: strain and nicotine pre-exposure effects on acquisition, Psychopharmacology, 129 (1997) 35-43.

[168] S. Deiana, L. Fattore, M.S. Spano, G. Cossu, E. Porcu, P. Fadda, W. Fratta, Strain and schedule-dependent differences in the acquisition, maintenance and extinction of intravenous cannabinoid self-administration in rats, Neuropharmacology, 52 (2007) 646-654.

[169] C. D'Arcy, J.E. Luevano, M. Miranda-Arango, J.A. Pipkin, J.A. Jackson, E. Castaneda, K.L. Gosselink, L.E. O'Dell, Extended access to methamphetamine self-administration up-regulates dopamine transporter levels 72 hours after withdrawal in rats, Behavioural brain research, 296 (2016) 125-128.

[170] G.C. Wagner, G.A. Ricaurte, L.S. Seiden, C.R. Schuster, R.J. Miller, J. Westley, Long-lasting depletions of striatal dopamine and loss of dopamine uptake sites following repeated administration of methamphetamine, Brain research, 181 (1980) 151-160.

[171] K.L. Preston, G.C. Wagner, C.R. Schuster, L.S. Seiden, Long-term effects of repeated methylamphetamine administration on monoamine neurons in the rhesus monkey brain, Brain research, 338 (1985) 243-248.

[172] D.J. Mooney, L.K. Hansen, R. Langer, J.P. Vacanti, D.E. Ingber, Extracellular matrix controls tubulin monomer levels in hepatocytes by regulating protein turnover, Molecular biology of the cell, 5 (1994) 1281-1288.

[173] D.C. Harvey, G. Lacan, S.P. Tanious, W.P. Melega, Recovery from methamphetamine induced long-term nigrostriatal dopaminergic deficits without substantia nigra cell loss, Brain research, 871 (2000) 259-270.

[174] W.A. Cass, M.W. Manning, Recovery of presynaptic dopaminergic functioning in rats treated with neurotoxic doses of methamphetamine, The Journal of neuroscience : the official journal of the Society for Neuroscience, 19 (1999) 7653-7660.

[175] J.F. Bowyer, G.D. Newport, G.W. Lipe, L.T. Frame, A further evaluation of the effects of K+ depolarization on glutamate-evoked [3H]dopamine release from striatal slices, The Journal of pharmacology and experimental therapeutics, 261 (1992) 72-80.

[176] R.C. Callaghan, J.K. Cunningham, J. Sykes, S.J. Kish, Increased risk of Parkinson's disease in individuals hospitalized with conditions related to the use of methamphetamine or other amphetamine-type drugs, Drug and alcohol dependence, 120 (2012) 35-40.

[177] D. Wloga, J. Gaertig, Post-translational modifications of microtubules, Journal of cell science, 123 (2010) 3447-3455.

[178] E. Schulze, D.J. Asai, J.C. Bulinski, M. Kirschner, Posttranslational modification and microtubule stability, The Journal of cell biology, 105 (1987) 2167-2177.

[179] A. Brown, Y. Li, T. Slaughter, M.M. Black, Composite microtubules of the axon: quantitative analysis of tyrosinated and acetylated tubulin along individual axonal microtubules, Journal of cell science, 104 (Pt 2) (1993) 339-352.

[180] N.A. Reed, D. Cai, T.L. Blasius, G.T. Jih, E. Meyhofer, J. Gaertig, K.J. Verhey, Microtubule acetylation promotes kinesin-1 binding and transport, Current biology : CB, 16 (2006) 2166-2172.

[181] Y. Konishi, M. Setou, Tubulin tyrosination navigates the kinesin-1 motor domain to axons, Nature neuroscience, 12 (2009) 559-567.

[182] M.A. Tischfield, H.N. Baris, C. Wu, G. Rudolph, L. Van Maldergem, W. He, W.M. Chan, C. Andrews, J.L. Demer, R.L. Robertson, D.A. Mackey, J.B. Ruddle, T.D. Bird, I. Gottlob, C. Pieh, E.I. Traboulsi, S.L. Pomeroy, D.G. Hunter, J.S. Soul, A. Newlin, L.J. Sabol, E.J. Doherty, C.E. de Uzcategui, N. de Uzcategui, M.L. Collins, E.C. Sener, B. Wabbels, H. Hellebrand, T. Meitinger, T. de Berardinis, A. Magli, C. Schiavi, M. Pastore-Trossello, F. Koc, A.M. Wong, A.V. Levin, M.T. Geraghty, M. Descartes, M. Flaherty, R.V. Jamieson, H.U. Moller, I. Meuthen, D.F. Callen, J. Kerwin, S. Lindsay, A. Meindl,

M.L. Gupta, Jr., D. Pellman, E.C. Engle, Human TUBB3 mutations perturb microtubule dynamics, kinesin interactions, and axon guidance, Cell, 140 (2010) 74-87.

[183] J. Guo, M. Qiang, R.F. Luduena, The distribution of beta-tubulin isotypes in cultured neurons from embryonic, newborn, and adult mouse brains, Brain research, 1420 (2011) 8-18.

[184] M. Hari, H. Yang, C. Zeng, M. Canizales, F. Cabral, Expression of class III beta-tubulin reduces microtubule assembly and confers resistance to paclitaxel, Cell motility and the cytoskeleton, 56 (2003) 45-56.

[185] E. Narvi, K. Jaakkola, S. Winsel, C. Oetken-Lindholm, P. Halonen, L. Kallio, M.J. Kallio, Altered TUBB3 expression contributes to the epothilone response of mitotic cells, British journal of cancer, 108 (2013) 82-90.

[186] P.W. Baas, M.M. Black, Individual microtubules in the axon consist of domains that differ in both composition and stability, The Journal of cell biology, 111 (1990) 495-509.

[187] K.R. Brunden, Y. Yao, J.S. Potuzak, N.I. Ferrer, C. Ballatore, M.J. James, A.M. Hogan, J.Q. Trojanowski, A.B. Smith, 3rd, V.M. Lee, The characterization of microtubule-stabilizing drugs as possible therapeutic agents for Alzheimer's disease and related tauopathies, Pharmacological research : the official journal of the Italian Pharmacological Society, 63 (2011) 341-351.

[188] Y. Fan, G. Wali, R. Sutharsan, B. Bellette, D.I. Crane, C.M. Sue, A. Mackay-Sim, Low dose tubulin-binding drugs rescue peroxisome trafficking deficit in patient-derived stem cells in Hereditary Spastic Paraplegia, Biology open, 3 (2014) 494-502.

[189] P.D. Altland, B. Highman, M. Parker, Induction of hypothermia by dimethyl sulfoxide in rats exposed to cold: tissue and enzyme changes, Proc Soc Exp Biol Med, 123 (1966) 853-859.

[190] J. Robinson, Y. Engelborghs, Tubulin polymerization in dimethyl sulfoxide, The Journal of biological chemistry, 257 (1982) 5367-5371.

[191] G. Cavaletti, N. Oggioni, F. Sala, G. Pezzoni, E. Cavalletti, P. Marmiroli, M.G. Petruccioli, L. Frattola, G. Tredici, Effect on the peripheral nervous system of systemically administered dimethylsulfoxide in the rat: a neurophysiological and pathological study, Toxicology letters, 118 (2000) 103-107.

[192] A. Kleindienst, J.G. Dunbar, R. Glisson, K. Okuno, A. Marmarou, Effect of dimethyl sulfoxide on blood-brain barrier integrity following middle cerebral artery occlusion in the rat, Acta neurochirurgica. Supplement, 96 (2006) 258-262.

[193] J.F. Bowyer, A.W. Tank, G.D. Newport, W. Slikker, Jr., S.F. Ali, R.R. Holson, The influence of environmental temperature on the transient effects of methamphetamine on dopamine levels and dopamine release in rat striatum, The Journal of pharmacology and experimental therapeutics, 260 (1992) 817-824.

[194] W.F. Sette, Adoption of new guidelines and data requirements for more extensive neurotoxicity testing under FIFRA, Toxicology and industrial health, 5 (1989) 181-194.

[195] B.K. Yamamoto, W. Zhu, The effects of methamphetamine on the production of free radicals and oxidative stress, The Journal of pharmacology and experimental therapeutics, 287 (1998) 107-114.

[196] S. Jayanthi, X. Deng, P.A. Noailles, B. Ladenheim, J.L. Cadet, Methamphetamine induces neuronal apoptosis via cross-talks between endoplasmic reticulum and mitochondria-dependent death cascades, FASEB journal : official publication of the Federation of American Societies for Experimental Biology, 18 (2004) 238-251.

[197] J.P. Zhu, W. Xu, J.A. Angulo, Disparity in the temporal appearance of methamphetamine-induced apoptosis and depletion of dopamine terminal markers in the striatum of mice, Brain research, 1049 (2005) 171-181.

[198] J.F. Bowyer, L.T. Frame, P. Clausing, K. Nagamoto-Combs, C.A. Osterhout, C.R. Sterling, A.W. Tank, Long-term effects of amphetamine neurotoxicity on tyrosine hydroxylase mRNA and protein in aged rats, The Journal of pharmacology and experimental therapeutics, 286 (1998) 1074-1085.

[199] B.K. Yamamoto, A. Moszczynska, G.A. Gudelsky, Amphetamine toxicities: classical and emerging mechanisms, Annals of the New York Academy of Sciences, 1187 (2010) 101-121.

[200] K.J. Verhey, J. Gaertig, The tubulin code, Cell Cycle, 6 (2007) 2152-2160.

[201] C. Janke, The tubulin code: molecular components, readout mechanisms, and functions, The Journal of cell biology, 206 (2014) 461-472.

[202] A. Wehenkel, C. Janke, Towards elucidating the tubulin code, Nature cell biology, 16 (2014) 303-305.

[203] G. Liao, G.G. Gundersen, Kinesin is a candidate for cross-bridging microtubules and intermediate filaments. Selective binding of kinesin to detyrosinated tubulin and vimentin, The Journal of biological chemistry, 273 (1998) 9797-9803.

[204] C. Erck, L. Peris, A. Andrieux, C. Meissirel, A.D. Gruber, M. Vernet, A. Schweitzer, Y. Saoudi, H. Pointu, C. Bosc, P.A. Salin, D. Job, J. Wehland, A vital role of tubulin-tyrosine-ligase for neuronal organization, Proceedings of the National Academy of Sciences of the United States of America, 102 (2005) 7853-7858.

[205] L. Peris, M. Thery, J. Faure, Y. Saoudi, L. Lafanechere, J.K. Chilton, P. Gordon-Weeks, N. Galjart, M. Bornens, L. Wordeman, J. Wehland, A. Andrieux, D. Job, Tubulin tyrosination is a major factor affecting the recruitment of CAP-Gly proteins at microtubule plus ends, The Journal of cell biology, 174 (2006) 839-849.

[206] A.J. Moughamian, G.E. Osborn, J.E. Lazarus, S. Maday, E.L. Holzbaur, Ordered recruitment of dynactin to the microtubule plus-end is required for efficient initiation of retrograde axonal transport, The Journal of neuroscience : the official journal of the Society for Neuroscience, 33 (2013) 13190-13203.

[207] E. Chevalier-Larsen, E.L. Holzbaur, Axonal transport and neurodegenerative disease, Biochimica et biophysica acta, 1762 (2006) 1094-1108.

[208] M. Lin, P. Chandramani-Shivalingappa, H. Jin, A. Ghosh, V. Anantharam, S. Ali, A.G. Kanthasamy, A. Kanthasamy, Methamphetamine-induced neurotoxicity linked to ubiquitin-proteasome system dysfunction and autophagy-related changes that can be modulated by protein kinase C delta in dopaminergic neuronal cells, Neuroscience, 210 (2012) 308-332.

[209] H.L. Wen, Y.T. Lin, C.H. Ting, S. Lin-Chao, H. Li, H.M. Hsieh-Li, Stathmin, a microtubule-destabilizing protein, is dysregulated in spinal muscular atrophy, Human molecular genetics, 19 (2010) 1766-1778.

[210] J.R. Menezes, M.B. Luskin, Expression of neuron-specific tubulin defines a novel population in the proliferative layers of the developing telencephalon, The Journal of neuroscience : the official journal of the Society for Neuroscience, 14 (1994) 5399-5416.

[211] A.J. Roskams, X. Cai, G.V. Ronnett, Expression of neuron-specific beta-III tubulin during olfactory neurogenesis in the embryonic and adult rat, Neuroscience, 83 (1998) 191-200.

[212] M. Mariani, R. Karki, M. Spennato, D. Pandya, S. He, M. Andreoli, P. Fiedler, C. Ferlini, Class III beta-tubulin in normal and cancer tissues, Gene, 563 (2015) 109-114.

[213] H. Ujike, M. Takaki, M. Kodama, S. Kuroda, Gene expression related to synaptogenesis, neuritogenesis, and MAP kinase in behavioral sensitization to psychostimulants, Annals of the New York Academy of Sciences, 965 (2002) 55-67.

[214] I.K. Tulloch, L. Afanador, L. Baker, D. Ordonez, H. Payne, I. Mexhitaj, E. Olivares, A. Chowdhury, J.A. Angulo, Methamphetamine induces low levels of neurogenesis in striatal neuron subpopulations and differential motor performance, Neurotoxicity research, 26 (2014) 115-129.

[215] V.K. Godena, N. Brookes-Hocking, A. Moller, G. Shaw, M. Oswald, R.M. Sancho, C.C. Miller, A.J. Whitworth, K.J. De Vos, Increasing microtubule acetylation rescues axonal transport and locomotor deficits caused by LRRK2 Roc-COR domain mutations, Nature communications, 5 (2014) 5245.

[216] A. Cheng, A.L. Scott, B. Ladenheim, K. Chen, X. Ouyang, J.D. Lathia, M. Mughal, J.L. Cadet, M.P. Mattson, J.C. Shih, Monoamine oxidases regulate telencephalic neural

progenitors in late embryonic and early postnatal development, The Journal of neuroscience : the official journal of the Society for Neuroscience, 30 (2010) 10752-10762.

[217] C. Janke, M. Kneussel, Tubulin post-translational modifications: encoding functions on the neuronal microtubule cytoskeleton, Trends in neurosciences, 33 (2010) 362-372.

[218] J. Ruschel, F. Hellal, K.C. Flynn, S. Dupraz, D.A. Elliott, A. Tedeschi, M. Bates, C. Sliwinski, G. Brook, K. Dobrindt, M. Peitz, O. Brustle, M.D. Norenberg, A. Blesch, N. Weidner, M.B. Bunge, J.L. Bixby, F. Bradke, Axonal regeneration. Systemic administration of epothilone B promotes axon regeneration after spinal cord injury, Science, 348 (2015) 347-352.

[219] C.D. Scripture, W.D. Figg, A. Sparreboom, Peripheral neuropathy induced by paclitaxel: recent insights and future perspectives, Current neuropharmacology, 4 (2006) 165-172.

[220] M. Tomas, P. Marin, L. Megias, G. Egea, J. Renau-Piqueras, Ethanol perturbs the secretory pathway in astrocytes, Neurobiology of disease, 20 (2005) 773-784.

[221] W. Bilecki, A. Wawrzczak-Bargiela, R. Przewlocki, Regulation of kinesin light chain 1 level correlates with the development of morphine reward in the mouse brain, The European journal of neuroscience, 30 (2009) 1101-1110.

[222] J.P. Jedynak, J.M. Uslaner, J.A. Esteban, T.E. Robinson, Methamphetamine-induced structural plasticity in the dorsal striatum, The European journal of neuroscience, 25 (2007) 847-853.

[223] Y. Ren, W. Liu, H. Jiang, Q. Jiang, J. Feng, Selective vulnerability of dopaminergic neurons to microtubule depolymerization, The Journal of biological chemistry, 280 (2005) 34105-34112.

[224] M.A. Franker, C.C. Hoogenraad, Microtubule-based transport - basic mechanisms, traffic rules and role in neurological pathogenesis, Journal of cell science, 126 (2013) 2319-2329.

[225] O. Mercado-Gomez, P. Ferrera, C. Arias, Histopathologic changes induced by the microtubule-stabilizing agent Taxol in the rat hippocampus in vivo, Journal of neuroscience research, 78 (2004) 553-562.

[226] K. Stamer, R. Vogel, E. Thies, E. Mandelkow, E.M. Mandelkow, Tau blocks traffic of organelles, neurofilaments, and APP vesicles in neurons and enhances oxidative stress, The Journal of cell biology, 156 (2002) 1051-1063.

[227] P. Brun, M. Begou, A. Andrieux, L. Mouly-Badina, M. Clerget, A. Schweitzer, H. Scarna, B. Renaud, D. Job, M.F. Suaud-Chagny, Dopaminergic transmission in STOP null mice, Journal of neurochemistry, 94 (2005) 63-73.

[228] C. Bouvrais-Veret, S. Weiss, N. Hanoun, A. Andrieux, A. Schweitzer, D. Job, M. Hamon, B. Giros, M.P. Martres, Microtubule-associated STOP protein deletion triggers restricted changes in dopaminergic neurotransmission, Journal of neurochemistry, 104 (2008) 745-756.

[229] H.A. Boger, L.D. Middaugh, K.S. Patrick, S. Ramamoorthy, E.D. Denehy, H. Zhu, A.M. Pacchioni, A.C. Granholm, J.F. McGinty, Long-term consequences of methamphetamine exposure in young adults are exacerbated in glial cell line-derived

neurotrophic factor heterozygous mice, The Journal of neuroscience : the official journal of the Society for Neuroscience, 27 (2007) 8816-8825.

[230] A. Brown, Axonal transport of membranous and nonmembranous cargoes: a unified perspective, The Journal of cell biology, 160 (2003) 817-821.

[231] D. Lechardeur, M.N. Castel, M. Reibaud, D. Scherman, P.M. Laduron, Axonal transport of dopamine-containing vesicles labelled in vivo with [3H]reserpine, The European journal of neuroscience, 5 (1993) 449-453.

[232] N.R. Herring, T.L. Schaefer, G.A. Gudelsky, C.V. Vorhees, M.T. Williams, Effect of +-methamphetamine on path integration learning, novel object recognition, and neurotoxicity in rats, Psychopharmacology, 199 (2008) 637-650.

[233] A.W. Fjorback, S. Sundbye, J.C. Dachsel, S. Sinning, O. Wiborg, P.H. Jensen, P25alpha / TPPP expression increases plasma membrane presentation of the dopamine transporter and enhances cellular sensitivity to dopamine toxicity, The FEBS journal, 278 (2011) 493-505.

[234] H. Higashi, K. Inanaga, S. Nishi, N. Uchimura, Enhancement of dopamine actions on rat nucleus accumbens neurones in vitro after methamphetamine pre-treatment, The Journal of physiology, 408 (1989) 587-603.

[235] R. Kuczenski, D.S. Segal, M.L. Aizenstein, Amphetamine, cocaine, and fencamfamine: relationship between locomotor and stereotypy response profiles and caudate and accumbens dopamine dynamics, The Journal of neuroscience : the official journal of the Society for Neuroscience, 11 (1991) 2703-2712.

[236] E.H. Chartoff, M.S. Szczypka, R.D. Palmiter, D.M. Dorsa, Endogenous neurotensin attenuates dopamine-dependent locomotion and stereotypy, Brain research, 1022 (2004) 71-80.

[237] J.T. Kevenaar, C.C. Hoogenraad, The axonal cytoskeleton: from organization to function, Frontiers in molecular neuroscience, 8 (2015) 44.

[238] R. Castino, G. Lazzeri, P. Lenzi, N. Bellio, C. Follo, M. Ferrucci, F. Fornai, C. Isidoro, Suppression of autophagy precipitates neuronal cell death following low doses of methamphetamine, Journal of neurochemistry, 106 (2008) 1426-1439.

[239] S. Hayashi, A. Yamamoto, F. You, K. Yamashita, Y. Ikegame, M. Tawada, T. Yoshimori, S. Shimizu, S. Nakashima, The stent-eluting drugs sirolimus and paclitaxel suppress healing of the endothelium by induction of autophagy, The American journal of pathology, 175 (2009) 2226-2234.

[240] N.E. LaPointe, G. Morfini, S.T. Brady, S.C. Feinstein, L. Wilson, M.A. Jordan, Effects of eribulin, vincristine, paclitaxel and ixabepilone on fast axonal transport and kinesin-1 driven microtubule gliding: implications for chemotherapy-induced peripheral neuropathy, Neurotoxicology, 37 (2013) 231-239.

[241] V. Fournet, A. Schweitzer, C. Chevarin, J.C. Deloulme, M. Hamon, B. Giros, A. Andrieux, M.P. Martres, The deletion of STOP/MAP6 protein in mice triggers highly altered mood and impaired cognitive performances, Journal of neurochemistry, 121 (2012) 99-114.

[242] V. Fournet, G. de Lavilleon, A. Schweitzer, B. Giros, A. Andrieux, M.P. Martres, Both chronic treatments by epothilone D and fluoxetine increase the short-term memory

and differentially alter the mood status of STOP/MAP6 KO mice, Journal of neurochemistry, 123 (2012) 982-996.

[243] A. Daoust, S. Bohic, Y. Saoudi, C. Debacker, S. Gory-Faure, A. Andrieux, E.L. Barbier, J.C. Deloulme, Neuronal transport defects of the MAP6 KO mouse - a model of schizophrenia - and alleviation by Epothilone D treatment, as observed using MEMRI, NeuroImage, 96 (2014) 133-142.

[244] T.E. Robinson, K.C. Berridge, The neural basis of drug craving: an incentive-sensitization theory of addiction, Brain research. Brain research reviews, 18 (1993) 247-291.

[245] W. Schultz, Multiple dopamine functions at different time courses, Annual review of neuroscience, 30 (2007) 259-288.

[246] D.J. Nutt, A. Lingford-Hughes, D. Erritzoe, P.R. Stokes, The dopamine theory of addiction: 40 years of highs and lows, Nature reviews. Neuroscience, 16 (2015) 305-312.

[247] W. Dauer, S. Przedborski, Parkinson's disease: mechanisms and models, Neuron, 39 (2003) 889-909.

[248] G.E. Alexander, Biology of Parkinson's disease: pathogenesis and pathophysiology of a multisystem neurodegenerative disorder, Dialogues in clinical neuroscience, 6 (2004) 259-280.

[249] P. Mazzoni, B. Shabbott, J.C. Cortes, Motor control abnormalities in Parkinson's disease, Cold Spring Harbor perspectives in medicine, 2 (2012) a009282.

[250] A. Alttoa, P. Seeman, K. Koiv, M. Eller, J. Harro, Rats with persistently high exploratory activity have both higher extracellular dopamine levels and higher proportion of D(2) (High) receptors in the striatum, Synapse, 63 (2009) 443-446.

[251] F.A. Perez, R.D. Palmiter, Parkin-deficient mice are not a robust model of parkinsonism, Proc Natl Acad Sci U S A, 102 (2005) 2174-2179.

[252] J. Menendez, J.A. Rodriguez-Navarro, R.M. Solano, M.J. Casarejos, I. Rodal, R. Guerrero, M.P. Sanchez, J. Avila, M.A. Mena, J.G. de Yebenes, Suppression of Parkin enhances nigrostriatal and motor neuron lesion in mice over-expressing human-mutated tau protein, Human molecular genetics, 15 (2006) 2045-2058.

[253] T. Kitada, A. Pisani, M. Karouani, M. Haburcak, G. Martella, A. Tscherter, P. Platania, B. Wu, E.N. Pothos, J. Shen, Impaired dopamine release and synaptic plasticity in the striatum of parkin-/- mice, Journal of neurochemistry, 110 (2009) 613-621.

[254] G. Oyama, K. Yoshimi, S. Natori, Y. Chikaoka, Y.R. Ren, M. Funayama, Y. Shimo, R. Takahashi, T. Nakazato, S. Kitazawa, N. Hattori, Impaired in vivo dopamine release in parkin knockout mice, Brain research, 1352 (2010) 214-222.

[255] Y. Takamatsu, H. Shiotsuki, S. Kasai, S. Sato, T. Iwamura, N. Hattori, K. Ikeda, Enhanced Hyperthermia Induced by MDMA in Parkin Knockout Mice, Curr Neuropharmacol, 9 (2011) 96-99.

[256] Y. Zhang, B.A. Barres, Astrocyte heterogeneity: an underappreciated topic in neurobiology, Curr Opin Neurobiol, 20 (2010) 588-594.

[257] J.E. Burda, M.V. Sofroniew, Reactive gliosis and the multicellular response to CNS damage and disease, Neuron, 81 (2014) 229-248.

[258] J.P. O'Callaghan, D.B. Miller, Neurotoxicity profiles of substituted amphetamines in the C57BL/6J mouse, J Pharmacol Exp Ther, 270 (1994) 741-751.

[259] G.D. Cappon, L.L. Morford, C.V. Vorhees, Ontogeny of methamphetamine-induced neurotoxicity and associated hyperthermic response, Brain Res Dev Brain Res, 103 (1997) 155-162.

[260] M.A. Cambray-Deakin, R.D. Burgoyne, Posttranslational modifications of alpha-tubulin: acetylated and detyrosinated forms in axons of rat cerebellum, J Cell Biol, 104 (1987) 1569-1574.

[261] P.W. Baas, T. Slaughter, A. Brown, M.M. Black, Microtubule dynamics in axons and dendrites, J Neurosci Res, 30 (1991) 134-153.

[262] H. Chauhan, B.A. Killinger, C.V. Miller, A. Moszczynska, Single and binge methamphetamine administrations have different effects on the levels of dopamine D2 autoreceptor and dopamine transporter in rat striatum, Int J Mol Sci, 15 (2014) 5884-5906.

[263] K.A. Mark, J.J. Soghomonian, B.K. Yamamoto, High-dose methamphetamine acutely activates the striatonigral pathway to increase striatal glutamate and mediate long-term dopamine toxicity, The Journal of neuroscience : the official journal of the Society for Neuroscience, 24 (2004) 11449-11456.

[264] B.A. Killinger, A. Moszczynska, Epothilone D prevents binge methamphetamine-mediated loss of striatal dopaminergic markers, J Neurochem, 136 (2016) 510-525.

[265] M.S. Quinton, B.K. Yamamoto, Causes and consequences of methamphetamine and MDMA toxicity, AAPS J, 8 (2006) E337-347.

[266] N.R. Swerdlow, A.S. Krupin, M.J. Bongiovanni, J.M. Shoemaker, J.C. Goins, R.P. Hammer, Jr., Heritable differences in the dopaminergic regulation of behavior in rats: relationship to D2-like receptor G-protein function, Neuropsychopharmacology, 31 (2006) 721-729.

[267] A.J. Lees, J.C. Fernando, G. Curzon, Serotonergic involvement in behavioural responses to amphetamine at high dosage, Neuropharmacology, 18 (1979) 153-158.

[268] D. Dawbarn, C.J. Pycock, Motor effects following application of putative excitatory amino acid antagonists to the region of the mesencephalic dopamine cell bodies in the rat, Naunyn Schmiedebergs Arch Pharmacol, 318 (1981) 100-104.

[269] Y.A. Grimbergen, J.W. Langston, R.A. Roos, B.R. Bloem, Postural instability in Parkinson's disease: the adrenergic hypothesis and the locus coeruleus, Expert Rev Neurother, 9 (2009) 279-290.

[270] L.H. Conti, D.S. Segal, R. Kuczenski, Maintenance of amphetamine-induced stereotypy and locomotion requires ongoing dopamine receptor activation, Psychopharmacology (Berl), 130 (1997) 183-188.

[271] E. Bezard, S. Dovero, C. Prunier, P. Ravenscroft, S. Chalon, D. Guilloteau, A.R. Crossman, B. Bioulac, J.M. Brotchie, C.E. Gross, Relationship between the appearance of symptoms and the level of nigrostriatal degeneration in a progressive 1-methyl-4-phenyl-1,2,3,6-tetrahydropyridine-lesioned macaque model of Parkinson's disease, The Journal of neuroscience : the official journal of the Society for Neuroscience, 21 (2001) 6853-6861.

[272] J.F. Bowyer, S. Ali, High doses of methamphetamine that cause disruption of the blood-brain barrier in limbic regions produce extensive neuronal degeneration in mouse hippocampus, Synapse, 60 (2006) 521-532.

[273] R.A. Singh, T.A. Kosten, B.M. Kinsey, X. Shen, A.Y. Lopez, T.R. Kosten, F.M. Orson, Dose-dependent changes in the locomotor responses to methamphetamine in BALB/c mice: low doses induce hypolocomotion, Pharmacol Biochem Behav, 103 (2012) 230-236.

[274] D.M. Thomas, D.M. Francescutti-Verbeem, D.M. Kuhn, The newly synthesized pool of dopamine determines the severity of methamphetamine-induced neurotoxicity, J Neurochem, 105 (2008) 605-616.

[275] Y. Lee, D.A. Stevens, S.U. Kang, H. Jiang, Y.I. Lee, H.S. Ko, L.A. Scarffe, G.E. Umanah, H. Kang, S. Ham, T.I. Kam, K. Allen, S. Brahmachari, J.W. Kim, S. Neifert, S.P. Yun, F.C. Fiesel, W. Springer, V.L. Dawson, J.H. Shin, T.M. Dawson, PINK1 Primes Parkin-Mediated Ubiquitination of PARIS in Dopaminergic Neuronal Survival, Cell Rep, 18 (2017) 918-932.

[276] R. Moratalla, M. Xu, S. Tonegawa, A.M. Graybiel, Cellular responses to psychomotor stimulant and neuroleptic drugs are abnormal in mice lacking the D1 dopamine receptor, Proc Natl Acad Sci U S A, 93 (1996) 14928-14933.

[277] D. Centonze, C. Grande, E. Saulle, A.B. Martin, P. Gubellini, N. Pavon, A. Pisani, G. Bernardi, R. Moratalla, P. Calabresi, Distinct roles of D1 and D5 dopamine receptors in motor activity and striatal synaptic plasticity, J Neurosci, 23 (2003) 8506-8512.

[278] M. Fukada, A. Nakayama, T. Mamiya, T.P. Yao, Y. Kawaguchi, Dopaminergic abnormalities in Hdac6-deficient mice, Neuropharmacology, 110 (2016) 470-479.

[279] S.F. Ali, G.D. Newport, R.R. Holson, W. Slikker, Jr., J.F. Bowyer, Low environmental temperatures or pharmacologic agents that produce hypothermia decrease methamphetamine neurotoxicity in mice, Brain Res, 658 (1994) 33-38.

[280] E.A. Kiyatkin, H.S. Sharma, Expression of heat shock protein (HSP 72 kDa) during acute methamphetamine intoxication depends on brain hyperthermia: neurotoxicity or neuroprotection?, J Neural Transm (Vienna), 118 (2011) 47-60.

[281] J.A. Olzmann, L. Li, M.V. Chudaev, J. Chen, F.A. Perez, R.D. Palmiter, L.S. Chin, Parkin-mediated K63-linked polyubiquitination targets misfolded DJ-1 to aggresomes via binding to HDAC6, J Cell Biol, 178 (2007) 1025-1038.

[282] C.R. Taylor, R.M. Levenson, Quantification of immunohistochemistry--issues concerning methods, utility and semiquantitative assessment II, Histopathology, 49 (2006) 411-424.

[283] R.A. Walker, Quantification of immunohistochemistry--issues concerning methods, utility and semiquantitative assessment I, Histopathology, 49 (2006) 406-410.

[284] S.C. Taylor, A. Posch, The design of a quantitative western blot experiment, BioMed research international, 2014 (2014) 361590.

[285] D. Zhang, X. Hu, L. Qian, J.P. O'Callaghan, J.S. Hong, Astrogliosis in CNS pathologies: is there a role for microglia?, Molecular neurobiology, 41 (2010) 232-241.

[286] C.L. Beites, H. Xie, R. Bowser, W.S. Trimble, The septin CDCrel-1 binds syntaxin and inhibits exocytosis, Nature neuroscience, 2 (1999) 434-439.

[287] N. Wu, P.R. Joshi, C. Cepeda, E. Masliah, M.S. Levine, Alpha-synuclein overexpression in mice alters synaptic communication in the corticostriatal pathway, Journal of neuroscience research, 88 (2010) 1764-1776.

[288] P. Garcia-Reitbock, O. Anichtchik, A. Bellucci, M. Iovino, C. Ballini, E. Fineberg, B. Ghetti, L. Della Corte, P. Spano, G.K. Tofaris, M. Goedert, M.G. Spillantini, SNARE protein redistribution and synaptic failure in a transgenic mouse model of Parkinson's disease, Brain : a journal of neurology, 133 (2010) 2032-2044.

[289] T. Rhinesmith, B.A. Killinger, A. Sharma, A. Moszczynska, Multimer-PAGE: A Method for Capturing and Resolving Protein Complexes in Biological Samples, J Vis Exp, DOI 10.3791/55341(2017).

[290] M. Goedert, M.G. Spillantini, K. Del Tredici, H. Braak, 100 years of Lewy pathology, Nature reviews. Neurology, 9 (2013) 13-24.

[291] J. Burre, M. Sharma, T.C. Sudhof, alpha-Synuclein assembles into higher-order multimers upon membrane binding to promote SNARE complex formation, Proceedings of the National Academy of Sciences of the United States of America, 111 (2014) E4274-4283.

[292] J. Burre, M. Sharma, T.C. Sudhof, Definition of a molecular pathway mediating alpha-synuclein neurotoxicity, The Journal of neuroscience : the official journal of the Society for Neuroscience, 35 (2015) 5221-5232.

[293] U. Dettmer, A.J. Newman, F. Soldner, E.S. Luth, N.C. Kim, V.E. von Saucken, J.B. Sanderson, R. Jaenisch, T. Bartels, D. Selkoe, Parkinson-causing alpha-synuclein missense

mutations shift native tetramers to monomers as a mechanism for disease initiation, Nat Commun, 6 (2015) 7314.

[294] U. Dettmer, A.J. Newman, E.S. Luth, T. Bartels, D. Selkoe, In vivo cross-linking reveals principally oligomeric forms of alpha-synuclein and beta-synuclein in neurons and non-neural cells, J Biol Chem, 288 (2013) 6371-6385.

[295] V.N. Uversky, H.J. Lee, J. Li, A.L. Fink, S.J. Lee, Stabilization of partially folded conformation during alpha-synuclein oligomerization in both purified and cytosolic preparations, The Journal of biological chemistry, 276 (2001) 43495-43498.

[296] C. Huang, G. Ren, H. Zhou, C.C. Wang, A new method for purification of recombinant human alpha-synuclein in Escherichia coli, Protein expression and purification, 42 (2005) 173-177.

[297] J. Folch, M. Lees, G.H. Sloane Stanley, A simple method for the isolation and purification of total lipides from animal tissues, The Journal of biological chemistry, 226 (1957) 497-509.

[298] I. Wittig, H.P. Braun, H. Schagger, Blue native PAGE, Nature protocols, 1 (2006) 418-428.

[299] G. Shearer, Jr., A syringe-based gradient former for linear and exponential gradients, Analytical biochemistry, 221 (1994) 397-400.

[300] A. McMahon, H. Lu, I.A. Butovich, The spectrophotometric sulfo-phospho-vanillin assessment of total lipids in human meibomian gland secretions, Lipids, 48 (2013) 513-525.

[301] I. Wittig, H. Schagger, Native electrophoretic techniques to identify protein-protein interactions, Proteomics, 9 (2009) 5214-5223.

[302] A.M. Seddon, P. Curnow, P.J. Booth, Membrane proteins, lipids and detergents: not just a soap opera, Biochimica et biophysica acta, 1666 (2004) 105-117.

[303] D.J. Samsonoff C, Almog R, Berns DS The use of Coomassie Brillian Blue for critical micelle concentration determination of detergents., J Colloid Interface Sci, DOI (1986) 325-329.

[304] P.G. Crichton, M. Harding, J.J. Ruprecht, Y. Lee, E.R. Kunji, Lipid, detergent, and Coomassie Blue G-250 affect the migration of small membrane proteins in blue native gels: mitochondrial carriers migrate as monomers not dimers, The Journal of biological chemistry, 288 (2013) 22163-22173.

[305] P. Banerjee, A. Dasgupta, B.A. Chromy, G. Dawson, Differential solubilization of membrane lipids by detergents: coenrichment of the sheep brain serotonin 5-HT1A receptor with phospholipids containing predominantly saturated fatty acids, Archives of biochemistry and biophysics, 305 (1993) 68-77.

[306] A.K. Bhuyan, On the mechanism of SDS-induced protein denaturation, Biopolymers, 93 (2010) 186-199.

[307] A.G. Therien, F.E. Grant, C.M. Deber, Interhelical hydrogen bonds in the CFTR membrane domain, Nature structural biology, 8 (2001) 597-601.

[308] A. Rath, M. Glibowicka, V.G. Nadeau, G. Chen, C.M. Deber, Detergent binding explains anomalous SDS-PAGE migration of membrane proteins, Proceedings of the National Academy of Sciences of the United States of America, 106 (2009) 1760-1765.

[309] W.S. Davidson, A. Jonas, D.F. Clayton, J.M. George, Stabilization of alpha-synuclein secondary structure upon binding to synthetic membranes, The Journal of biological chemistry, 273 (1998) 9443-9449.

[310] A. Leitner, T. Walzthoeni, A. Kahraman, F. Herzog, O. Rinner, M. Beck, R. Aebersold, Probing native protein structures by chemical cross-linking, mass spectrometry, and bioinformatics, Molecular & cellular proteomics : MCP, 9 (2010) 1634-1649.

[311] J. Gubbens, E. Ruijter, L.E. de Fays, J.M. Damen, B. de Kruijff, M. Slijper, D.T. Rijkers, R.M. Liskamp, A.I. de Kroon, Photocrosslinking and click chemistry enable the specific detection of proteins interacting with phospholipids at the membrane interface, Chemistry & biology, 16 (2009) 3-14.

[312] C. Van Humbeeck, E. Waelkens, O. Corti, A. Brice, W. Vandenberghe, Parkin occurs in a stable, non-covalent, approximately 110-kDa complex in brain, The European journal of neuroscience, 27 (2008) 284-293.

[313] A.J. Newman, D. Selkoe, U. Dettmer, A new method for quantitative immunoblotting of endogenous alpha-synuclein, PloS one, 8 (2013) e81314.

[314] X. Zhao, Y. Zhou, A.M. Weissmiller, M.L. Pearn, W.C. Mobley, C. Wu, Real-time imaging of axonal transport of quantum dot-labeled BDNF in primary neurons, Journal of visualized experiments : JoVE, DOI 10.3791/51899(2014) 51899.

[315] Y. Ren, J. Zhao, J. Feng, Parkin binds to alpha/beta tubulin and increases their ubiquitination and degradation, The Journal of neuroscience : the official journal of the Society for Neuroscience, 23 (2003) 3316-3324.

[316] J. Zhao, Y. Ren, Q. Jiang, J. Feng, Parkin is recruited to the centrosome in response to inhibition of proteasomes, J Cell Sci, 116 (2003) 4011-4019.

[317] Y. Ren, H. Jiang, F. Yang, K. Nakaso, J. Feng, Parkin protects dopaminergic neurons against microtubule-depolymerizing toxins by attenuating microtubule-associated protein kinase activation, The Journal of biological chemistry, 284 (2009) 4009-4017.

[318] J. Feng, Microtubule: a common target for parkin and Parkinson's disease toxins, Neuroscientist, 12 (2006) 469-476.

[319] F. Yang, Q. Jiang, J. Zhao, Y. Ren, M.D. Sutton, J. Feng, Parkin stabilizes microtubules through strong binding mediated by three independent domains, The Journal of biological chemistry, 280 (2005) 17154-17162.

[320] W. Kim, E.J. Bennett, E.L. Huttlin, A. Guo, J. Li, A. Possemato, M.E. Sowa, R. Rad, J. Rush, M.J. Comb, J.W. Harper, S.P. Gygi, Systematic and quantitative assessment of the ubiquitin-modified proteome, Mol Cell, 44 (2011) 325-340.

[321] A. Mirecki, P. Fitzmaurice, L. Ang, K.S. Kalasinsky, F.J. Peretti, S.S. Aiken, D.J. Wickham, A. Sherwin, J.N. Nobrega, H.J. Forman, S.J. Kish, Brain antioxidant systems in human methamphetamine users, J Neurochem, 89 (2004) 1396-1408.

[322] M.W. Warren, F.H. Kobeissy, M.C. Liu, R.L. Hayes, M.S. Gold, K.K. Wang, Concurrent calpain and caspase-3 mediated proteolysis of alpha II-spectrin and tau in rat brain after methamphetamine exposure: a similar profile to traumatic brain injury, Life Sci, 78 (2005) 301-309.

[323] M. Dubey, P. Chaudhury, H. Kabiru, T.B. Shea, Tau inhibits anterograde axonal transport and perturbs stability in growing axonal neurites in part by displacing kinesin

cargo: neurofilaments attenuate tau-mediated neurite instability, Cell Motil Cytoskeleton, 65 (2008) 89-99.

[324] H. Li, S.H. Li, Z.X. Yu, P. Shelbourne, X.J. Li, Huntingtin aggregate-associated axonal degeneration is an early pathological event in Huntington's disease mice, J Neurosci, 21 (2001) 8473-8481.

[325] G.B. Stokin, C. Lillo, T.L. Falzone, R.G. Brusch, E. Rockenstein, S.L. Mount, R. Raman, P. Davies, E. Masliah, D.S. Williams, L.S. Goldstein, Axonopathy and transport deficits early in the pathogenesis of Alzheimer's disease, Science, 307 (2005) 1282-1288.

[326] G.J. Wang, N.D. Volkow, L. Chang, E. Miller, M. Sedler, R. Hitzemann, W. Zhu, J. Logan, Y. Ma, J.S. Fowler, Partial recovery of brain metabolism in methamphetamine abusers after protracted abstinence, Am J Psychiatry, 161 (2004) 242-248.

[327] I. Boileau, T. McCluskey, J. Tong, Y. Furukawa, S. Houle, S.J. Kish, Rapid Recovery of Vesicular Dopamine Levels in Methamphetamine Users in Early Abstinence, Neuropsychopharmacology, 41 (2016) 1179-1187.

[328] M. Denham, M. Dottori, Neural differentiation of induced pluripotent stem cells, Methods Mol Biol, 793 (2011) 99-110.

[329] L. Ma, Y. Liu, S.C. Zhang, Directed differentiation of dopamine neurons from human pluripotent stem cells, Methods Mol Biol, 767 (2011) 411-418.

[330] H. Nakamura, N. Yamashita, Y. Kanamaru, T. Tachibana, Y. Sekino, S. Chen, T. Gotoh, F. Tanaka, Y. Goshima, Quantitative analysis of intraneuronal transport in human iPS neurons, J Pharmacol Sci, 128 (2015) 170-178.

[331] S. Goodin, M.P. Kane, E.H. Rubin, Epothilones: mechanism of action and biologic activity, J Clin Oncol, 22 (2004) 2015-2025.

[332] U. Vaishampayan, R.E. Parchment, B.R. Jasti, M. Hussain, Taxanes: an overview of the pharmacokinetics and pharmacodynamics, Urology, 54 (1999) 22-29.

[333] J.P. Kesby, A. Chang, A. Markou, S. Semenova, Modeling human methamphetamine use patterns in mice: chronic and binge methamphetamine exposure, reward function and neurochemistry, Addict Biol, DOI 10.1111/adb.12502(2017).

[334] J.L. St Martin, J. Klucken, T.F. Outeiro, P. Nguyen, C. Keller-McGandy, I. Cantuti-Castelvetri, T.N. Grammatopoulos, D.G. Standaert, B.T. Hyman, P.J. McLean, Dopaminergic neuron loss and up-regulation of chaperone protein mRNA induced by targeted over-expression of alpha-synuclein in mouse substantia nigra, J Neurochem, 100 (2007) 1449-1457.

ABSTRACT

AXONAL TRANSPORT, PARKIN, AND A-SYNUCLEIN; NOVEL THERAPEUTIC TARGETS TO TREAT METHAMPHETAMINE NEUROTOXICITY

by

BRYAN KILLINGER

December 2017

Advisor: Dr. Anna Moszczynska

Major: Pharmaceutical Sciences

Degree: Doctor of Philosophy

Methamphetamine (METH) is a commonly abuse psychostimulant. Exposure to chronic high doses of METH can result in neurotoxicity primarily characterized by damage to striatal dopaminergic (DAergic) axons. There are currently no therapeutic interventions for METH neurotoxicity. To some extent damage to striatal DAergic axons is reversible and DAergic axon function may return following abstinence from METH. The reversible nature of METH neurotoxicity suggests that normal striatal function could be restored following exposure to METH. However, potential targets to treat METH neurotoxicity are needed. Axonal transport is required for restoration of DAergic axon components

damaged or lost following METH. Here we investigated several potential novel drug targets to treat METH neurotoxicity including with emphasis on targeting axonal transport. We also investigated the E3 ligase parkin and the aggregation prone nerve terminal protein α-synuclein. To investigate the role of axonal transport in METH neurotoxicity we treated a rat model of METH neurotoxicity with axonal transport enhancing drug, epothilone D. Results show that epothilone D could to some extent prevent METH-induced damage to DAergic axons in the striatum. To investigate parkin's role in METH neurotoxicity we treated parkin knockout rats with a neurotoxic dose of METH. We found that parkin knockout rats were hypersensitive to the METH induced DAergic neurotoxicity, confirming the neuroprotective role of parkin for DAergic neurons. To investigate the role of α-synuclein in METH neurotoxicity we developed a novel method of measuring α-synuclein oligomerization in complex biological samples. In conclusion, here we lay the experimental foundation for three potential targets of METH neurotoxicity.

AUTOBIOGRAPHICAL STATEMENT

Education

2012-2017	PhD, Pharmaceutical Sciences Wayne State University, Detroit, MI,
2009	MA, Psychology Western Michigan University, Kalamazoo, MI
2008	BS, Psychology Western Michigan University, Kalamazoo, MI

Publications

1) Killinger BA and Labrie V. (2017) Vertebrate food products as a potential source of prion-like α-synuclein. NPJ Parkinson's disease.

2) Rhinesmith T, Killinger BA, Sharma A, Moszczynska A (2017). Multimer-PAGE: A Method for Capturing and Resolving Protein Complexes in Biological Samples. JoVE.

3) Luong D, Kesharwani P, Killinger BA, Moszczynska A, Sarkar FH, Padhye S, Rishi AK, Iyer AK (2016). Solubility enhancement and targeted delivery of a potent anticancer flavonoid analogue to cancer cells using ligand decorated dendrimer nano-architectures. Journal of Colloid Interface Science.

4) Killinger, B. A. and A. Moszczynska (2016). Characterization of alpha-Synuclein Multimer Stoichiometry in Complex Biological Samples by Electrophoresis. Analytical Chemistry.

5) Killinger, B. A. and A. Moszczynska (2016). Epothilone D prevents binge methamphetamine-mediated loss of striatal dopaminergic markers. Journal of Neurochemistry. 136(3): 510-525.

6) Moszczynska, A., Flack, A., Qui, P., Muotri, A., Killinger, B.A. (2015). Neurotoxic Methamphetamine Doses Increase Line-1 Expression in the Neurogenic Zones of the Rat Brain. Scientific reports.

7) Nadithe, V., Liu, R., Killinger, B.A., Movassaghian, S., Kim, N.H., Moszczynska, A.B., Masters, K.S., Gellman, S.H. and Merkel, O.M. (2015). Screening nylon-3 polymers, a new class of cationic amphiphiles, for siRNA delivery. Molecular Pharmacology, 12, 362-374.

8) Chauhan, H., Killinger, B.A., et al. (2014). Single and binge methamphetamine administrations have different effects on the levels of dopamine D2 autoreceptor and dopamine transporter in rat striatum. International Journal of Molecular Sciences 15(4): 5884-5906.

9) Killinger, B.A., Mrudang S., Moszczynska A. (2013). Co-administration of betulinic acid and methamphetamine causes toxicity to dopaminergic and serotonergic nerve terminals in the striatum of late adolescent rats. Journal of Neurochemistry.

10) Liu, B., Traini, R., Killinger, B., Schneider, B, Moszczynska, A. (2013) Overexpression of parkin in the rat nigrostriatal dopamine system protects against methamphetamine neurotoxicity. Experimental Neurology. Sep; 247:359-72.

11) Killinger, B.A., Peet, M.M., Baker, L.E. (2010) Salvinorin A Fails to Substitute for the Discriminative Stimulus Effects of LSD or Ketamine in Sprague-Dawley Rats. Pharmacology, Biochemistry, and Behavior, 96: 260-265.

12) Baker, L.E., Panos, J.J., Killinger, B.A., Peet, M.M., Bell, L.M., Haliw, L.A., Walker, S.L. (2009) Comparison of the Discriminative Stimulus Effects of Salvinorin A and its Derivatives to U69, 593 and U50,488 in Rats. Psychopharmacology. 203: 203-211.